Title

Determining the cellular and circuit mechanisms underlying visual processing in the LGN.

Author

Sanchez, Alyssa

Publication Date

2024

Peer reviewed|Thesis/dissertation

Determining the Cellular and Circuit Mechanisms Underlying Visual Processing in the LGN.

By

ALYSSA NICOLE SANCHEZ

DISSERTATION

Submitted in partial satisfaction of the requirements of the degree of

DOCTOR OF PHILOSOPHY

in

Neuroscience

in the

OFFICE OF GRADUATE STUDIES

of the

UNIVERSITY OF CALIFORNIA

DAVIS

Approved:

_____

W. Martin Usrey, Chair

_____

Gregg Recanzone

_____

Jochen Ditterich

_____

Tim Hanks

_____

Murray Sherman

Committee in Charge

2024

Dedicated with love,

to my mother,

and Hubert Sanchez, in memoriam.

Table of contents

List of Figures

Abstract

This dissertation highlights unique aspects of the LGN for visual processing in the hopes to reframe the traditional view that the LGN is simply a relay center between the retina and primary visual cortex. It begins with a general introduction outlining the early visual system in the domestic cat and non-human primate, and sets up the rest of the dissertation to include an examination of unique LGN visual processing. Within the second chapter of this dissertation is an investigation of the unique biophysical membrane properties of the LGN to understand how the phenomena of bursting changes as a function of contrast in the anesthetized cat. In the third chapter of this dissertation, there is an investigation of corticogeniculate feedback's effects on LGN processing as a function of stimulus size in the awake-behaving non-human primate. In the general discussion chapter, there is an exploration of how bursting and corticogeniculate feedback could interact with one another to facilitate (and modulate) LGN visual processing. Lastly, there is an appendix chapter, consisting of a review of the early visual processing system in rodents, felines, and non-human primates. As the LGN is a ubiquitous part of the thalamus and an extremely important brain region for the visual system, understanding the LGN's interactions with other parts of the early visual system is integral to understanding how the LGN contributes to visual processing and the LGN's contribution to higher-level aspects of vision.

Acknowledgements

I would like to thank my graduate advisor and dissertation committee chair, Dr. W. Martin Usrey. Thank you for sharing your expertise in studying the function of the early visual system, your tremendous knowledge about anatomy, your surgical skills training and experience, and your in-depth understanding of the animal models studied for the visual system. Your guidance in my writing and scientific thinking was important for my individual and academic growth and allowed me to gain the expertise necessary to complete my PhD work and continue on in systems neuroscience. Your professional guidance was extremely important in navigating my PhD and remaining in neuroscience. You have fostered within me a forever appreciation of understanding basic systems neuroscience and the importance of understanding early visual processing for understanding how the visual system works to allow us to interact with the world around us.

I would like to thank my other members of my dissertation for their time, along with their scientific thoughts, opinions, and contributions to my dissertation work. To Dr. Jochen Ditterich, thank you for your supportive and helpful contributions during my dissertation work, allowing me to analyze my data further with a better understanding of ascribing data findings to visual processing as a whole. Thank you to Dr. Tim Hanks for your expertise in understanding circuit dynamics, for your assistance in thinking about interactions between feedforward and feedback projections, and for your supportive and kind words during my entire dissertation work. To Dr. Murray Sherman, thank you for your intellectual thoughts regarding my entire dissertation, for providing unique insights for understanding the role of bursting in the LGN, and for helping me develop critical

thinking about how to understand the relationship between my data and understanding its impacts on the feedback visual processing circuit. Lastly, to Dr. Gregg Recanzone, thank you for your entire support during my PhD, for being a rotation mentor to me during my first year, for your time and advice on my posters and presentations after, for your professional and personal advice in my professional endeavors, and for your development of my ability to critically think about the function of feedback on visual processing.

I would like to give a special thank my project scientist, lab mate, friend, and academic mentor Dr. Henry Alitto. You helped me learn how to simultaneously record from two cortical regions, and helped me develop tools needed for my feedback project. Thank you for being a consistent and reliable resource for me during my PhD. You helped me with my daily questions, thoughts, and concerns during my entire research collection, from my beginning days to the very end. You were irreplaceable for helping me develop my scientific thinking and data analysis skills. You assisted me both scientifically and personally, and I will be forever grateful for being able to work with you during my time in the Usrey Lab.

I would like to give thanks to the rest of the Usrey Lab members that helped me during my PhD. Thank you, Dr. Scottie Alexander for always helping me with my coding questions and providing intellectual input to my scientific projects. Thank you, Dr. Jeffrey Johnson and Dr. Dan Sperka for your never-ending assistance with my data collection, from rig maintenance, Spike2 scripts, and general computer issues. Both of your time, patience, and encouragement helped me tremendously. To my lab manager Katie Neverkovec, thank you for being a special person and friend during my PhD, who

helped me personally during my time in graduate school and helped me learn how to do non-human primate handling and training.

Thank you to all the other young women in the Annex, who have helped me find newfound motivation to continue in science and assist young women who also want to pursue careers in science. You help remind me of the reason I wanted to work with women in STEM and have become beacons of encouragement during my PhD.

I want to give thanks to my loving community of friends, family, and partner, your undying support and encouragement allowed me to finish my PhD and finish my dissertation project. To my mom, thank you for always believing in me and my academic endeavors even when I doubted my own abilities. To my closest friends Flavia and Rose, thank you for your support, kindness, and encouragement during my dissertation. You brought lightness and joy during my PhD, encouraging me to always stay healthy physically, mentally, and emotionally. To my other friends, thank you for bringing joy and encouraging me during my challenging times. To Andres, thank you for your unwavering support during my last PhD year and writing of my dissertation. Your love, encouragement, and assistance with Qiwi allowed me to put my full energy into my dissertation work, focus on being healthy mentally and physically, and find a postdoctoral position after my PhD. To my rainbow chicken Qiwi, thank you for being a birb.

I want to give my most heartfelt gratitude to all of the animals who made my PhD and dissertation work possible. They provided lighthearted moments during difficult times and difficult data collection days. I want to specifically thank Baloo for training me on animal handling, and I want to thank Tomi Jon and Wimpy for their unwavering

patience and entire time spent with me during my PhD. For their contributions to science and my academic career, I will be forever grateful.

Finally, thanks to the funding sources that made my PhD and dissertation work possible from the National Eye Institute (grants EY015387, EY013588, EY012576, and MH082174).

Chapter 1: General Introduction

This dissertation examines the cellular and circuit mechanisms underlying visual response dynamics in the lateral geniculate nucleus of the thalamus (LGN). The pathway from eye to cortex involves projections from retinal ganglion cells that make synapses in the lateral geniculate nucleus (LGN) and projections from the LGN that synapse in primary visual cortex (V1). Traditionally, the LGN is thought of as a "relay center" between the retina and cortex, simply consolidating retinal inputs to be sent to cortex; however, there are important and unique response dynamics in the LGN that arguably make it more than a "relay" of retinal information. Of note within this dissertation, geniculate cells have unique membrane properties that allows them to respond to visual stimuli with burst or tonic activity patterns. Although bursts are particularly effective in driving cortical responses, there are many open and unresolved questions about their role in visual processing. Chapter 2 is focused on experiments in the anesthetized cat to determine the relationship between burst and tonic activity in encoding information about stimulus contrast. Geniculate cells also receive many extraretinal inputs, which can modulate geniculate responses to retinal input. A particularly prominent source of extraretinal input is feedback directly from visual cortex, but the function(s) of corticogeniculate feedback remains to be determined. Chapter 3 is focused on corticogeniculate feedback and explores it function using optogenetics to manipulate feedback in behaving macaque monkeys. The overall goal of this dissertation is to explore and characterize the unique aspects of geniculate visual processing that go beyond the view that the LGN is a simple "relay" for retinal activity in route to cortex. Within this dissertation two animal models are utilized, domestic cats

(*Felis catus*) and rhesus macaques (*Macaca mulatta*), taking advantage of the unique features that each offer.

The retinogeniculocortical pathway of the visual system is well-studied across animal models both anatomically and physiologically (Livingstone and Hubel, 1984; Merigan and Maunsell, 1994; Sincich and Horton, 2005). Irrespective of animal species, the pathway begins in the retina and includes projections to and synapses in the LGN before continuing on to V1. This pathway is denoted as the retinogeniculocortical pathway. After V1, visual information is further sent to downstream cortical areas for additional visual processing. Importantly, research focusing on the retinogeniculocortical pathway is critical for understanding how visual information is encoded, consolidated, and processed within the visual system to allow animals to successfully interact with the world. At the level of the retina, visual information leaves the eye via retinal ganglion cells (RGCs). The classification of RGCs in the retina depends on characterizing their preferences to various aspects of visual information, including: 1. center/surround organization of their receptive field (Kuffler, 1952, 1953; Barlow et al., 1954); 2. their cell size/receptive field size (Boycott and Wassle, 1991; Brown and Masland, 2001); 3. linear/nonlinear spatial summation (Enroth-Cugell and Robson, 1966; Enroth-Cugell, Robson, Schweitzer-Tong, and Watson, 1983); 4. response to standing contrast over time (Cleland, Dubin, and Levick, 1971a); 5. sustained/transient axonal velocity (Cleland, Dubin, and Levick, 1971b); 6. response to stimulus contrast (Kaplan and Shapley, 1986); 7. response to stimulus speed (Hamasaki and Cohen, 1977; Cohen, Winters, and Hamasaki, 1980; Cleland and Harding, 1983); and 8. chromatic organization of their receptive field (Dacey, 2000). In both carnivores and primates,

RGCs can be comparatively grouped, although they have different names for the classifications. In carnivores, RGCs are classified into Y, X, or W cells. These same cell types are also known as α, β, or γ cells (Boycott and Wassle, 1991). In general, X cells respond more linearly to sinusoidal stimuli and have more sustained responses, whereas Y cells have non-linear and transient responses (Enroth-Cugell and Robsen, 1966). In the primate, RGCs are classified as either parasol or midget cells. Despite this difference in their names, carnivore and primate RGCs have similar distinctions for their visual responses. For comparison of carnivore RGCs to primate RGCs, Y cells, α cells, and parasol cells respond similarly to visual stimuli while X cells, β cells, and midget cells respond similarly to visual stimuli. Overall, previous literature has demonstrated that for these groupings of RGCs, the following distinctions can be made between the two groups of RGCs:

	X cells/β cells; midget cells	Y cells/α cells; parasol cells
Center/Surround Organization	On/Off; Off/On	On/Off; Off/On
Cell Size/Receptive Field Size	small	large
Spatial Summation	linear	nonlinear
Response to Standing Contrast	sustained	transient
Axonal Velocity	slow	fast
Response to Stimulus Contrast	poor	very good
Response to Stimulus Speed	poor	very good
Receptive Field Chromaticity	color component*	broadband
**For trichromatic primates*		

This knowledge has important implications for understanding the feedforward visual pathway, as these RGCs set up parallel streams of visual information flow to

cortex. Anatomically, the two groups of RGCs selectively project onto unique LGN cell classes. In carnivores, RGC populations of Y cells/α cells project onto Y cells in the LGN (either in layer A or A1) while X cells/β cells project onto X cells in the LGN (either in layer A or A1). In comparison, parasol cells project onto the magnocellular layers of the LGN (layers 1-2) while midget cells project onto the parvocellular layers of the LGN (layers 3-6) in the primate. This distinction between the two animal models in which their RGC cell types project to different LGN layers is due to differences in the anatomical structure of the LGN between the two species. In carnivores, the LGN has two predominant layers, which receive separate input from the contralateral eye (layer A) and ipsilateral eye (layer A1) to be relayed to V1. Thus, RGCs from both cell-type groupings need to project to each LGN layer. In comparison, for the primate, the LGN has six layers, moving dorsally to ventrally the LGN layers receive contralateral (layer 6), ipsilateral (layer 5), contralateral (layer 4), ipsilateral (layer 3 and layer 2), and contralateral (layer 1) inputs to be relayed to V1. Additionally, both species have an additional group of retinal and LGN neurons known as the W cells (cats) and koniocellular neurons (monkeys). Less is known about these cell types and they will not be a focus of this dissertation; however, they are included in the Appendix for additional information. Despite the difference in the number of LGN layers for these two animal models, the LGN and its general structure is highly conserved across animals (Figure 1, see also Appendix Figure 1). Additionally, despite differences in the number of LGN layers, carnivores and primates are well-selected animal models for studying the LGN, as both animal models have binocular vision and rely heavily on their vision for

navigating the world around them, making them ideal species to study visual processing.

As mentioned above, the LGN has historically been thought of as a simple relay for visual information leaving the eye to reach the cortex. At the level of the LGN, it is largely argued that the LGN cells serve to simply consolidate the multiple of retinal RGC inputs it receives for further processing upstream (Reid and Alonso, 1995; Alonso et al., 2001; Reid and Usrey, 2004). Each relay cell receives ~1-5 RGC inputs from the retina to consolidate and send to cortex (for review, see Cleland, 1986; Reid and Usrey, 2004). As a result, LGN cells that receive RGC input are referred to as geniculate relay cells. This belief is, in large part, due to previous literature which has demonstrated that a majority of an LGN relay cell's response to visual information is inherited from the retina directly, making retinal inputs the primary driving input for LGN relay cell activity (Kaplan and Shapley, 1984; Usrey et al., 1999; Sincich et al., 2007; Sherman and Guillery, 2009; Rathbun et al., 2010). Looking at the previous table of visual processing by RGC type, LGN relay cells have the following preferences for visual processing:

	X cells; Parvo-cells	Y cells; Magno-cells
Center/Surround Organization	On/Off; Off/On	On/Off; Off/On
Cell Size/Receptive Field Size	small	large
Spatial Summation	linear	nonlinear
Response to Standing Contrast	sustained	transient
Axonal Velocity	slow	fast
Response to Stimulus Contrast	poor	very good
Response to Stimulus Speed	poor	very good
Receptive Field Chromaticity	color-component	broadband

In the primate, parvocellular cells have small receptive fields with color-opponency and have slow, sustained responses, responding poorly to lower contrast stimuli, while magnocellular cells have larger receptive fields, broadband responses for color, and faster, transient responses, responding well to lower contrast stimuli (Dreher et al., 1976; Sherman et al., 1976; Shapley et al., 1981; Schiller et al., 1990). Additionally, parvocellular cells are associated with color vision and high acuity vision while magnocellular cells are better suited for perception of motion (DeYoe and Van Essen, 1988; Livingston and Hubel, 1988; Merigan and Maunsell, 1993). This parallel processing of visual information from retina is encoded and relayed to V1 through geniculate relay cell spiking activity.

Geniculate relay cells can communicate information to V1 under two different spiking modes. Relay cells can (and typically) send information to cortex in tonic mode, or burst mode. In order to produce bursts, geniculate relay cells require unique channels in their cell membranes that allow for Ca^{2+} influx via T-type Ca^{2+} channels, which in turn leads to activation of voltage-gated Na+ channels and rapid trains of spike within very short timeframes (Jahnsen and Llinás, 1984). Although bursts are often associated with states of drowsiness (Weyand et al., 2001; Bezdudnaya et al., 2006; Bereshpolova et al., 2011), they are also known to convey visual information to cortex and are particularly effective in evoking cortical responses in V1 (Dan et al., 1996; Usrey et al., 1998; Wang et al., 2007; Martinez et al., 2014; Butts et al., 2016; Fisher et al., 2017; Alitto et al., 2019b; reviewed in Sherman and Guillery, 2009; Usrey and Alitto, 2015; Usrey and Sherman, 2022). Previous work has demonstrated that the occurrence of thalamic bursts depends on (1) de-inactivating the inactivation gate of T-type Ca^{2+}

channels and (2) opening the activation gate in of T-type Ca^{2+} channels. Notably, the number of spikes in a burst, and thus its ability to drive cortex, also depends on (1) the ratio of T-type Ca^{2+}channels in the de-inactivated vs. inactivated state and (2) the subsequent rate of depolarizing voltage change (δv/δt) (Deschênes et al., 1984; Destexhe and Sejnowski, 2002; Hong et al., 2014). This phenomenon of bursting and its function in visual processing is further discussed in Chapter 2, where LGN relay cell bursting is studied as a function of changes in stimulus contrast. As burst spikes increase the timing precision and spatial focus of cortical responses (Borden et al., 2022) understanding how bursting changes as a function of stimulus contrast is an important step in understanding the mechanism for why bursting is effective in evoking cortical responses and why the LGN would have this unique cell membrane to do so (Shapley, 1978; Swadlow and Gusev, 2001; Alitto, Weyand and Usrey, 2005; Rathbun et al., 2016;see also Usrey et al., 1998).

The ubiquitous preservation of the LGN's structure, its relay cell bursting, and continued anatomical separation of parallel visual characteristics across animals facilitates efficient encoding and processing in the visual pathway. From the LGN, the parallel pathway continues to V1, where inputs from the parvocellular layers project to layer 4A and layer 4Cβ of V1 while inputs from the magnocellular layers project to layer 4Cα of V1. Finally, once visual information reaches V1, aspects of visual processing begin to mix from the parallel pathways. For example, the beginning of binocular processing of visual information is found in V1 in addition to V1 ocular dominance columns (Hubel and Wiesel, 1969). At the level of V1, new aspects of visual processing can occur including the ability for cells to have preferences for the orientation of visual

stimuli. This is due to the convergence of LGN relay cell activity onto V1. From V1, visual information is sent further upstream in the visual pathway, either directly to V2 or via the pulvinar in the thalamus where it is sent to higher levels for visual processing (reviewed in Sherman and Guillery, 2009).

While the general features of LGN receptive fields are inherited from the retina (Kaplan and Shapley, 1984; Usrey et al., 1999; Sincich et al., 2007; Sherman and Guillery, 2009; Rathbun et al., 2010), it is important to note that nonretinal inputs onto geniculate relay cells largely outnumber those coming from the retina. For an LGN relay cell, only ~5-10% of synapses made onto LGN neurons come from retinal inputs (Hamos et al., 1987). Thus, a majority of inputs to the LGN relay cell come from extraretinal inputs, and a substantial amount of those come from corticogeniculate feedback from layer 6 of V1, sometimes outnumbering RGC inputs by almost 10:1 (Erisir et al., 1997a, b; Guillery, 1969). Importantly, in carnivores and primates, corticogeniculate feedback from V1 is also anatomically separated and thus processed in parallel. In old world primates, feedback inputs from V1 from the upper tier of layer 6 project to the parvocellular layers and feedback inputs from the lower tier of layer 6 project to the magnocellular layers of the LGN (Fitzpatrick et al., 1994; Usrey, 1994, Figure 2). Additionally, the upper and lower tiers of layer 6 are anatomically separated, with a layer between that does not project to the LGN (Fitzpatrick et al., 1994). In cat, LGN-projecting cortical feedback neurons are also separated from other layer 6 neurons (Carey et al., 1980; LeVay and Sherk, 1981; Katz, 1987). Comparing the percentage of corticogeniculate feedback cells in V1, feedback cells are ~20% of layer 6 cells in macaque (Usrey, 1994) and ~50% of layer 6 cells in cat (Gilbert and Kelly, 1975; Katz,

1987). These feedback projections are known to monosynaptically excite geniculate relay cells or disynaptically inhibit geniculate relay cells via local inhibitory neurons in the LGN or the thalamic reticular nucleus (TRN) (Sherman and Guillery, 2006). The TRN's role in feedback is not currently well-understood.

As relay cells inherit most of their receptive field properties from retina, what function could these nonretinal inputs have on geniculate relay cell visual processing? One possibility is to modulate the gain of relay cell activity to visual inputs (McClurkin et al., 1994; Alitto and Usrey, 2015). Although the retina is the source of driving input to the LGN, not all retinal spikes are transmitted to V1 from the LGN. Thus, the opportunity exists to increase or decrease the responsiveness of LGN cells to retinal input. This filtering of retinal spiking can affect the timing of geniculate relay cell responses to the presentation of visual stimuli (Silitto et al., 1994). This selective filtering of retinal spikes is due to several reasons, including, but not limited to, prior retinal activity, prior LGN spiking, visual environment statistics, and behavioral state (Livingstone and Hubel, 1981; Mastronarde, 1987; Usrey et al., 1998; Lesica and Stanley, 2004; Alitto et al., 2005; Denning and Reinagel, 2005; Rathbun et al., 2007, 2010; Weyand, 2007; Chen et al., 2008; Uglesich et al., 2009; Bereshpolova et al., 2011; Moore et al., 2014; Stoelzel et al., 2015). In Chapter 3, we will explore the function of corticogeniculate feedback further, particularly investigating the idea that feedback could selectively modulate geniculate relay cell activity based on relay cell type. In this study, corticogeniculate feedback is viewed as having the potential to selectively amplify visual features, enhancing specific aspects of relay cell activity of retinal visual information to cortex. Lastly, as different geniculate relay cell types process different aspects of visual

information, corticogeniculate feedback could assist in selectively modulating cell types. In the general discussion chapter (Chapter 4), we explore how the unique aspects of LGN relay cells could interact during visual processing, along with the benefits for LGN relay cells to be able to modulate their activity to appropriately filter retinal inputs to cortex.

Figures

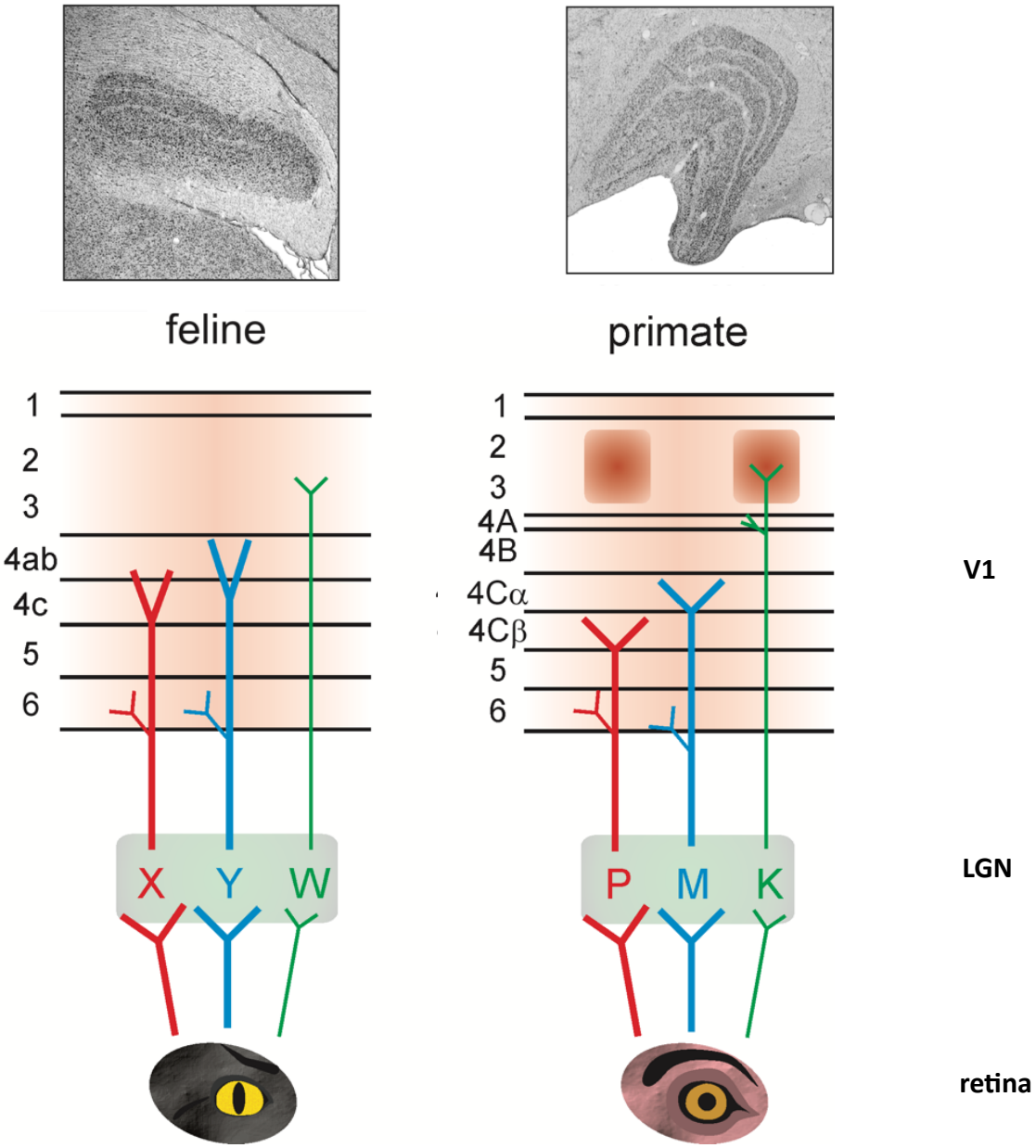

Figure 1. Overview of the LGN and visual pathway in feline and primate animal models. Top: Nissl-stained LGN in feline and primate. Bottom: overview of the visual pathway's feedforward inputs in feline and primate.

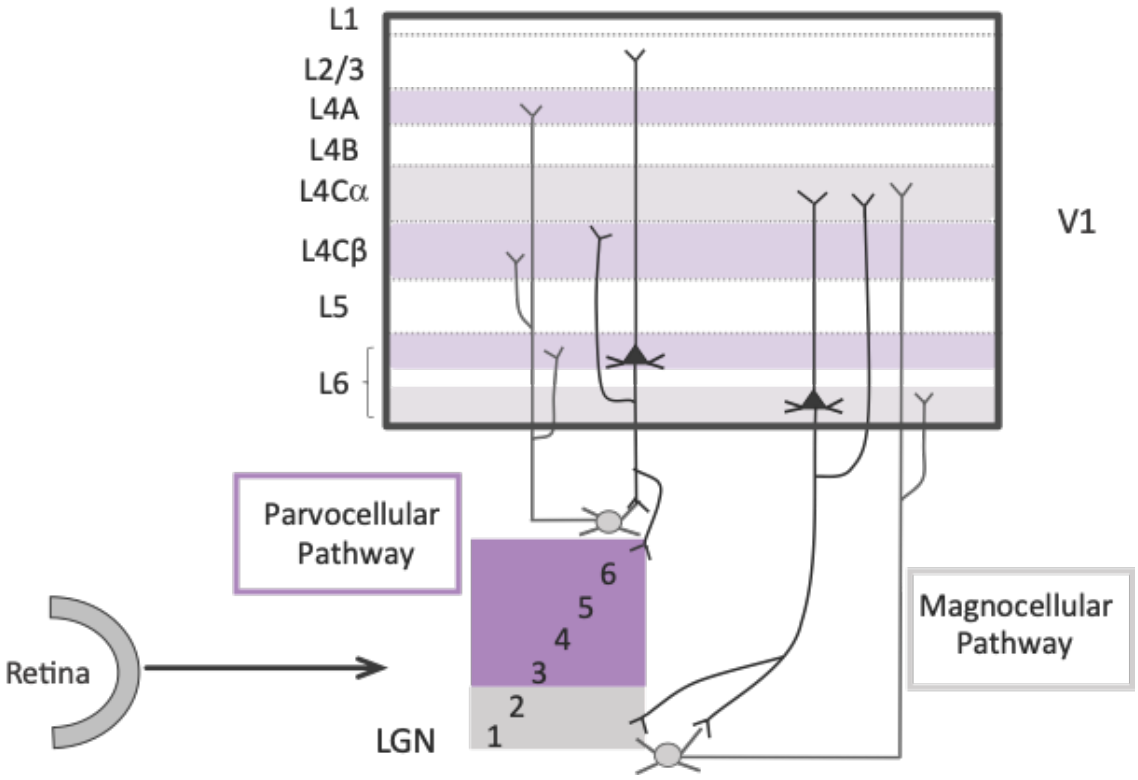

Figure 2. Overview of the corticogeniculate feedback visual pathway. Overview of the anatomy of the retinogeniculocortical visual pathway. This demonstrates the parallel feedforward pathway of the parvocellular pathway (purple) and the magnocellular pathway (gray) to primary visual cortex (V1). These pathways synapse to unique target layers in V1 and, in addition, receive unique feedback projections form layer 6 feedback cells.

Chapter 2: Stimulus contrast modulates burst activity in the lateral geniculate nucleus

For citations of this chapter, please refer to its published citation: Sanchez, A.N., Alitto, H.J., Rathbun, D.L., Fisher, T.G., Usrey, W.M. Stimulus contrast modulates burst activity in the lateral geniculate nucleus. Curr. Res. Neurobiol. 2023 Jun 10;4:100096. doi: 10.1016/j.crneur.2023.10009.6 PMID: 37397805; PMCID: PMC10313900.

Abstract

Burst activity is a ubiquitous feature of thalamic neurons and is well documented for visual neurons in the lateral geniculate nucleus (LGN). Although bursts are often associated with states of drowsiness, they are also known to convey visual information to cortex and are particularly effective in evoking cortical responses. The occurrence of thalamic bursts depends on (1) the inactivation gate of T-type Ca^{2+} channels (T-channels), which become de-inactivated following periods of increased membrane hyperpolarization, and (2) the opening of the T-channel activation gate, which has voltage-threshold and rate-of-change (δv/δt) requirements. Given the time/voltage relationship for the generation of Ca^{2+} potentials that underlie burst events, it is reasonable to predict that geniculate bursts are influenced by the luminance contrast of drifting grating stimuli, with the null phase of higher contrast stimuli evoking greater hyperpolarization followed by a larger dv/dt than the null phase of lower contrast stimuli. To determine the relationship between stimulus contrast and burst activity, we recorded the spiking activity of cat LGN neurons while presenting drifting sine-wave gratings that varied in luminance contrast. Results show that burst rate, reliability, and timing precision are significantly greater with higher contrast stimuli compared with lower contrast stimuli. Additional analysis from simultaneous recordings of synaptically connected retinal ganglion cells and LGN neurons further reveals the time/voltage dynamics underlying burst activity. Together, these results support the hypothesis that stimulus contrast and the biophysical properties underlying the state of T-type Ca^{2+} channels interact to influence burst activity, presumably to facilitate thalamocortical communication and stimulus detection (see Graphical Abstract).

Introduction

Visual information reaches the cerebral cortex primarily via the retino-geniculo-cortical pathway. Neurons in the lateral geniculate nucleus (LGN) of the thalamus receive direct input from retinal ganglion cells and convey this information to target neurons in primary visual cortex (V1). Although LGN projection neurons are often viewed as passive relay cells, they are known to transform retinal signals in several dynamic ways, including transformations in the temporal domain (Dan et al., 1996; Usrey et al., 1998, Wang et al., 2007; Martinez et al., 2014; Butts et al., 2016; Fisher et al., 2017; Alitto et al., 2019b). A prominent example of such a transformation is the shift in LGN firing between tonic spiking and burst spiking (reviewed in Sherman and Guillery, 2009; Usrey and Alitto, 2015; Usrey and Sherman, 2022). Importantly, LGN neurons switch between these two forms of spiking based on the time/voltage history of their membrane potential (Jahnsen and Llinás, 1984). Thus, these two types of activity, tonic activity and burst activity, could be differentially engaged by distinct patterns of visual stimulation and, consequently, be used to differentially encode information about stimuli being provided to cortex. This view is supported by past work showing bursts can transmit visual information and occur reliably to specific patterns of visual stimuli (Guido et al., 1995; Reinagel et al., 1999; Rivadulla et al., 2003; Lesica and Stanley, 2004; Alitto et al., 2005).

LGN projection neurons in tonic mode respond to excitatory inputs with regularly spaced action potentials, generally in proportion to the strength of the stimulus (Llinás and Jahnsen, 1982; Huguenard and McCormick, 1992). In comparison, LGN projection neurons in burst mode generate tight clusters of spikes, referred to as “bursts”. Whether

or not LGN neurons produce tonic or burst spikes depends on the state of their voltage-gated, T-type Ca^{2+} channels (or T-channels). T-channels have two gates, an inactivation gate and an activation gate (Tsien et al., 1988; Crunelli et al., 2005). Once T-channels are de-inactivated following a sufficient period of hyperpolarization, an appropriate depolarizing stimulus can open the activation gate, thereby generating a depolarizing Ca^{2+} potential (or T-potential; McCormick and Huguenard, 1992 Huguenard and McCormick, 1992; Huguenard, 1996; Perez-Reyes, 2003). If the T-potential crosses the threshold to open voltage-gated Na^{+} channels, then a short train of high-frequency, Na^{+}-based action potentials, referred to as a burst, will result (Suzuki and Rogawski, 1989; McCormick and Huguenard, 1992; Huguenard and McCormick, 1992; Huguenard, 1996; Perez-Reyes, 2003). Notably, the magnitude of the T-potential and the number of spikes in a burst depend on (1) the ratio of T-channels in the de-inactivated vs. inactivated state, which depends, in turn, on the depth and duration of hyperpolarization in the cell, and (2) the subsequent rate of depolarizing voltage change ($\delta v/\delta t$) (Deschênes et al., 1984; Destexhe and Sejnowski, 2002; Hong et al., 2014). If the T-channels are primarily in the inactivated state or the depolarization is too slow, then tonic spiking occurs. Although visually evoked bursts are more common in anesthetized and drowsy animals than in alert animals, visually evoked bursts occur across brain states (Weyand et al., 2001; Bezdudnaya et al., 2006; Bereshpolova et al., 2011) and, when they occur, burst spikes are particularly effective in evoking cortical responses (Swadlow and Gusev, 2001; see also Usrey et al., 1998) and increase the timing precision and spatial focus of cortical responses (Borden et al., 2022).

Across mammals, the majority of LGN neurons have either On-center or Off-center receptive fields (Kuffler, 1953; Hubel and Wiesel, 1961), the former being (i) depolarized by light increments over the center of their receptive fields and (ii) hyperpolarized by light decrements over the same region, and the latter showing the reverse pattern. With these receptive-field properties in mind, a drifting grating stimulus should evoke alternating periods of depolarization and hyperpolarization in both types of cells, with the magnitude of hyperpolarization and depolarization and the rate of voltage change, being dictated by the contrast and phase of the time varying stimulus (Wang et al., 2007). Based on these properties and assumptions, we made single-unit recordings from LGN neurons in the anesthetized cat to test the hypothesis that bursts are affected by stimulus contrast, with burst activity being more frequent and temporally precise with higher contrast stimuli compared with lower contrast stimuli. We also performed simultaneous intraocular and LGN recordings to examine the spiking patterns of synaptically connected retinal ganglion cells and LGN neurons to compare the influence of contrast on the relationship between interspike interval and retinogeniculate communication and high-frequency responses in the LGN. Results show that bursts occur more frequently with higher contrast stimuli and more consistently with respect to the phase of the stimulus cycle when compared to tonic spikes. These results support the view that burst and tonic firing modes can differentially encode information about visual stimuli and the external world.

Materials and methods

Animal preparation.

Ten adult cats, both sexes, were used for this study. All experimental procedures were conducted with the consent of the Animal Care and Use Committee at the University of California, Davis and followed National Institutes of Health guidelines. The analyses performed on spikes trains for this study come from a combination of new unpublished data and data that contributed to previous, but unrelated, studies on the retinogeniculate pathway (Alitto et al., 2019b; Rathbun et al., 2010, 2016).

All surgical procedures were performed while animals were anesthetized. Surgical anesthesia was induced with ketamine (10 mg/kg, i.m.) and xylazine/dexmedetomidine (1mg/kg, i.m.) and maintained with either thiopental sodium (20 mg/kg, i.v., supplemented as needed) or propofol (4-6mg/kg/h, i.v., supplemented as needed) and sufentanil citrate (0.1-25ug/kg/h, i.v., supplemented as needed) along with isoflurane (0.5-1.5%) in a 2:1 mix of oxygen and nitrous oxide. Tracheotomies were performed, and animals were placed in a stereotaxic apparatus where they were mechanically ventilated and given atropine (0.04mg/kg, i.m.), dexamethasone (0.2mg/kg, i.m.), and baytril (5mg/kg, i.m.). Animals' vitals were monitored throughout the experiment, including the EEG, ECG, CO_2, and temperature. If physiological monitoring indicated a decreased level of anesthesia (increased heart rate, CO_2, and/or high-frequency activity in the EEG), additional thiopental sodium or propofol and sufentanil citrate was given, and the rate of continuous infusion was increased. For each animal, a scalp incision was made, and skin edges were infused with lidocaine (2%). A single craniotomy was made over the LGN, the dura was removed, and the

craniotomy was filled with agarose to protect the underlying brain. Eyes were fixed and adhered to metal posts, fitted with contact lenses, and focused on a tangent screen located 172 cm in front of the animal. Flurbiprofen sodium drops were administered (0.3%) to prevent miosis, atropine drops were administered (1%) for pupil dilation, and phenylephrine drops (2.5%) were administered to retract the nictitating membranes. Once all surgical procedures were complete, animals remained anesthetized with maintenance doses of anesthetic agents (either thiopental sodium, 2–3 mg/kg/h, i.v. or propofol, 4-6mg/kg/h, i.v., and sufentanil citrate, 0.1-25ug/kg/h, i.v., and isoflurane, 0.1-0.5% in a 2:1 mix of oxygen and nitrous oxide). Before administering paralytic, animals were monitored for one hour to ensure a stable plane of anesthesia. Once a steady plane of maintenance anesthesia was established, animals were paralyzed with vecuronium bromide (0.2 mg/kg/h, i.v.). At the end of data collection, animals were euthanized with Euthasol (100 mg/kg, i.v.).

Electrophysiological recording and visual stimuli.

Single-unit extracellular recordings were made from LGN cells in layers A and A1 using parylene-coated tungsten electrodes (AM systems, Sequim, WA). In a subset of experiments, a second electrode was inserted into the retina to provide simultaneous recordings from synaptically connected retinal ganglion cells and LGN neurons (procedures described in Alitto et al., 2019b; Rathbun et al., 2010, 2016). Neural responses were amplified, filtered, and recorded to a computer equipped with a Power 1401 data acquisition interface and Spike 2 software package (Cambridge Electronic Design, Cambridge, UK). Spike isolation was based upon waveform analysis and the presence of a refractory period, assessed from the autocorrelogram.

Visual stimuli were generated using a VSG2/5 visual stimulus generator (Cambridge Research Systems, Rochester, UK) and presented on a gamma-calibrated Sony monitor running at 140 Hz. Mean luminance of the monitor was 38 cd/m^2. The visual responses of individual LGN neurons were mapped and assessed using white-noise stimuli and drifting sine-wave gratings. White-noise stimuli consisted of a 16 by 16 grid of black and white squares. Each square was temporally modulated according to a 2^{15}-1 length m-sequence (Sutter, 1987; Reid and Shapley, 1992; Reid et al., 1997). Individual squares in the stimulus were updated with each monitor frame (~4 min for a complete sequence). Between 4 and 16 squares of the stimulus overlapped receptive field centers of each individual neuron. White-noise stimuli were used to quantify the spatiotemporal receptive field properties of each cell for purposes of cell classification (Usrey et al., 1999). We also determined each cell's preferred size and spatial frequency using drifting sine-wave gratings (4 Hz) centered over the cell's receptive field. Once the preferred location, size, and spatial frequency were determined, cells were presented with multiple repeats of a drifting grating stimulus that varied in contrast (2.5%, 5%, 10%, 20%, 40%, 60%, 80%, and 100%; random order). With each repeat of the stimulus, gratings were shown for 4 seconds and were interleaved with 4 seconds of mean gray.

Identification of LGN burst and tonic spikes.

We used two well-established criteria to identify bursts in the spike trains of LGN neurons, (Lu et al., 1992; Swadlow and Gusev, 2001; Weyand et al., 2001; Lesica and Stanley, 2004; Alitto et al., 2005, 2011; Denning and Reinagel, 2005; Bezdudnaya et al., 2006; Bereshpolova et al., 2011; Alitto et al., 2019b). These criteria were: (1) a

preceding interspike interval (ISI) of >100 ms, and (2) one or more subsequent spikes that followed with ISIs of <4 ms (Figure 1). Spikes that met these criteria were labeled burst spikes, and all other spikes were labeled tonic spikes. The first spike of a burst is referred to as the cardinal spike. Some of the analyses used the cardinal spike of each burst to represent a burst "event", whereas others used all spikes within a burst (described below). Throughout the paper, we use the terms long-ISI and high-frequency events to refer to the first and second criteria for a burst, respectively.

Tonic vs. burst analysis: firing rate.

Burst and tonic responses that occurred during low- and high-contrast stimulation were compared. The cutoff for low- and high-contrast stimuli was based each cell's contrast response function, where the low-contrast condition was any contrast value that elicited ≤ 30% of maximum firing rate and the high-contrast condition was any contrast value that elicited ≥ 75% of maximum firing rate of the cell. For the high- and low-contrast conditions, we calculated the firing rate of burst and tonic spikes as well as the average number of spikes within each burst event. To quantify the contrast-dependent changes in tonic and burst activity, we calculated a modulation index at each contrast level. The modulation index for each cell was calculated as follows:

$$modulation\ index(x) = \frac{firing\ rate(x) - firing\ rate_{spontaneous}}{firing\ rate(x) + firing\ rate_{spontaneous}}$$

Here, x = stimulus contrast. Tonic f1 was used for tonic firing rate, while bursts/cycle was used for the burst firing rate (i.e., bursts per cycle of the drifting grating). To compare the modulation indices across cells, we computed the effective contrast:

$$effective\ contrast\ (x) = \frac{firing\ rate(x)}{\max\ (firing\ rate)}$$

For example, if the cell's response was 20 spikes/s at 30% contrast, with a maximum firing rate of 40 spikes/s, then the effective contrast was 0.5.

***Tonic vs. burst analysis: pairwise phase consistency*.**

To assess response timing across the stimulus cycle, we calculated Pairwise Phase Consistency (PPC) for tonic and burst spikes across different contrast conditions (Vinck et al., 2010). The phase for each spike (burst or tonic, spike time relative to stimulus onset) at the drift rate of the visual stimulus (4 Hz) was calculated as:

$$\Phi_i = 2\pi * \frac{modulus(spike\ time_i, cycle\ duration)}{cycle\ duration}$$

PPC was then calculated for each spiking category (burst vs tonic) and each stimulus condition (low vs high contrast):

$$ppc = \sum_i \sum_{j<i} \frac{\cos \Phi_i * \cos \Phi_j + \sin \Phi_i * \sin \Phi_j}{.5n(n-1)}$$

Here, n is the number of spikes in each category/condition. Low PPC values near zero indicate no consistent relationship between the spike timing and phase of the visual stimulus, whereas PPC values near 1.0 indicate that the spikes always occur at the same phase of the visual stimulus.

Retinal spike efficacy.

To quantify the influence of contrast-dependent bursting on retinogeniculate communication, we measured the retinal efficacy (percentage of retinal spikes that evoked a postsynaptic spike or burst event) for a subpopulation of the LGN cells (n=14) in which simultaneous recordings were made from one of their retinal inputs (via intraocular recordings) as a function of ongoing LGN ISI during high- and low-contrast

conditions. Synaptic connectivity was assessed using cross-correlation analysis, as described in Fisher et al. (2017). Changes in retinal spike efficacy were assessed as a function of ongoing LGN ISI, which is defined as the time since the previous LGN spike at the time of a given retinal spike. For example, if a retinal spike occurred at 3.753 s and the last LGN spike occurred at 3.750s, then the retinal spike is said to occur during a 0.003 ongoing LGN ISI. We have previously shown that ongoing LGN ISI can be used as a reliable proxy for burst probability (Alitto et al, 2019b). In particular, (1) the probability of a high-frequency LGN event increases as the LGN ISI increases beyond 50 ms, in a manner that cannot be explained by passive mechanisms, indicating the likely involvement of T-Type Ca^{2+} channels, and (2) coincident with the increase of high-frequency probability at long LGN ISIs, there is an increase in retinal spike efficacy that is also difficult to explain by passive mechanisms. To quantify the relationship between contrast-dependent changes in retinal spike efficacy and contrast-dependent changes in LGN burst rate at long LGN ISIs, we modeled changes in retinal spike efficacy using generalized linear mixed-effects model (fitglme, Matlab version R2021a, MathWorks) with predictors of tonic f1, burst rate, and stimulus contrast. Cell identity was used as a random variable.

Poisson expectation of thalamic burst rate.

To address the possibility that changes in contrast-dependent burst rates were simply a statistical consequence of overall changes in firing rate, we estimated the frequency of burst events from a nonhomogeneous Poisson spiking model. Spike times were simulated based on a time-varying sinusoidal function where firing rates were set by the cell's f1 and f0:

*mean spike count (t) = f1*sin(2*pi*t*f) + f0.*

Here, t = time, f = the drift frequency of the visual stimulus, f1 = response at the frequency of the visual stimulus, and f0 = mean response. The sinusoidal model was then rectified such that negative spike counts were set to zero. For each LGN neuron, 100 trials were simulated: 4s stimulus on, 4s stimulus off, to match how the experimental data were collected. Simulated spike trains were analyzed similar to the experimental data to quantify the amount of burst activity that would be predicted to occur simply as a result of the cell's firing rate. For each neuron, the mean and standard deviation of the simulated data were estimated through bootstrap to determine if the neuron's experimental burst rate was significantly greater than that found in the simulated data.

Statistical testing

All analyses were done in Matlab version 2021a. For significance testing, t-tests were used for normally distributed variables (verified with a Kolmogorov–Smirnov test); sign tests were used for non-normally distributed variables (e.g., bounded indices).

Results

We recorded a total of 511,002 spikes (including 39,107 burst events comprised of 90,068 burst spikes) from 21 LGN neurons (11 on-center cells, 10 off-center cells; 6 X cells, 15 Y cells) in the anesthetized cat during visual stimulation with drifting sinusoidal gratings that varied in luminance contrast to determine the relationship between stimulus contrast and burst versus tonic spiking. For the analyses described below, there were not any statistically significant differences between subtypes of LGN cells (on vs. off, X vs. Y). For a subset of the LGN cells (n=14; 373,325 spikes, total) we also simultaneously recorded the spiking activity of one of their retinal ganglion cell inputs (999,044 retinal spikes, total) via a second electrode inserted into the eye. We were particularly interested in determining whether high-contrast stimuli, with presumably greater null phase hyperpolarization for priming T-type Ca^{2+} channels and a greater rate of depolarization ($\delta v/\delta t$) during the transition from the null phase to the preferred phase, evoked more geniculate bursts than low-contrast stimuli. Recordings were divided into low- and high-contrast trials based on each cell's contrast response function (see Materials and Methods). Geniculate spikes were classified as burst or tonic using previously established criteria (Lu et al., 1992), whereby a burst has a sequence of two or more spikes, with the initial spike having a preceding interspike interval (ISI) >100 ms and subsequent spikes having ISIs < 4ms (Figure 1). All non-burst spikes were classified as tonic spikes.

Thalamic bursting is modulated by stimulus contrast.

On average, bursting events were more common (>2x more frequent) with high-contrast stimuli than they were with low-contrast stimuli. This contrast-dependent

increase in LGN bursting was clearly observed in single-cell raster plots (Figure 2A-B), PSTHs (Figure 2C-D), and cycle histograms (Figure 2E-F) and was robust across our sample of LGN neurons (Figure 3A; mean burst events per cycle: high contrast = 0.27 ±0.01, low contrast = 0.12 ±0.01, $p<10^{-3}$, t-test). There was also a small, but significant, increase in the number of spikes within a burst with high-contrast stimuli compared to low-contrast stimuli (Figure 3B; mean spikes/burst: high contrast = 2.25 ±0.03, low contrast = 2.15 ±0.03; p = 0.03, t-test). Across cells, the contrast response function for burst spikes was similar in shape to the contrast response function for tonic spikes (Figure 3C); however, the influence of contrast on bursting activity was weaker than the influence of contrast on tonic spikes, particularly at high contrasts where tonic spikes have a higher ceiling (limited by the action potential refractory periods) than burst spikes (limited by the 100 ms ISI lockout period). This can be seen by plotting the contrast modulation index as a function of effective contrast (see Materials and Methods) for both tonic and burst spikes across the sample of LGN neurons (Figure 3C). Comparing the modulation index for burst spikes and tonic spikes, the modulation index covaries for both burst and tonic firing, and it is higher for tonic spikes compared to bursts. This reflects the upper bound on the two categories of spikes; bursts can only happen once per cycle (due to the 100ms lockout), whereas tonic spikes can occur more than once. Overall, there was a tight correlation between the modulation of tonic spiking and burst spiking across all contrasts (Figure 3D, $r = 0.7$, $p < 10^{-4}$).

Having found a positive relationship between stimulus contrast and burst probability, we next asked whether stimulus contrast affected the consistency of burst activity within the temporal domain. To address this question, we performed a Pairwise

Phase Consistency (PPC) analysis to quantify the consistency of the stimulus phase when bursts occurred (see Materials and Methods). With this analysis, higher PPC values indicate greater consistency of responses with respect to stimulus phase and lower values indicate less consistency. On average, PPC values for burst activity were significantly greater for high-contrast stimuli than for low-contrast stimuli (Figure 4A; high-contrast mean PPC = 0.67 ±0.06, low-contrast mean PPC = 0.44 ±0.06; $p = 7.29 \times 10^{-4}$, sign test. A similar relationship was also found for tonic spikes (Figure 4B; high contrast mean PPC = 0.47 ±0.05, low contrast mean PPC = 0.35 ±0.05; p = 0.002, sign test); however, across cells and contrast values, PPC values were typically greater for bursts than for tonic spikes (Figure 4C and D; low-contrast: burst PPC vs. tonic PPC, p = 0.019, sign test; high contrast: burst PPC vs. tonic PPC, p = 0.007, sign test). Thus, high-contrast stimuli are more likely to evoke bursts than low-contrast stimuli, and bursts under high-contrast conditions have greater phase consistency. Both features are consistent with the notion that bursts can carry contrast information to the cortex.

Changes in retinal spike efficacy can be partially explained by contrast-dependent changes in bursting.

Previous work has shown that the ability of retinal spikes to drive spiking in the LGN (retinal spike efficacy) is modulated by bursting in the LGN (Alitto et al, 2019b). Although this work did not directly measure LGN Ca^{2+} potentials, the relative arrival of retinal spikes to the time since a previous LGN spike (ongoing LGN ISI, $ISI_{ongoing}$; see Materials and Methods) influenced several aspects of visual processing in the LGN, including retinal spike efficacy, in a manner consistent with the biophysics of T-type Ca^{2+}

channels. In this way, $ISI_{ongoing}$ can be used to infer the relative probability of thalamic burst mode in a manner that is complementary to the traditional criteria.

To examine the relationship between retinal spike efficacy and burst probability under low- and high-contrast conditions, we analyzed the spike trains of synaptically connected retinal ganglion cells and LGN neurons (see Materials and Methods). Figures 5A1, 5B1, and 5C1 show the relationship between ongoing ISI and retinal efficacy for 3 representative pairs of synaptically connected neurons. Also depicted in these figures (gray shading) are 3 ranges of ongoing ISI that were used to compare the probability of retinal evoked geniculate spikes under low- and high-contrast conditions (Figure 5A2-A4, B2-B4, C2-C4). Results from these 3 examples and the entire sample of simultaneously recorded neurons (Figure 5D1) show that the relationship between retinal spike efficacy and burst probability, as assessed by $ISI_{ongoing}$, is highly nonlinear. Specifically, when the $ISI_{ongoing}$ is short (< 30ms; indicated with black arrow in A1-D1) and Ca^{2+} potentials are unlikely to occur, there is a negative relationship between retinal efficacy and $ISI_{ongoing}$. Interestingly, in this region of the ISI-efficacy curve, low-contrast spikes are more effective than high-contrast spikes in driving LGN activity, particularly at the shortest $ISI_{ongoing}$ (< 30ms, zone 2 in panels A1, B1, and C1). This finding is consistent with LGN contrast gain control mechanisms, similar to what has been previously reported (Alitto et al, 2019a).

More importantly for the current study, our results reveal a contrast-dependent increase in retinal spike efficacy as the $ISI_{ongoing}$ increases beyond 50ms and the probability of burst mode increases. To quantify this contrast-dependent effect, we compared retinal spike efficacy found during mid-duration $ISI_{ongoing}$ (30-60ms, zone 3 in

panels A1, B1, and C1) to long-duration $ISI_{ongoing}$ (>100ms, zone 4 in panels A1, B1, and C1) (Figure 5D2). These specific ranges were selected to exclude the short-duration $ISI_{ongoing}$ range where temporal summation dominates ISI-efficacy curves. Results show a significant increase in retinal spike efficacy during long-duration $ISI_{ongoing}$ relative to mid-duration $ISI_{ongoing}$ with both high- and low-contrast stimuli (high-contrast stimuli: retinal efficacy with mid-duration $ISI_{ongoing}$ = 0.053 +/- 0.012 SE, with long-duration $ISI_{ongoing}$ = 0.161 +/- 0.024 SE, $p = 9.76x10^{-4}$; low-contrast stimuli: retinal efficacy with mid-duration $ISI_{ongoing}$ = 0.053 +/- 0.015 SE, with long-duration $ISI_{ongoing}$ = 0.092 +/- 0.023 SE, p = 0.007, sign test); however, the effect was significantly greater with high-contrast stimuli (p = 0.007, sign test), and may include a component involving convergent input from other, non-recorded, retinal ganglion cells.

To establish a more direct link between contrast-dependent changes in ISI-efficacy curves and burst rate, we next created a generalized linear mixed-effects model of the change in spike efficacy (Δ_{eff}) using contrast, burst rate, and the fundamental frequency (f1) of the spiking response. This simple linear model did a good job at predicting Δ_{eff} observed between mid-duration and long-duration $ISI_{ongoing}$ (Figure 5D3, explained variance = 0.4). Both burst rate and f1 were significantly positive predictors of Δ_{eff} ($ß_{burst}$= 0.024, tstat = 2.24, p = 0.01; $ß_{f1}$ = 0.026, tstat = 2.59, p = 0.02), while contrast was not predictive of Δ_{eff} ($ß_{con}$ = -0.007, tstat = 0.24, p = 0.81). This indicates an indirect relationship between contrast and Δ_{eff}. One parsimonious explanation of these results is that changing contrast drives changes in burst rate, which is a reliable proxy for an underlying neural mechanism, (e.g., state of the T-Type Ca^{2+} channels), that then drives the Δ_{eff}. Mathematically, this indirect relationship between stimulus contrast and

Δeff is supported by the finding that contrast is a significant predictor when it is the only variable in the model ($ß_{con}$ = 0.048, tstat = 3.43, p = 0.01).

Measures of contrast-dependent changes in LGN burst rate are not a trivial consequence of changes in firing rate.

While the increase in burst rate with stimulus contrast is consistent with the biophysical properties of T-type Ca^{2+} channels, it is also possible that the increase in burst rate is not related to the involvement of T-type Ca^{2+} channels, but rather is a trivial consequence of the contrast-dependent changes in firing rate. As described above, when the contrast of a drifting grating is increased, there is increased excitation during the neuron's preferred phase and increased inhibition during the neuron's null phase. Consequently, there is an increase in the absolute number of high-frequency spikes (ISI < 0.004s, Figure 6A and C) and the number of long-ISI spikes (ISI > 0.1s, Figure 6B and C), as well as the probability of high-frequency spikes (Figure 6D and 6F) and the probability of long ISI spikes (Figure 6E and 6F). This raises the possibility that the increase in burst rate is a trivial consequence of the increased number of high-frequency spikes and long-ISI spikes. This explanation for the contrast-dependent increase in burst frequency assumes a Poisson distribution of LGN spike times; consequently, it can be accepted or ruled out by an analysis of the interdependence of high-frequency events and long-ISI spikes.

Under Poisson expectations, the probability of a high-frequency event, the second component of a burst, does not depend on the preceding ISI. However, consistent with the involvement of T-type Ca^{2+} channels, results show that the probability of a high-frequency spike is highly modulated by the preceding ISI for both

low-contrast and high-contrast conditions (Figure 7A-D). As predicted by the time/voltage relationship for de-inactivating T-Type Ca^{2+} channels (i.e., the greater the hyperpolarization, the less time required) the modulation of high-frequency probability was steeper and evident at shorter preceding ISIs with high-contrast stimuli compared with low-contrast stimuli. Importantly, this relationship was absent in the spike trains of retinal ganglion cells, which also experience increased preferred phase excitation and null-phase suppression, but do not exhibit bursting activity (Figure 7E).

The modulation of high-frequency event probability by the preceding ISI clearly violates the assumption of Poisson distributions. However, it is possible that these non-Poisson spike interactions, including contrast-dependent increases in thalamic burst rate, can be accounted for by a time-varying Poisson spiking model that accounts for the sinusoidal nature of LGN firing rates in response to drifting sine-wave gratings. To examine this possibility, we simulated LGN spike rates using a time-varying Poisson model where the spike rates were set by a sinusoidal function and the neurons' firing rates (see Materials and Methods). In this way we quantified how the experimentally measured burst rates compared to burst rates seen in the simulated spike trains. If the contrast-dependent burst rate could be explained simply by the increase in firing rate, then we should observe similar burst rates in the experimental and simulated data.

Consistent with the involvement of T-type Ca^{2+} channels, the observed burst rate far exceeded the Poisson expectation during both low-contrast (Figure 8A, experimental = 0.125 +/- 0.025 SE, simulated = 0.009 +/- 0.0013 SE, $p < 0.0015$, t-test) and high-contrast (Figure 8B, experimental = 0.273 +/- 0.048 SE, simulated = 0.0412 +/- 0.004 SE, $p < 0.0015$, t-test) stimulation, indicating the involvement of nonlinear processes

such as the voltage dependence of T-Type Ca^{2+} channels. Lastly, after removing the small, but present, “statistical” bursts (i.e., those occurring with Poisson expectation) from the observed measure of bursts, there remained a robust contrast-dependent increase in burst rate (Figure 8C, low-contrast adjusted burst rate = 0.116+/- 0.025 SE, high-contrast adjusted burst rate = 0.232+/- 0.048 SE, p = 0.009, t-test).

Discussion

The goal of this study was to test the hypothesis that luminance contrast can influence the response mode (burst vs. tonic spiking) of LGN neurons. To explore the relationship between stimulus contrast and response mode, we recorded the activity of LGN neurons in the anesthetized cat during visual stimulation with low-contrast and high-contrast drifting sine-wave gratings. Fundamental to the reasoning behind these experiments was knowledge about the biophysical properties of the T-type Ca^{2+} channels that underlie bursts, assumptions about the membrane potential dynamics of LGN cells during stimulation with high- and low-contrast stimuli, and past work demonstrating bursts are unique events in the LGN and largely absent in the retina (Weyand, 2007; Alitto et al., 2019b; but see Sincich et al., 2007).

T-type channels have two gates, an inactivation gate and an activation gate (Tsien et al., 1988; Crunelli et al., 2005). For calcium entry to occur, the inactivation gate must be in the de-inactivated state, a state that requires a sufficient period and depth of hyperpolarization (generally > 100 ms and below a cell’s typical resting potential), and the activation gate must be opened, a process that requires depolarization with voltage/time ($\delta v/\delta t$) constraints (Jahnsen and Llinás, 1984; Suzuki and Rogawski, 1989). Drifting gratings, with greater luminance modulation (higher contrast) and

presumably greater membrane potential dynamics, would therefore seem better suited for opening T-type channels compared with gratings with less luminance modulation (lower contrast).

With opening of the T-type channels, Ca^{2+} influx evokes a T-potential that brings the membrane potential of a cell toward the threshold for activating voltage-gated Na^{+} channels (Jahnsen and Llinás, 1984; Suzuki and Rogawski, 1989). Because T-potentials last longer than the duration of an individual Na^{+} spike, a burst of Na^{+} spikes can ride on the T-potential (Wang et al., 1991; McCormick and Huguenard, 1992 Huguenard and McCormick, 1992; Huguenard, 1996; Perez-Reyes, 2003). However, if the T-type channels are inactivated and/or the $\delta v/\delta t$ of depolarization is insufficient to open their activation gate, then depolarizing inputs to a cell will evoke tonic spikes without bursts, generally in proportion to the strength of their excitatory inputs. Consistent with these assumptions and predictions, we found the burst frequency, the number of spikes in a burst, and the timing precision of bursts were all significantly greater with higher contrast stimuli compared with lower contrast stimuli.

Stimulus contrast affects the interspike interval (ISI) dynamics of bursts.

Based on results from intracellular recordings from which sub-threshold T-potentials and suprathreshold bursts could be more clearly ascertained, two criteria were established for identifying burst events in extracellular recordings: (1) a preceding interspike interval (ISI) of >100 ms and (2) subsequent ISIs <4 ms (Figure 1; Lu et al., 1992). The first criterion is believed to reflect the de-inactivation requirements of T-type Ca^{2+} channels; however, it is also known that the time/voltage relationship for de-inactivation is dynamic, with less time required for greater hyperpolarization and more time required

for less hyperpolarization (McCormick and Huguenard, 1992; Huguenard and McCormick, 1992; Huguenard, 1996; Perez-Reyes, 2003). Consistent with this understanding, we found that high-frequency responses (ISIs < 4ms; the second criterion for a burst) were associated with shorter preceding ISIs (the first criterion for a burst) with higher contrast stimuli compared with lower contrast stimuli. This indicates that at higher contrast values (and presumably greater depth of hyperpolarization), the period of hyperpolarization (or ISI interval) needed to elicit a high-frequency burst is shortened from the generally accepted value of 100 ms. With lower contrast stimuli and in the absence of visual stimulation (i.e., spontaneous activity), the 100 ms criterion that is typically applied for identifying bursts was evident and seemed appropriate (Lu et al., 1992). These findings suggest that greater hyperpolarization not only increases the likelihood of a burst, but also shortens the time required to elicit a burst event.

Contrast levels modulate the reliability of bursts.

An analysis of the timing of bursts with respect to the phase of the drifting grating revealed bursts occur more reliably and temporally precise with higher contrast stimuli compared with lower contrast stimuli. Moreover, at each contrast level (high or low) the timing of burst spikes was more consistent compared with the timing of tonic spikes. These findings likely also reflect the time-voltage relationship of T-type Ca^{2+}channels, with higher contrast stimuli having a greater $\delta v/\delta t$ that results in a more reliable crossing of the T-channel threshold in a noisy background. Consistent with this view, results from a study using white-noise stimuli reported the suppressive phase of the spike-triggered average was significantly greater in magnitude and duration for burst spikes compared with tonic spikes (Alitto et al., 2005; see also Reinagel et al., 1999; Kepecs et al., 2002;

Lesica and Stanley, 2004; Lesica et al., 2006; Zeldenrust et al., 2018, Mease et al., 2017). Similarly, previous work examining the temporal-frequency tuning properties of LGN neurons as a function of burstiness, reports LGN neurons shifting from low-pass to band-pass filtering with increased burstiness.

Indirect inference of T-Type Ca^{2+} potentials

Unlike studies using intracellular or whole-cell recording methods where the involvement of T-type Ca^{2+} channels in thalamic bursts can be directly assessed, studies using extracellular recording methods have relied on the criteria (preceding ISI >100 ms, subsequent ISIs < 4 ms) established by Lu et al. (1992) to distinguish bursts. While these criteria have been shown to do an extremely good job at identifying bursts that rely on T-type Ca^{2+} channels, it must be acknowledged that misclassification can occur and that a single set of criteria may not apply equally well to different stimulus conditions and/or behavioral states. For instance, because the time required to de-inactivate (prime) T-type Ca^{2+} channels decreases as cells are more deeply hyperpolarized, it is likely that some thalamic bursts under these conditions with preceding ISIs <100 ms will be incorrectly excluded. Consistent with this view, there was an increase in high-frequency probability with high-contrast stimuli (and presumably greater null-phase hyperpolarization) with preceding ISIs <100 ms that was not seen with low-contrast stimuli (and presumably less null-phase hyperpolarization) (Figure 7, panel D2; see also Alitto et al., 2019b).

Perhaps a larger concern is the occurrence of “statistical bursts”, events identified as bursts that are simply the result of the temporal coincidence of a long preceding ISI followed by high-frequency spikes, without the involvement of T-type Ca^{2+}

channels. This was a particular concern for the current study, as the possibility that the contrast-dependent increase in thalamic bursts might be a trivial consequence of the increase in firing rate (i.e., more statistical bursts at higher contrast). To address the possibility, we modeled LGN spiking using Poisson spiking statistics. A defining feature of Poisson processes is that each event occurs independent of every other event. Neuronal refractory periods, both absolute and relative, are a clear violation of Poisson assumptions; however, for the sake of simplicity, this biological inaccuracy was tolerated. A second violation of Poisson spiking relevant to this study is the phase-dependent, sinusoidal nature of LGN responses to drifting sine-wave gratings. This violation could not be ignored as it clearly affects the distribution of both long ISIs and high-frequency events. We therefore model LGN spiking as a sine function, with a firing rate set by the observed mean and f1, as the best approximation of LGN spiking that did not explicitly contain the non-Poisson characteristics associated with the biophysical properties of T-type Ca^{2+} channels. For most cells in this study (15/21), but not for cells with very low burst rates, results from this modeling effort indicate contrast-dependent bursting cannot be explained by the statistics of having higher firing rates. This finding, along with the small increase in the simulated burst rate under high-contrast conditions, emphasizes the importance of quantifying the possibility of statistical bursts in data collected in different conditions.

Bursts and thalamocortical processing.

Our results show that LGN bursts can be driven by specific patterns of visual stimulation and that stimulus contrast affects burst frequency and timing. Similar findings have been reported for higher order thalamic neurons in the mouse whisker system (Mease et al

2017), emphasizing the generality and importance of thalamic bursts across sensory systems. Moreover, all thalamic nuclei receive corticothalamic feedback from pyramidal neurons in layer 6 (reviewed in Usrey and Sherman, 2019). As this source of input can influence the membrane of thalamic neurons via monosynaptic excitation and disynaptic inhibition, layer 6 neurons have the opportunity to shift thalamic neurons between burst and tonic activity modes (Hirai et al., 2018; Mease et al., 2014). Provided there exists a cortical readout for bursts, bursts appear well suited for conveying contrast information to the cortex. Like other feedforward synapses, it is generally believed that thalamocortical synapses experience synaptic depression (Stratford et al., 1996; Gil et al., 1999; Chung et al., 2002). If so, then the long ISI that precedes a burst should reduce the amount of depression and thereby increase thalamocortical burst efficacy. In addition, the rapid train of spikes within a burst should evoke postsynaptic temporal summation (see Usrey et al., 2000; Usrey 2002) and thereby lead to a similar increase in burst efficacy. Although direct measures of burst effectiveness in driving responses in visual cortex have yet to be performed, related studies have been performed in the somatosensory pathway of rabbits and mice where burst spikes are more effective than tonic spikes in driving cortical responses (Swadlow and Gusev, 2001) and increase the timing precision and spatial focus of cortical responses (Borden et al, 2022), respectively. If LGN bursts are similarly more effective at driving cortical responses, then visually evoked bursts would seem to have the properties needed to represent a distinct mode for processing and conveying visual information to the cortex.

Figures

Graphical Abstract

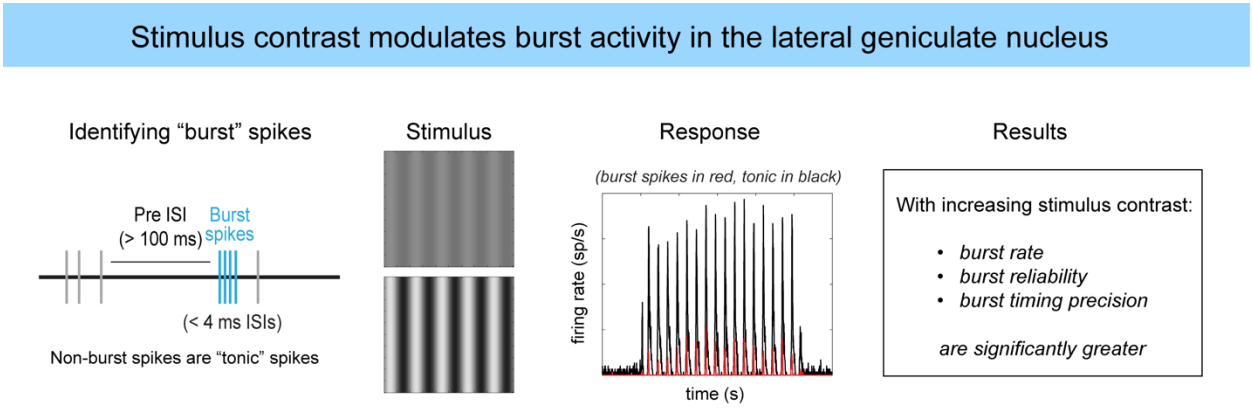

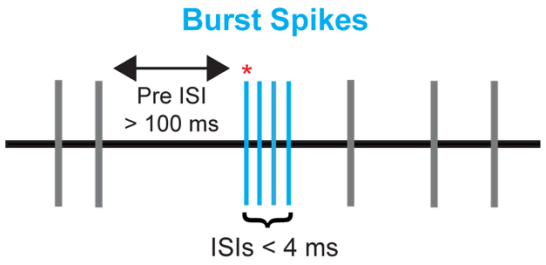

Figure 1. Identification of burst spikes using criteria established by Lu et al. (1992). In this diagram, time is moving left to right and the vertical lines indicate spikes. Bursts are defined as (i) a cardinal spike (indicated with red *) that follows an ISI >100 ms, and (ii) subsequent spikes that occur with ISIs <4 ms. In this example, the burst spikes are shown in blue and the tonic spikes are shown in gray.

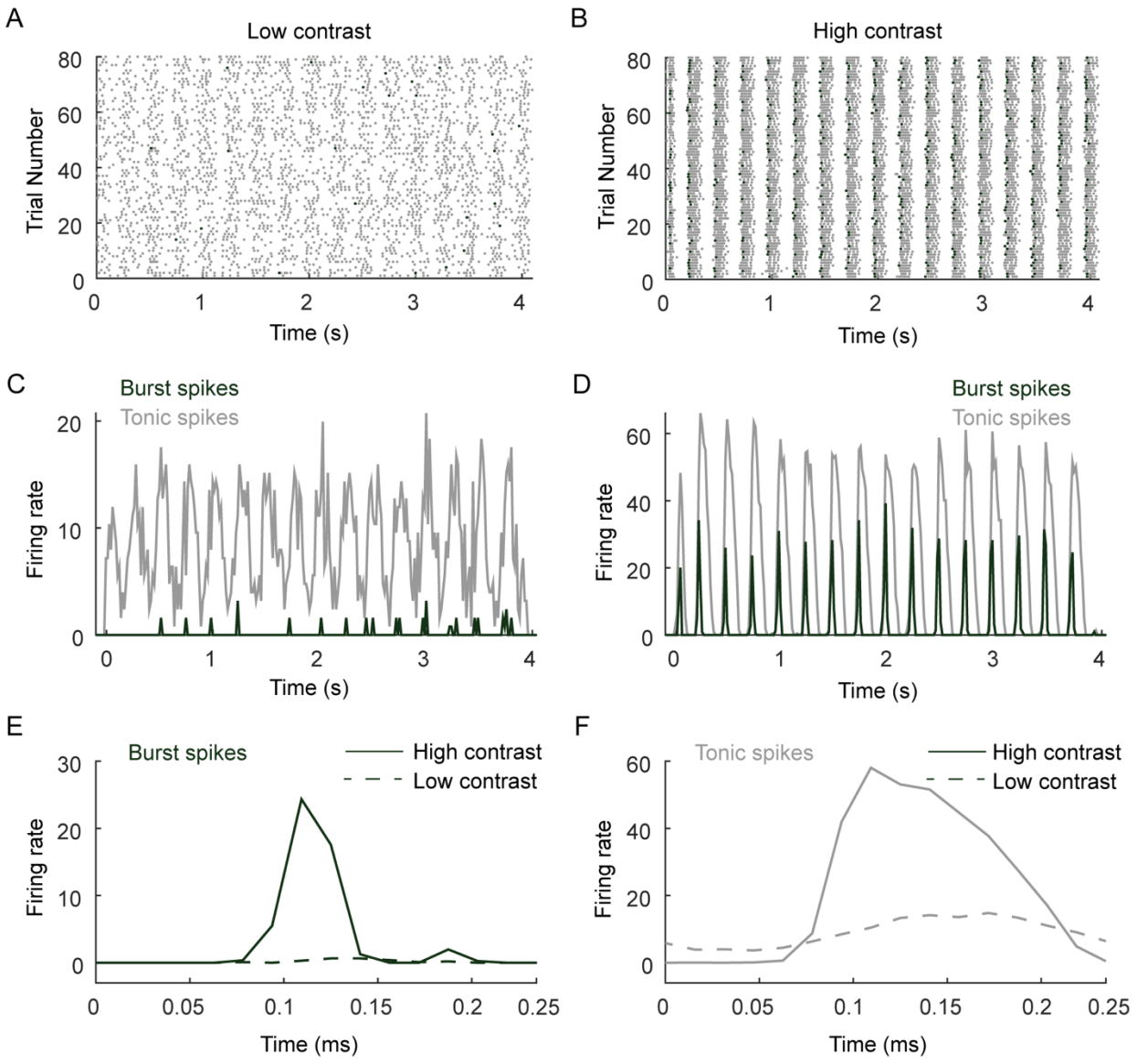

Figure 2. Burst and tonic responses from a representative LGN neuron during high- and low-contrast visual stimulation. **A** and **B**. Raster plots showing the neuron's spiking activity across 80 4-second trials of a 4 Hz drifting sinusoidal grating stimulus at low contrast (**A**) and high contrast (**B**; see Materials and Methods). Burst spikes indicated in dark green; tonic spikes indicated in shades of gray. Note: at the time scale shown, the multiple spikes that occur during a single burst appear as a single marker. **C** and **D**. PSTHs showing the firing rate of burst spikes (dark green) and tonic spikes (shades of

gray) during stimulation with (**C**) low-contrast drifting gratings and (**D**) high-contrast drifting gratings. **E** and **F**. Cycle histograms showing the relative timing and duration of burst spikes (**E**) and tonic spikes (**F**) with low-contrast drifting gratings (dashed lines) and high-contrast drifting gratings (solid lines).

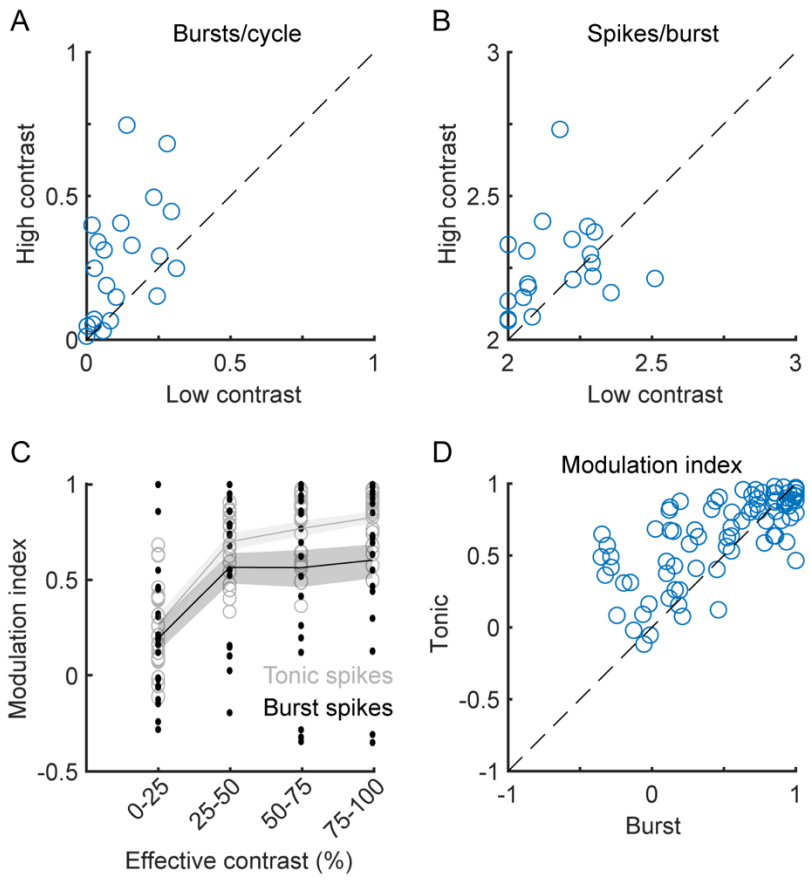

Figure 3. Burst activity during high- and low-contrast visual stimulation. **A.** Scatter plot showing the average burst rate (burst events per cycle of the drifting grating stimulus) for 21 LGN neurons stimulated with high- and low-contrast gratings. Burst rate is significantly greater for high-contrast stimuli compared to low-contrast stimuli ($p<10^{-3}$, t-test). **B.** Scatterplot showing the average number of spikes per burst for 21 neurons stimulated with high- and low-contrast gratings. There was a small, but significant, increase in the number of spikes per burst with high-contrast stimuli compared to low-contrast stimuli ($p=0.03$, t-test). **C.** Modulation index as a function of effective contrast (see Materials and Methods). At each effective contrast level, gray circles represent the modulation index of tonic spikes for each neuron examined at that contrast, and black dots represent the modulation index of burst spikes for each neuron examined at that

contrast (tonic spikes (gray circles and gray line): mean +/- SE = 0.27 +/-0.05, 0.70 +/-0.04, 0.77 +/-0.04, 0.82 +/-0.03 for 25%, 50%, 75%, and 100% contrast, respectively; burst spikes (black dot and black line): mean +/- SE = 0.19 +/-0.08, 0.56 +/-0.08, 0.56 +/- 0.10, 0.60 +/- 0.09 for 25%, 50%, 75%, and 100% contrast, respectively). **D.** Scatterplot showing the burst modulation index versus the tonic modulation index. The modulation index was significantly greater for tonic spikes than for burst spikes (tonic: mean 0.638 +/-0.032 SE; burst: mean 0,483 +/-0.047 SE, p = 0.0198 sign test).

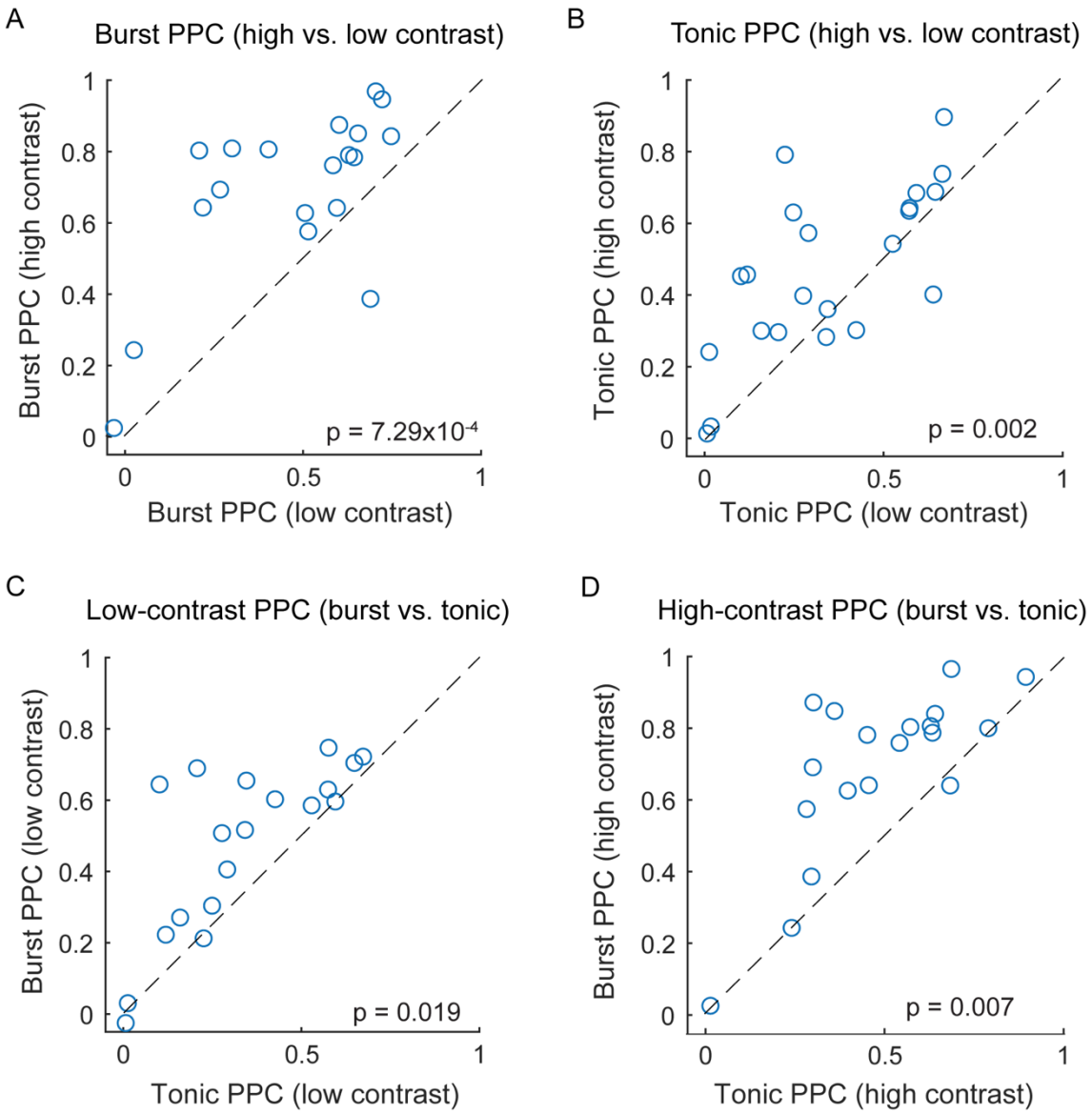

Figure 4. Scatterplots showing pairwise phase consistency (PPC) values for burst and tonic spikes when stimulated with low- and high-contrast gratings. **A** and **B**. Comparison of PPC values from recordings with high-contrast and low-contrast stimulation for burst spikes (**A**) and tonic spikes (**B**). PPC values for burst spikes and tonic spikes were significantly greater, on average, when cells were stimulated with high-contrast stimuli compared with low-contrast stimuli ($p = 7.29 \times 10^{-4}$ and $p = 0.002$, respectively; sign test). **C** and **D**. On average, PPC values were greater for burst spikes than for tonic spikes

when cells were excited with low-contrast stimuli (**C**, p = 0.019, sign test) and when excited with high-contrast stimuli (**D**; p = 0.007, sign test).

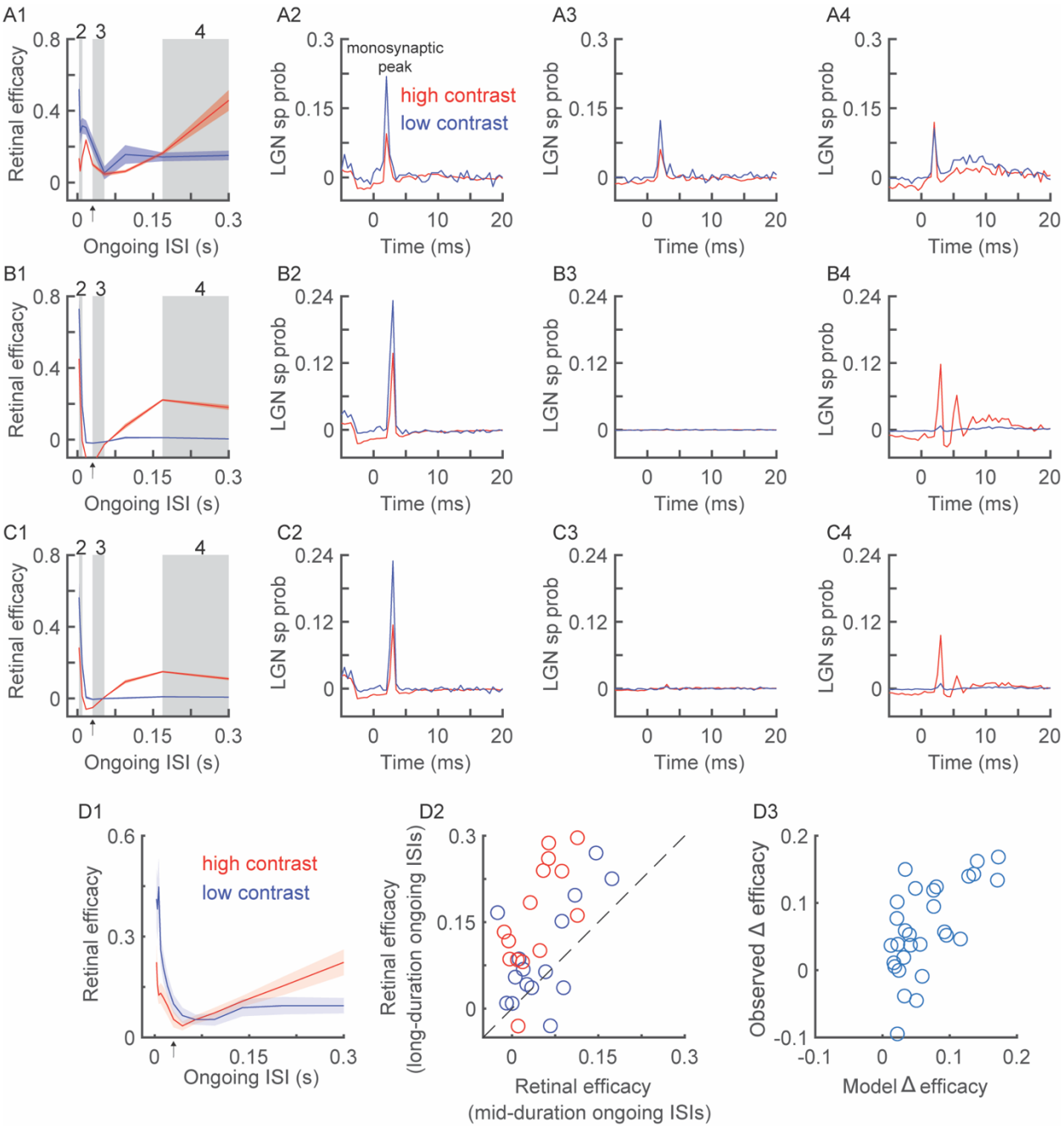

Figure 5. The relationship between contrast-dependent retinal spike efficacy and contrast-dependent burst rate. **A1.** Example ongoing ISI-efficacy curves for low-contrast (blue) and high-contrast (red) trials. The three gray boxes indicate three regions of interest: (2) short-ongoing LGN ISIs (<30ms) where retinal spike efficacy is dominated by temporal summation, (3) mid-duration ongoing LGN ISIs (30-60ms) where retinal

spike efficacy is at a minimum, and (4) long-duration ongoing LGN ISIs (>100ms) where the inferred activation of T-Type Ca^{2+} channels enhances retinal spike efficacy. The data are binned logarithmically. Arrow indicates where the ongoing ISI is 30ms. **A2.** LGN spike probability as a function of time since a retinal spike for short-ongoing ISIs, as defined above. The peak near 3.0 ms indicates a monosynaptic connection between the RGC-LGN pair. The area under the curve is used to calculate spike efficacy. **A3.** Similar to A1, but for mid-duration ongoing LGN ISIs. **A4.** Similar to A1, but for long-ongoing LGN ISIs. **B-C.** Similar to A for two additional example RGC-LGN pairs. **D1.** Similar to A1, but for the entire sample of RGC-LGN pairs. **D2.** Scatter plot of retinal efficacy during mid-duration ongoing LGN ISIs vs. retinal efficacy during long-duration ongoing LGN ISIs (low contrast: $p = 9.76x10^{-4}$; high contrast: $p = 0.007$, sign test). **D3.** A scatter plot of observed change in retinal spike efficacy plotted as a function of the output of a generalized linear model with significant predictors of burst rate and spike f1 ($ß_{burst}$= 0.024, tstat = 2.24, $p = 0.01$; $ß_{f1} = 0.026$, tstat = 2.59, $p = 0.02$).

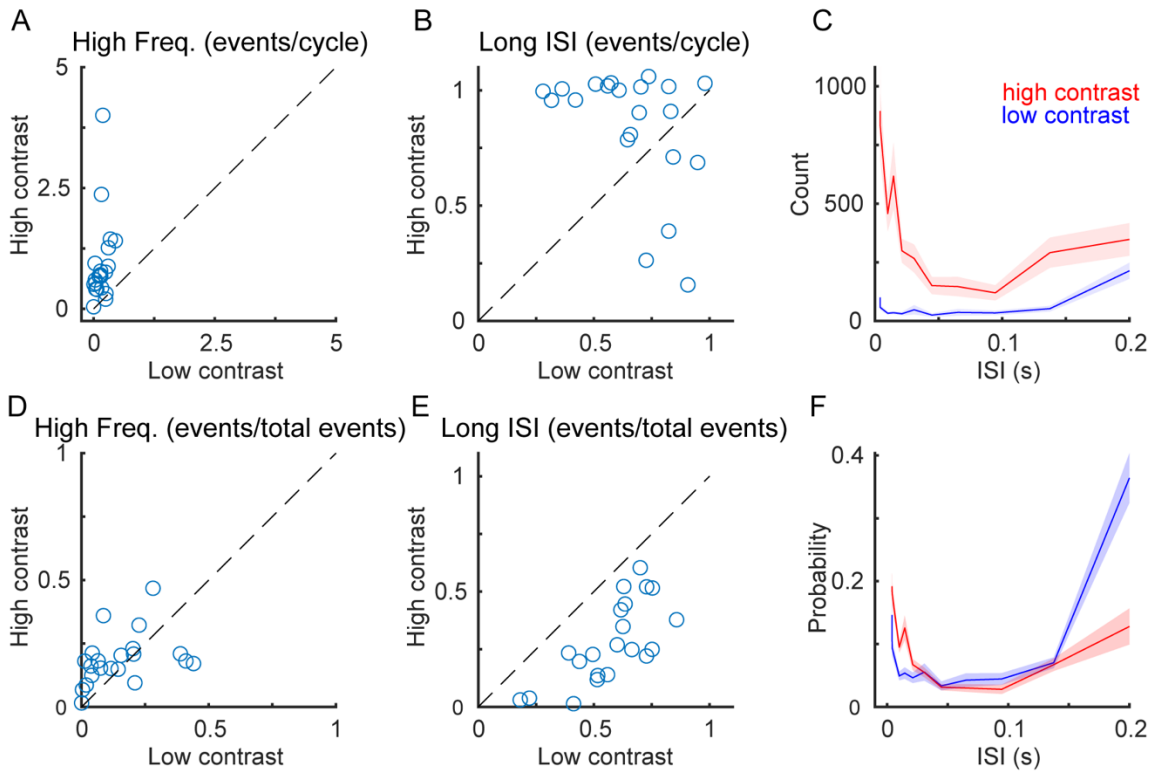

Figure 6. Increasing stimulus contrast results in an increase in the total number of long-ISIs and high-frequency events. **A.** The number of high-frequency LGN events (ISI < 4 ms, includes bursts) during low-contrast trials versus the number of high-frequency LGN events during high-contrast trials. **B.** The number of long-ISI LGN spikes (ISI > 100 ms, includes bursts) during low-contrast trials versus the number of long-ISI LGN spikes during high-contrast trials **C.** Average distribution of LGN ISIs across the entire sample. **D-F.** Similar to A-C, but count has been converted to probability.

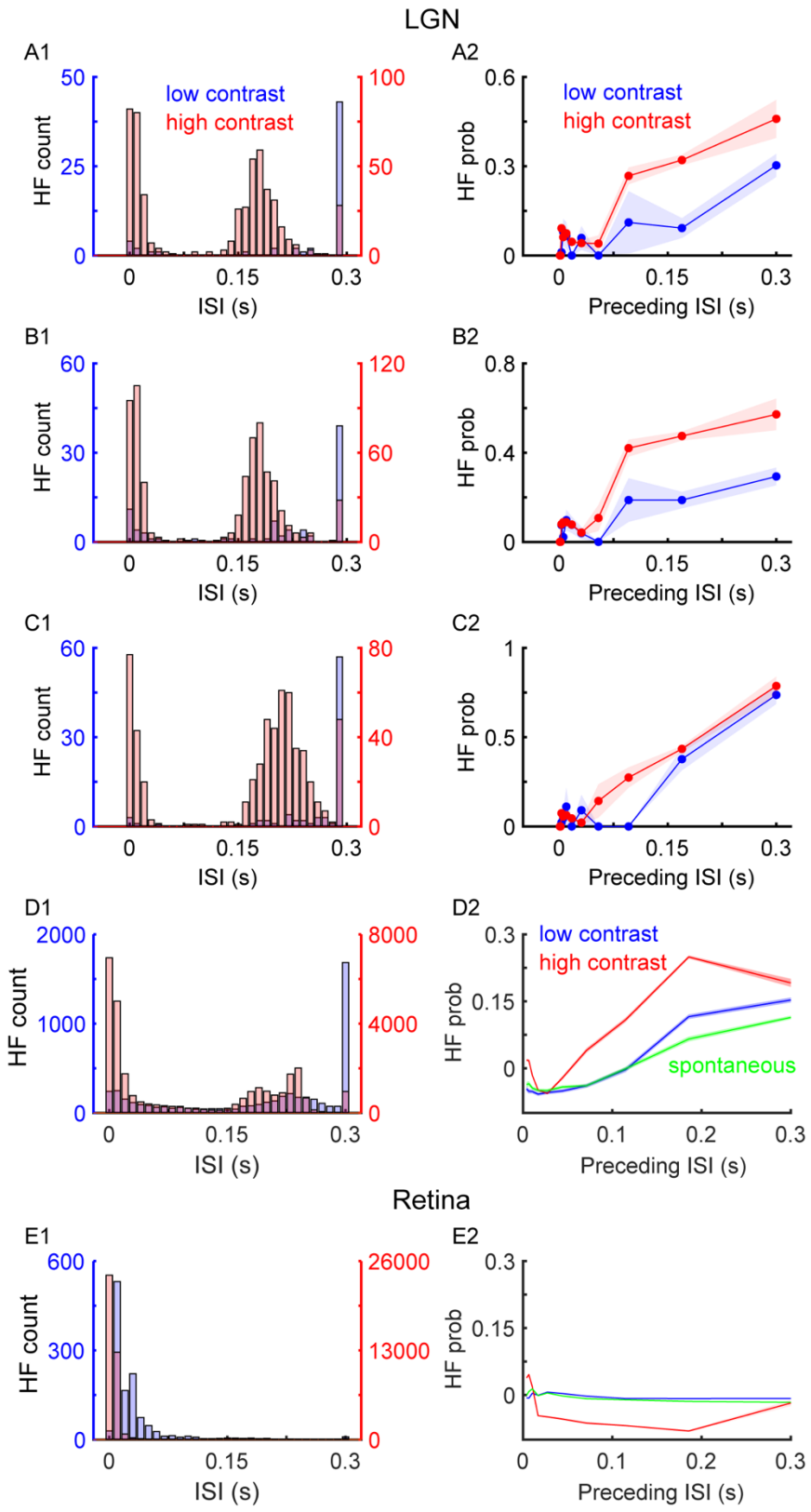
LGN
A1
A2
B1
B2
C1
C2
D1
D2
low contrast
high contrast
spontaneous
HF count
HF prob
ISI (s)
Preceding ISI (s)
Retina
E1
E2

Figure 7. The interdependence of long-ISIs and high-frequency events in the LGN. **A1.** Distribution of high-frequency events as a function of the preceding ISI for an example LGN neuron (blue = low-contrast trials, red = high-contrast trials). **A2.** The probability of high-frequency events as a function of preceding ISI. **B-C.** Similar to **A**, but for two additional, example LGN neurons. **D.** Similar to **A**, but for the entire sample of LGN neurons (green = spontaneous activity). **E.** Similar to **A**, but for the entire sample of retinal ganglion cells (green = spontaneous activity).

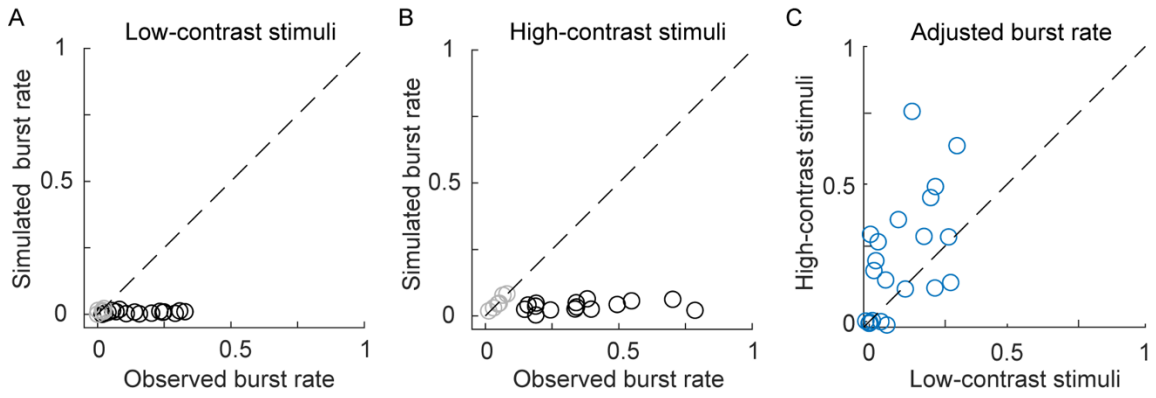

Figure 8. Contrast-dependent changes in LGN bursting activity cannot be explained by changes in firing rate. **A.** Observed LGN burst rate as a function of the Poisson expectation during low-contrast visual stimulation ($p < 0.0015$, t-test; grey circles indicate no significant difference between observed and simulated burst rate, black circles indicate significant difference between observed and simulated burst rate). **B.** Similar to **A**, but for high-contrast stimulation ($p < 0.0015$, t-test). **C.** Scatterplot showing the adjusted burst rate (observed minus Poisson expectation) for LGN cells during high-contrast and low-contrast stimulation ($p = 0.009$, t-test).

Chapter 3: Corticogeniculate feedback modulation of LGN cell size tuning

Abstract

Within the LGN, primary driving inputs are inherited from retinal ganglion cells. However, the largest number of inputs for the LGN come from corticogeniculate feedback. These inputs are proposed to be modulatory, but their full effects on LGN cell activity remains unclear. As extraclassical surround responses seen in the LGN cannot be accounted for solely by retinal extraclassical surround responses, it is probable that the additional surround response comes from corticogeniculate feedback. Within this study, we explored the effects of feedback on LGN cell type, including parvocellular vs. magnocellular; on-cell vs. off-cell; and whether LGN cells experienced extraclassical surround facilitation vs. suppression. Utilizing optogenetic silencing of feedback, we compared geniculate cell responses under control and optogenetic conditions as a function of changing stimulus size. Interestingly, we found that feedback's effects on geniculate cells depended largely on what type of LGN cell it was projecting to.

Generally, we found two distinctions for how feedback modulates classical receptive field responses: for facilitation cells, LGN cells receive center suppression from V1; for suppression cells, LGN cells receive center excitation from V1 . Within the extraclassical surround, feedback's effects were as follows: for facilitation cells, LGN cells receive surround excitation from V1; for suppression cells, LGN cells receive surround suppression from V1. This suggests that for facilitation cells, feedback assists in extending receptive field boundaries, improving stimulus detection. For suppression cells, feedback effects help to sharpen receptive boundaries, improving stimulus discrimination.

Introduction

The visual pathway involves a feedforward retinogeniculocortical route, where visual information leaves the retina and travels to the lateral geniculate nucleus (LGN) of the thalamus before reaching primary visual cortex (V1). The visual information leaving the eye is communicated to V1 via geniculate relay cells in the LGN. In the thalamus, LGN relay cells inherit a majority of their receptive field preferences from the retina (Kaplan and Shapley, 1984; Usrey et al., 1999; Sincich et al., 2007; Sherman and Guillery, 2009; Rathbun et al., 2010), and consolidate information from multiple retinal inputs before it sends the visual information to V1 for further processing (Reid and Alonso, 1995; Alonso et al., 2001; Reid and Usrey, 2004). Previous literature has likened this step in visual processing to a simple relaying of information form the retina to V1. Despite this, work in our lab and others have focused on understanding the functional role of LGN relay cells beyond a simple relay center (for review, see Sherman and Guillery, 2002; Sherman, 2005; Sherman and Guillery, 2011; Sherman, 2012; Usrey and Alitto, 2015; Sherman, 2016; Sherman, 2017). Just as it is found in the retina, in the LGN each relay cell has a classical center/surround organization in which cells can either have either an on-center/off-surround or an off-center/on-surround structure (Kuffler 1952; 1953). The polarity of the classical center/surround receptive field determines the relay cell's response to light, with light exciting the center of on-center cells and dark exciting the surround, and vice versa for off-center cells. In addition to the classical receptive field, geniculate cells also have an additional extraclassical (EC) receptive field that extends over the classical receptive field and beyond into the surrounding space. This extraclassical receptive field plays an important role in size

tuning and adjusting the gain of visual responses (Jones et al., 2000; Solomon et al., 2002; Bonin et al., 2005; Alitto and Usrey, 2008; Mante et al., 2008; Alitto and Usrey, 2015a). Overall, the extraclassical receptive field functions to produce extraclassical surround suppression for a geniculate relay cell, such that a stimulus that covers both the classical receptive field and the extraclassical surround will result in a suppressed response from the cell. This is an inherent feature of the visual system, as extraclassical receptive fields exist in both the retina as well as in V1. This phenomenon has an important function for visual processing, as previous research conducted in the LGN indicates that extraclassical receptive fields likely contribute to various visual aspects including contrast gain control and perceptual “pop-out” (Sillito and Jones, 2002; Bonin et al., 2005). In addition, research has suggested that there may be both retinal and nonretinal contributions to the extraclassical receptive field in the LGN (Fisher, Alitto, and Usrey, 2017; Archer, Alitto, and Usrey, 2021), although the extent of each and their underlying mechanisms are sometimes contradictory in the literature; thus, clarity on this issue is needed.

Previous work from our laboratory has focused on determining both the retinal and nonretinal contributions to extraclassical surround suppression in the LGN (see Fisher, Alitto, and Usrey, 2017). Thus far, the data indicate that LGN extraclassical suppression is larger than can be accounted for solely by retinal mechanisms (Fisher et al., 2017). This suggests that additional extraclassical suppression is provided from nonretinal sources. The focus of this chapter is on elucidating the role of corticogeniculate feedback in generating extraclassical suppression in the LGN. Overall, understanding how extraclassical surround suppression arises within a geniculate cell is

inherently important for understanding visual processing, as this is the source of visual information reaching the primary visual cortex (V1), where extraclassical suppression is reported throughout all layers (Kapadia et al., 1999; Sceniak et al., 1999, 2001; Jones et al., 2000; Walker et al., 2000; Cavanaugh et al., 2002a; Levitt and Lund, 2002; Webb et al., 2005; Angelucci and Sainsbury, 2006; Smith et al., 2006).

Corticogeniculate feedback is a strong candidate for non-retinal contributions for extraclassical effects in the LGN. Anatomically, corticogeniculate neurons which are located in layer 6 of V1 provide dense feedback projections onto geniculate relay cells, either via monosynaptic excitatory synapses or disynaptic inhibitory synapses (Sherman and Guillery, 2006). The synapses made by corticogeniculate feedback neurons greatly outnumber those of the retina by approximately 10:1 despite the fact that geniculate receptive field properties (i.e., “classical” receptive field properties) are inherited from the retina (Erisir et al., 1997a, b; Guillery, 1969). Additionally, the feedback projections from layer 6 in V1 onto either magnocellular or parvocellular layers of the LGN arise from distinct populations of layer 6 neurons, with neurons in the upper portion of layer 6 projecting to the parvocellular layers of the LGN and neurons in the lower portion of layer 6 projecting to the magnocellular layers of the LGN (Fitzpatrick et al., 1994; Usrey, 1994). This suggests that feedback could have differential and stream-specific effects on both LGN neurons in the magnocellular and parvocellular layers. Along these lines, previous research in our lab has demonstrated that magnocellular neurons have more extraclassical surround suppression than parvocellular neurons (Alitto and Usrey, 2007). Additionally, evidence from our lab suggests that LGN on- and off-cells are differentially modulated by stimuli with increasing sizes, that extend into the extraclassical surround,

with magnocellular off-cells experiencing more extraclassical suppression compared to on-cells (Archer et al., 2021). With these results in mind, the role of feedback in establishing these cell-type specific effects remains to be determined, with some results from previous literature partially supporting the possibility (Murphy and Sillito, 1987; Sillito and Jones, 2002; Webb et al., 2002; Nolt et al., 2007) and results from other studies arguing against it (Sceniak et al., 2006). The inconsistency of these results is likely due, at least in part, the previous work using non-reversible methods to silence neurons in anesthetized animals where activity in the feedback pathway is already suppressed by anesthesia. Experiments are therefore needed that utilize reversible and conclusive methods in alert animals, as has been done with the experiments described in this chapter.

Utilizing optogenetics to silence corticogeniculate feedback cells in awake-behaving animals, this chapter examines and discusses the extent of extraclassical surround suppression in relay cells by making comparisons across magnocellular and parvocellular cells and further comparing on-cells and off-cells within the LGN. Overall, results show that feedback plays a major role in extraclassical effects among the different classes of LGN cells with extraclassical effects. This has important implications on understanding the role of feedback in visual processing and further elucidating the unique properties of geniculate cell responses beyond those inherited from the retina, supporting the idea that the LGN is more than just a relay station between retina and cortex.

Methods

General Animal Information

A total of five rhesus macaques were utilized for this chapter, 2 male and 3 females. The majority of data that contributed to this study came from one female animal, however data from the other four additional animals were included to demonstrate that the data are an appropriate representation to understanding feedback's role on visual processing in primates. The animals performed passive fixation for awake-behaving recordings. All of the experimental design and protocols were approved by the Institutional Animal Care and Use Committee at the University of California, Davis and complied with the National Institutes of Health and USDA guidelines.

Animal Surgical Preparation: Cranial Implantation

Prior to awake-behaving recording for fixation training, animals received headposts and cranial implants. An initial weight-dependent dosage of ketamine was intramuscularly injected to induce an anesthetic state. Appropriate animal preparation for aseptic surgery was performed by the vet staff. Anesthetic state was maintained via isoflurane anesthesia (1.5-2.0%) for the duration of the surgical procedure. Animals were placed in a stereotax while an implant was placed utilizing bone cement and titanium screws, including a centrally placed headpost, along with a hemispheric craniotomy cylinder over the LGN stereotaxic coordinates and an additional craniotomy cylinder over V1 over the same hemisphere. Each craniotomy cylinder was 2cm wide, with the center of the cylinder determined by MRI and DTI stereotaxic coordinates. The recording cylinder was placed over each craniotomy via bone cement to facilitate

access to the LGN or V1 for recording. Cranial implants were maintained a minimum of 3 times a week, but cleaned before every recording. Additionally, the granulation tissue within each cylinder was maintained 3 times a week via 5FU administration. Lastly, the implant edge was additionally maintained via a haircut once a week.

Animal Surgical Preparation: Optogenetic Expression

Following the same general anesthesia listed above, animals were injected with optogenetic virus into their primary visual cortex, either before or after cranial implantations were made. Each animal was injected via 50μl Hamilton syringes (Hamilton) with construct transfected via AAV5 with optogenetic tags of either Jaws (AAV5-hSyn-Jaws-KGC-GFP-ER2-Jaws, Addgene # 65014-AAVrg), or mDlx (AAV5-hSyn-mDlx-KGC-mCherry, Addgene #83898-AAVrg) into V1 in a spatially controlled manner.

Surgical injections involved stereotaxic lowering our Hamilton syringe 2.5mm below dura, injecting 1 μls (rate 300 nls/min), raising the syringe 750 μms and injecting another 1 μls (rate 300 nls/min), and raising the syringe another 750 μms and injecting a final 1 μls (rate 300 nls/min). Each injection location had a total of ~3000 μls of AAV injected, with each injection spaced ~1.5mm-2mm apart. A total of ~45 μls of AAV5 was injected into V1 over ~20-25 injections for each animal. After three months, optogenetic manipulation of corticogeniculate cells was tested in an awake-behaving animal before data collection. Our lab has elected to use AAV5 virus (a human synapsin promotor with either Jaws or mCherry and either a GFP or mDlx fluorescent tag, respectively). Both these were able to successfully transfect corticogeniculate feedback cells for rapidly reversible manipulations of neural activity.

Behavioral Training: Passive Fixation & Eye Tracking

In this chapter, animals were trained to passively fixate during recording for fluid reward. The cranial implant of a headpost prior to training allowed a stabilization of both head and eye position and a minimization of movement while the animal sat in a standard primate chair with their gaze centered on a display monitor. During passive fixation, animals were trained to look at a red fixation point on a mean luminance gray screen. The fixation point occurred on either left or right side of the screen depending on which hemisphere was being recorded from, and was always placed in the center of the screen such that it was equidistant from the top and bottom of the screen. Achievement of passive fixation required the animal to maintain fixation within a computer-controlled window centered around the fixation point. Over training, the passive fixation duration was increased as the window size of fixation decreased simultaneously until an animal was able to maintain passive fixation for at least 1.5 second within a 0.5° radius fixation window. Eye position and eye movements were measured utilizing an infrared video eye tracker (Applied Science Laboratory, Bedford), operating at 240 Hz, and horizontal/vertical eye position was converted to a voltage signal sampled at 1 kHz to be compatible with our Spike2 data acquisition system. Additionally, animals were trained to calibrate their eyes utilizing the Applied Science Laboratory calibration system prior to every training and recording session. This involved the animal looking at target points displayed at known eccentricities for the system. This guaranteed appropriate and accurate eye position for each session.

Single-cell Extracellular Recordings

Single-unit extracellular recordings were made from LGN cells using parylene-coated tungsten electrodes (AM systems, Sequim, WA). Electrodes were inserted into the LGN for recording geniculate cell relay activity. Guide-tubes were inserted ~10mm into the brain via the thalamus craniotomy and electrodes were lowered to the LGN for active recordings (Thomas Microdrive). Guide tubes were placed ~2mm into the V1 craniotomy and in-house optrodes were inserted into V1 (single-cell tungsten electrode glued to optic fiber) via Thomas Microdrives. Neural responses were amplified, filtered, and recorded to a computer equipped with a Power 1401 data acquisition interface and Spike 2 software package (Cambridge Electronic Design, Cambridge, UK). Spike isolation was based upon waveform analysis and the presence of a refractory period, assessed from their autocorrelograms.

Optogenetic Laser Information

Lasers were utilized during optogenetic trials (Shanghai Laser & Optics Century). Depending on whether animals expressed Jaws or mDLX, during optogenetic trials, a pulse of either red light (632 nm, RLM635T3-300FC) for Jaws or blue light (495 nm, BL473T3-300FC) for mDLX was temporarily presented in V1 via an inhouse optrode (single-unit parylene-coated tungsten electrodes glued to an optic fiber). Optogenetic lasers came on ~50 ms before visual stimuli appeared on the screen, and turned off ~50 ms after the trial ended. Laser activation was controlled via signals sent by Spike 2 software package and executed via a Power 1401 data acquisition interface for each trial.

General Visual Stimuli Presentation

Visual stimuli for the experiment were created with a VSG Visage visual stimulus generator (Cambridge Research Systems, Cambridge, England) and presented on a gamma-calibrated Mitsubishi FP4121SB monitor with a refresh rate of 120 Hz and a mean luminance of 38 cd/m^2. The monitor was viewed at a distance of 80 cm from the animal chair. Stimuli were presented under binocular vision and the stimulus monitor provided the only source of illumination in a painted black dark room. Optogenetic laser activation of V1 provided minimal illumination during optogenetic (opto) recording trials. During recording sessions, LGN receptive field location was determined for each neuron found by manually moving a circular drifting sine-wave patch grating on the monitor. Centering visual stimuli over the receptive field was actively maintained throughout the entire data collection recording period. At the beginning of each trial, the animal was given a period of time to acquire initial fixation of a fixation target, a small red spot (0.5° radius) presented on a mean luminance gray background on either the left or right side of the screen depending on which hemisphere was being recorded from. After an initial fixation of 500ms, for control trials, the stimulus appeared over the receptive field location for approximately 800ms in which animals were required to remain fixation. For optogenetic trials, after the initial fixation of 500ms, the optogenetic laser was activated 50 ms before the visual stimulus appeared over the LGN receptive field. Visual stimulus presentation parameters remained the same for the optogenetic trials, with the laser turning off 50ms before the trial ended. In total, each trial lasted for ~1.5s during which each animal maintained fixation to receive a small fluid reward. Between each trial within a block and between blocks, the animal was given a mean luminance gray screen in which they were able to freely move their eyes.

Trials were sorted into control and optogenetic blocks, having ~10 repeats of stimulus presentations within each block and a total of 7-10 repetitions of each block type. To minimize eye movement complications, trials were aborted if eye position deviated outside of the fixation window of 0.5°. A mean luminance gray screen was presented during the intertrial interval of ~150ms was interleaved between each stimulus presentation within a block. During the intertrial, animals were allowed to move their eyes freely. Additionally, between optogenetic and control block trials, animals had approximately 5s to freely move their eyes. Each experiment block had approximately 90 trials total, with a total of ~9000 trials collected each recording day. Each trial included a minimum of three aperture sizes (0.1°, 0.5°, and 5°) and three contrast values depending on whether the cell was magnocellular or parvocellular (i.e., magnocellular contrast values: 15%, 45%, and 100%; parvocellular contrast values: 50%, 80%, and 100%). Aperture sizes were labelled as center stimuli at 0.5° as they covered the LGN receptive field isolated and aperture sizes were labelled as surround stimuli at 5° as they covered the LGN receptive field isolated and its surround. As contrast values did not demonstrate an influence on processing of aperture sizes, analyses collapsed across contrast values. Additionally, the sine-wave gratings had a consistent spatial frequency of 1, temporal frequencies at either 4Hz or 5 Hz to optimally excite LGN cells for drifting stimuli, orientations typically at 90°, and initial phases that optimized LGN cell activity (0 for On and 180 for Off).

Cell Type Classification

Before data collection, LGN cells were isolated and classified. Drifting sine-wave patch gratings were centered over the LGN receptive field to characterize response

properties to luminance, contrast, orientation, temporal frequency and spatial frequency. To classify whether neurons were on- or off-cells, the initial phase of the drifting sine-wave gratings was changed from either 0 to 180. Excited by bright luminance were classified as on-center cells and neurons excited by dark luminance were classified as off-center cells. Visual stimuli were given initial drifting sine-wave phases that reflected maximal excitation for the LGN cell class. Cells were classified as magnocellular or parvocellular by looking at their general responses to contrast values and supplementally their responses to temporal frequencies. Cells that consistently responded to contrast values between 5%-50% and faster temporal frequencies were classified as magnocellular; cells that responded consistently to contrast values between 50%-100% were classified as parvocellular. These classifications were utilized to determine the contrast values of the drifting sine-wave gratings presented during data collection.

Post-data collection cells were classified as either being facilitation or suppression cells. This involved presenting drifting sine-wave gratings of varied aperture sizes to generate an area tuning curve. Aperture sizes were stepped between 0.1° and 5° in 10 steps and with at least 5 repeats to generate individual area tuning curves. To classify whether cells were facilitated or suppressed by surround stimuli of 5°, their F1 spiking activity to this size was compared to their spiking activity for center stimuli (0.5°):

$$LGN\ Cell\ Type_{Fac/Supp} = Spiking\ Activity_{surround} - Spiking\ Activity_{center}$$

For a cell to be classified as a Facilitation cell, the value above has to be > 0; for a cell to be classified as a Suppression cell, the value has to be < 0. For neurons that had a value of 0 they were not classified as either cell type and were excluded from these analyses. For a total breakdown of LGN cell type and the number of LGN cells that were found for each category, see Table 1.

Center Index Modulation

For our study, we wanted to understand feedback's influence on aperture size processing in the LGN. This involves a characterization of center index modulation, defined in our study as the difference of LGN spiking activity to center stimuli sine-wave gratings that covered the classical receptive field under control conditions and under optogenetic conditions:

$$\Delta \text{ Center Index} = \frac{(control\ center\ response - opto\ center\ response)}{control\ center\ response}$$

Here a value of 0 would indicate no difference between control and optogenetic conditions.

Surround Index Modulation

To characterize the modulation experienced for each LGN cell under surround stimuli presentations, a suppression index was calculated by comparing the difference of spiking activity under control and optogenetic conditions:

$$\Delta \text{ Surround Index} = \frac{(control\ surround\ response - opto\ surround\ response)}{control\ surround\ response}$$

Here, a value of 0 would indicate no difference between control and optogenetic conditions. This calculation did not remove the spiking activity of the center index from the surround index.

Total Surround Index Modulation

To calculate a total surround index, we took the change found in the surround index and removed the change found in the center index as follows:

Δ Total Surround Index = Δ Surround Index - Δ Center Index

This provided an isolated surround index modulation that removed the center influence in the value, as the surround aperture size covered both the classical receptive field and extended into the surround.

Suppression Index

A final suppression index was calculated for each cell type, comparing the overall suppression experienced for each LGN cell under both control and optogenetic conditions. The strength of extraclassical suppression was quantified using a suppression index calculated as follows:

$$Suppression\ Index = \frac{Response\ to\ surround\ grating}{Response\ to\ center\ grating}$$

For each cell, their calculated suppression index under control and optogenetic conditions were compared to one another.

Results

To understand the effects of feedback on area summation, also called stimulus size tuning, of different geniculate cell types, we first wanted to demonstrate that relay cells experience effects from the extraclassical surround. Although past efforts have focused on suppressive effects from the extraclassical surround, we wished to also determine whether facilitatory effects might also occur. Across the geniculate cells

included in this study (n = 142), a majority had either extraclassical surround suppression or extraclassical surround facilitation, regardless of whether a cell was classified as a parvocellular (n = 91 of 104 cells), magnocellular (n = 37 of 38 cells), on-center (n = 47 of 61 cells), off-center (n = 81 of 81 cells) cell (see Table 1, Figure 5). To determine whether a geniculate cell had extraclassical facilitation (facilitation cell) or extraclassical suppression (suppression cell), we varied the size of an aperture covering an underlying sine wave grating stimulus and examined each cell's area summation response function, comparing its spiking activity to a stimulus size corresponding to the classical receptive field to a stimulus that extended into the extraclassical surround. (Figure 3). By applying an index ($LGN\ Cell\ Type_{Fac/Supp} = Spiking\ Activity_{surround} - Spiking\ Activity_{center}$) to quantify the direction and magnitude of extraclassical effects, we sorted cells into categories with extraclassical facilitation (indices >0; n=44) and with extraclassical suppression (indices <0; n=84). Figure 6 shows area summation response functions from representative cells. It is important to note that ~90% of geniculate relay cells fell into one of these categories; however, ~10% of geniculate relay cells (n = 14) did not experience either extraclassical facilitation nor extraclassical suppression. These cells were excluded from further analyses focusing on comparisons made between extraclassical facilitation and extraclassical suppression. Although this classification of cell types was conducted independently of whether the cells were magnocellular vs. parvocellular or on vs. off, it is useful to note that cells with extraclassical facilitation were primarily (82%) classified as on cells and cells with extraclassical suppression were primarily (82%) classified as off cells, (see Table 1 for additional cell count breakdown) in our data.

Before further data analysis, it is important to depict examples of both LGN facilitation cells and suppression cells under control conditions (four sample cells, Figure 6). Previous work in our lab has demonstrated that while a majority of the relay cell's visual processing is inherited from its retinal inputs, retinal input alone is not sufficient to account for the total amount of extraclassical suppression seen in geniculate relay cells (Fisher et al., 2017). Instead, polysynaptic circuits involving corticogeniculate feedback to LGN have been proposed to influence extraclassical surround responses in the LGN (for review, see Sillito and Jones, 2002; Usrey and Alitto, 2015). To investigate whether feedback from V1 contributes to the additional extraclassical facilitation or extraclassical suppression found in geniculate relay cells, we optogenetically silenced corticogeniculate feedback neurons in V1using JAWS (a light-activated chloride pump; see Figure 2 for an example of expression) or mDLX (a light activated channelrhodopsin selectively expressed in inhibitory neurons. While the mechanism for silencing V1 feedback differed between these two opsins: JAWS transfects V1 feedback cells to directly inhibit activity and mDLX transfects GABA cells in V1 which indirectly inhibits V1 feedback cells upon laser activation, both opsins were found to successfully transfect V1 and reversibly silence V1 activity via laser activation (for sample V1 cells, see Figure 4). Because feedforward and feedback connections between the LGN and cortex are retinotopically aligned, all of the recordings and manipulations examined in this study were between cortical and geniculate neurons with receptive fields separated by no more than 3° of visual space. Despite this constraint of 3°, ~40% of cell pairs were within 1° of retinotopic overlap and ~60% were within 2° of retinotopic overlap; see Supplemental Figure 1).

Regardless of whether a cell was labelled as a facilitation or suppression cell, we found that silencing feedback during optogenetic trials affected geniculate cell activity. This included cells that were either magnocellular or parvocellular and cells that were either on-cells or off-cells (for example cells of each cell type, see Figure 5). Importantly, under control conditions for all geniculate cell types (Parvo-Off, Parvo-On, Magno-Off, and Magno-On), cells were able to experience either extraclassical surround facilitation or extraclassical surround suppression (Figure 5). Interestingly, effects from silencing feedback were not absolute in predicting whether a cell was magnocellular vs parvocellular or on vs. off (individual cells in Figure 5I, population average Figure 5J).

Focusing on understanding feedback's contributions to extraclassical surround receptive fields, we wanted to first characterize optogenetic effects on sample facilitation and suppression cells. Looking at four sample cells, two example facilitation cells and two example suppression cells, comparing control to optogenetic conditions, optogenetic inactivation changed the activity of each of these individual geniculate cells (Figure 6). For the sample cells that fell under either facilitation or suppression cell type categorization, the effects seen under optogenetic silencing of feedback were largely consistent. For the sample cells with extraclassical facilitation, responses to stimuli that extended into the extraclassical surround decreased when feedback neurons were silenced (Figure 6B1-B5) indicating the removal of net excitation. Interestingly, during optogenetic inactivation, these same cells increased their activity for stimuli restricted within the classical receptive field (Figure 6A1-A5) indicating the removal of net inhibition (presumably by mechanisms involving polysynaptic inhibition). For the sample cells with extraclassical suppression, optogenetic effects were essentially the opposite,

with responses to stimuli extending into the extraclassical surround increasing when feedback was silenced (Figure 6D1-D5) and responses to stimuli with the classical receptive field decreasing when feedback was silenced (Figure 6C1-C5) indicating the removal of net excitation. For both categories of cells, those with extraclassical suppression and those with extraclassical facilitation, this is the first report of a center/surround organization of feedback effects, with the center corresponding to the classical receptive field and the surround corresponding to the extraclassical surround.

To understand the full extent of the interactions between stimulus size and feedback effects on geniculate responses, we needed to methodically compare the geniculate relay cell's activity when the stimuli covered the classical receptive field (center) to when the stimuli covered both the classical receptive field and the extraclassical surround (surround). This required both a comparison of control activity to optogenetic inactivation of feedback, but also a breakdown of each individual relay cell's activity to both the center stimuli that was contained within its classical receptive field (typically ~0.5°) and to the surround stimuli that covered the classical receptive field and extended into the extraclassical surround receptive field. To first determine feedback's effects on geniculate cell processing of center stimuli, we analyzed control and optogenetic relay cell activity to visual stimuli that covered only the classical receptive field of the LGN cell. For each geniculate relay cell, center stimuli were tailored to the LGN relay cell preferences for contrast, spatial frequency, and luminance phase polarity, while the orientation of the grating was either at 90°, or tailored to the paired V1 cell's orientation preference (temporal frequency was either at 4 or 5 Hz for LGN processing). Under center stimuli presentation, each geniculate relay cell had a center index

modulation calculated by identifying the change in center activity for each individual cell with and without feedback's inputs (*Δ Center Index* $= \frac{(control\ center\ response - opto\ center\ response)}{control\ center\ response}$). Here, a center index value of 0 would indicate that the relay cell's response remained the same regardless of whether feedback to the cell was active or silenced. This would indicate that feedback does not have a role in modulating the relay cell's activity when processing information within the classical receptive field. Additionally, a value closer to 1 would indicate that the relay cell's overall activity in optogenetic trials was much lower than in control conditions. Conversely, a value closer to -1 would indicate that compared to control conditions, the geniculate relay cell's activity was much greater when feedback was silenced.

Looking at the distributions of geniculate relay cells, the center modulation index values were evenly distributed across both parvocellular geniculate cells (parvocellular mean center index = 0.03 +/- 0.01 SE, p = 0.0650, *t-test*), and magnocellular geniculate cells (magnocellular mean center index = 0.03 +/- 0.03 SE, p = 0.38, *t-test*) (Table 3, Figure 7). However, when the data were analyzed under all cells there was a significant center index modulation comparing center index distributions for facilitation vs. suppression cells (mean = 0.03 +/- 0.01 SE, *p = 0.0446*, *t-test*). In addition, the influence of feedback on center stimulus modulation was more consistent for each geniculate relay cell type, further indicating a distinction between the two (see Table 2). For facilitation cells, feedback contributes to the suppressed activity for center stimuli (e.g., a negative center index value, mean = -0.08 +/- 0.02 SE, *p = 3.68e-04*, *t-test*), and for suppression cells, feedback contributes to an enhanced activity for center stimuli (e.g., a positive center index value, mean = 0.08 +/- 0.02 SE, *p = 1.64e-05*, *t-test*). In

comparison, if we analyze the data by on-cell and off-cells, only off-cells were significantly different during feedback inactivation (on-cell mean = -0.03 +/- 0.02 SE, p = 0.055; off-cell mean = 0.07 +/- 0.02 SE, *p = 2.21e-04*). For a full list of cell type statistics of center index modulation, see Table 2 and Table 3.

We next assessed the influence of feedback on how geniculate cells processed stimuli that extended into the extraclassical surround. For each geniculate cells, we quantified surround modulation using an index (*Δ Surround Index* = $\frac{(control\ surround\ response - opto\ surround\ response)}{control\ surround\ response}$, see Table 4). Comparing all cells, the change in surround index was significant when comparing facilitation and suppression cells (mean = -0.03 +/- 0.01 SE, *p = 0.0473*, *t-test*). However, as surround stimuli not only covers the extraclassical receptive field but also the classical receptive field, this calculated value is not sufficient for characterizing the extraclassical surround response. Instead, we also performed a total surround index calculation, which is calculated as *Δ total surround index = Δ surround index - Δ center index*. This newly calculated total surround index now accounts for any antagonistic effects from stimuli covering the classical receptive field as well, by subtracting the center response from the equation (see Table 5). Just as with the center index, a surround index of 0 would indicate that the relay cell's response remained the same regardless of feedback's ability to provide input to the cell. This would indicate that feedback does not have a role in modulating the relay cell's activity when processing information beyond the classical receptive field into the surround. Additionally, a value closer to 1 would indicate that the relay cell's overall activity in optogenetic trials was much lower. Again, when looking at the distributions of surround index for parvocellular geniculate cells and magnocellular

geniculate cells the distribution of values was varied (Figure 8). Feedback effects on the change in surround index were as follows: facilitation cells responses decrease when feedback's input is removed and suppression cell responses increase when feedback is removed (facilitation total surround index mean = 0.02 +/- 0.02 SE, *p = 3.20e-04, t-test*; suppression total surround index mean = -0.049 +/- 0.018 SE, *p = 1.44e-06, t-test*; facilitation vs. suppression total surround index mean = -0.03 +/- 0.01 SE, *p = 0.01*, *t-test*, Figure 8). This suggests that feedback has approximately equal but opposing effects on individual geniculate relay cells when a stimulus covers the classical receptive field vs. when a stimulus extends beyond the classical receptive field into the surround. Again, a total surround index was calculated for on-cells and off-cells, and again off-cells were significant (on-cells mean = -0.01 +/- 0.02 SE, p = 0.27, *t-test*; off-cells mean =-0.04 +/- 0.02 SE, *p = 8.19e-05, t-test*).

To further compare how geniculate relay cell's processed center stimuli and surround stimuli, we compared effects (facilitation vs suppression) on the responses to center and surround stimuli. Plotting the comparison as a scatter plot, we see that facilitation cells had a larger and opposite-sign surround index compared to their center index (facilitation surround index mean = 0.02 +/- 0.02 SE, facilitation surround index mean = -0.049 +/- 0.02 SE; Table 6, Figure 9). Likewise, suppression cells had a larger and opposite-sign center index compared to the surround index (suppression center index mean = -0.08 +/- 0.02 SE; suppression center index mean = 0.08 +/- 0.02 SE; Table 2, Figure 9). Lastly, calculating a final suppression index for control and optogenetic silencing of feedback's inputs to geniculate relay cells demonstrated that the two geniculate cell classifications have a distributed separation of suppression

indices in their cell classifications (all cells control vs. optogenetic, p = 0.0601, *t-test*; Table 7, Figure 10). While this result may be expected as the criteria for whether a geniculate relay cell is classified as a facilitation or suppression cell was largely determined by similar analyses for initial cell classification, what was unexpected and very evident from the data, when you silence feedback, the separate distributions from these two cell populations now overlap, indicating that feedback is necessary for geniculate relay cells to properly process and encode stimuli of different aperture sizes (facilitation cells control vs. optogenetic, *p = 0.01, t-test*; suppression cells control vs. optogenetic, *p = 1.29e-05, t-test*; Table 6, Figure 10). This indicates that feedback is necessary for geniculate relay cells to either experience extraclassical surround facilitation or extraclassical surround suppression. For on-cell and off-cell comparisons, the off-cell suppression index was significantly different under control and optogenetic conditions (off-cell control mean = 0.23 +/- 0.02 SE; off-center optogenetic mean = 0.12 +/- 0.03 SE, *p = 7.18e-04, t-test*, Table 6). For a full comparison of suppression index values across cell classification, refer to Table 7. Under our analyses, corticogeniculate feedback modulation was not limited to the extraclassical receptive field response. Our breakdown of geniculate relay cell receptive field responses further demonstrates that responses to stimuli that extend over the classical receptive field also include effects of feedback onto geniculate relay cells.

In total, feedback effects on geniculate responses to stimulus size entirely depends on the type of LGN cell involved. Our work demonstrates that when you look at inactivation of V1 feedback when stimuli are restricted to the geniculate cell's classical receptive field, V1 feedback provides center suppression to LGN cells with

extraclassical facilitation, whereas feedback provides center excitation to LGN cells with extraclassical suppression (Figure 11). Furthermore, when determining the effect of feedback on how geniculate cell' process stimuli that extends into their extraclassical surround, LGN facilitation cells receive surround excitation from feedback and LGN suppression cells receive surround suppression from feedback (Figure 11). Thus, corticogeniculate feedback is accounting for additional refinement of how geniculate cells process stimulus size. As inactivation of feedback input affects a cell's ability to respond to stimuli that are either constrained to the classical receptive field or extend into the extraclassical surround, feedback an important role in the processing of visual information in the LGN.

Discussion

Overall, this study demonstrates that the processing of stimulus size in the LGN depends on corticogeniculate feedback input from V1. Feedback inputs not only determine the geniculate cell's responses to stimuli within the extraclassical surround, but also modulate the geniculate cell's responses to stimuli restricted to the classical receptive field. This suggests that while classical receptive field responses are largely inherited by the retina, V1 feedback is providing modulatory input to adjust the gain of geniculate relay cell center responses. Previous literature has demonstrated that extraclassical surround suppression is greater in magnocellular cells compared to parvocellular cells and in off-cells compared to on-cells (Archer et al., 2021). Our results

are consistent with these findings and goes on to demonstrate a role for feedback in the effects.

Interestingly, our data indicates that the strength of extraclassical suppression in some parvocellular neurons can be as great as that in magnocellular neurons, a finding not previously noted in the literature. This could be for several reasons, one being our data has a larger sample of parvocellular cells compared to magnocellular cells. With a larger sample of magnocellular cells, our data might show even greater levels of extraclassical surround suppression in magnocellular cells. In our dataset, regardless of whether a cell was magnocellular or parvocellular, a slight majority of cells were off-cells (n = 81; 57%), which are known to exhibit more extraclassical surround suppression compared to on-cells. Again, with additional data, it is possible that further distinctions in geniculate cell processing of extraclassical surround stimuli may be seen. Despite this, our collected cells had a comparable distribution of on-: off-cells under both parvocellular (45 on:59 off) and magnocellular (16 on: 22 off) cell types. However, it is important to note that for comparisons between facilitation and suppression cells, cells excluded from that analysis were entirely on-cells (n = 14) and majority of those excluded cells were also classified as parvocellular (n = 13 of 14 excluded cells). This indicates that while it is possible for parvocellular cells to experience extraclassical surround suppression, many cells in parvocellular layers do not. It is possible, instead, that as off-cells experience more extraclassical surround suppression, they have equal opportunity to express this suppression in both parvocellular and magnocellular layers. As magnocellular cells are better at responding to low levels of contrast, the visual stimuli used in these experiments were selected to evoke to a response midway in the

cell's contrast response function. It is possible that under equivalent contrast values for visual stimuli, we might find greater distinctions in the extraclassical surround suppression experienced by magnocellular cells compared to parvocellular cells.

The functional roles of visual processing for parvocellular and magnocellular cells are as follows: parvocellular processes are associated with color vision and high acuity vision and magnocellular processes are associated with the perception of motion (DeYoe and Van Essen, 1988; Livingston and Hubel, 1988; Merigan and Maunsell, 1993). With this in mind, it is understandable that the extent of extraclassical surround suppression in the two populations could have different extents, and it is further understandable that they would receive V1 feedback input from different populations of layer 6 neurons. Our data suggests that depending on what visual information is being encoded, feedback's modulatory effects could be even further varied, promoting a heterogeneous model for feedback as originally discussed in Figure 1A. As each of the presentations of stimuli were tailored to the geniculate cell's visual preferences, if the stimuli were varied beyond the geniculate cell's preferences, the effects of corticogeniculate feedback could vary. If other properties of the visual stimulus were methodically varied or if this study was performed using natural images, feedback's modulatory responses might vary in magnitude and possibly even switch between net excitation and net suppression.

A methodological limitation in our study that deserves discussion is the limited extent of silencing feedback using optogenetics and light delivered via a fiber optic. Because the area of cortex that can influence a geniculate cell via feedback is almost certainly greater than the area silenced with optogenetics, the effects reported are likely

much less in magnitude than what the complete pathway can provide. Perhaps the use of DREADS which does not have the same restrictions on the footprint of inactivation to silence feedback neurons might reveal this additional influence, although this loses the ability to quickly compare inactivation to control conditions. Additionally, when suppressive effects are found, we cannot discern whether these are mediated by disynaptic interactions involving local interneurons or neurons in the thalamic reticular nucleus, both of which receive feedback input and provide GABAergic synapses onto LGN relay cells.

Furthermore, this study is only the beginning steps of understanding the role of feedback in visual processing in the awake-behaving animal, as the animals used in this study were only tasked with fixating their eyes, results could vary with great engagement with the visual stimulus, perhaps having the animal perform a discrimination involving stimulus size. Somewhat related, arousal levels are likely to influence the effects of feedback, as arousal is known to modulate feedback's activity higher in the visual processing stream, such as from V2 (area 18) to V1 of primates and carnivores (Briggs et al., 2016; Hasse et al., 2019; for review see Lin and Kaas, 1977). For instance, it is plausible that higher cognitive engagement or increased levels of arousal would recruit either more activity from individual feedback cells or more feedback cells. Conversely, low arousal could lower feedback's activity, or perhaps turn it off altogether as previous literature studying feedback effects on the LGN were inconsistent and oftentimes conflicting, probably because V1 feedback activity is largely silent in anesthetized states (Briggs and Usrey, 2007a) and geniculate activity is much lower as well (Alitto et al., 2011). An ability to further quantify and further isolate the

silencing of feedback inputs to geniculate relay cells would elucidate how levels of arousal could modify feedback activity and feedback recruitment.

Previous research has further demonstrated that within higher levels of the visual system, corticocortical feedback circuits are known to modulate their synaptic targets based on higher-level cognitive aspects such as conveying attention signals to lower levels of the visual system or communicating necessary information about context and task demand (Buffalo et al. 2010, Gregoriou et al. 2009, Michalareas et al. 2016, Noudoost et al. 2010, van Kerkoerle et al. 2014). As such, lastly it is hypothesized that feedback could be mitigated by not only general arousal state but also by items such as context and active task demand. Future work should analyze both pupil size as a proxy for general arousal, along with other psychometric measurements such as heart rate, breathing rate, and lastly measurements of arousal indicators such as acetylcholine levels. Some research suggests that corticogeniculate feedback differs depending on arousal signals (Stoelzel et al., 2017). Anatomically, feedback has parallel stream inputs to magnocellular and parvocellular cells from unique subregions of layer 6 (Fitzpatrick et al., 1994; Usrey, 1994), consequently the aspect of visual processing that should be prioritized based on task demand could be modulated at the level of the relay cell. Our current data suggest that extraclassical surround suppression could serve to sharpen the receptive field boundaries of geniculate cells. In contrast, extraclassical surround facilitation might serve to extend the receptive field boundaries of geniculate cells, thereby improving stimulus detection. As other aspects of visual processing are selectively studied with respect to feedback inactivation, it is likely that geniculate relay cells require varied aspects of feedback input to properly process a visual scene. Work

under anesthetized optogenetic activation of feedback has demonstrated that feedback can reduce the response latency of LGN relay neurons to incoming visual inputs (Hasse & Briggs, 2017). This evidence supports the proposal that feedback facilitates visual processing of LGN neurons to respond more precisely, reduce response variability, narrow their receptive fields, and, thus, increase their capacity to convey information about visual stimuli (Murphy et al., 2021). The work performed in this dissertation further supports feedback assisting in receptive field sizes, and demonstrate that burst mode can function to improve both LGN reliability and timing precision as a function of contrast. It is possible that with inhibition of feedback, the rate in which LGN cells fire in either tonic or burst mode can change, potentially increasing the rate of bursting as it is demonstrated to effectively drive cortex.

Current research of corticogeniculate feedback proposes various contexts for feedback modulation, including top-down information about context, attention, reward, task goals, and arousal (Bondy et al., 2018; for review, see Briggs, 2020). Outside of these possibilities, certain literature has also proposed that corticogeniculate feedback is involved in higher visual functions such as probabilistic inference (for a review, see Cumming & Nienborg 2016), or predictive coding (Edwards et al. 2017, Pennartz et al. 2019, Rao & Ballard 1999). Finally, as the relationship of feedback from V1 to the LGN is preserved across all sensory modalities and multiple animal models, understanding feedback's role in visual processing of stimulus size will help us understand how the brain communicates from cortex to the thalamus to process sensory information and interact with the environment.

Figures

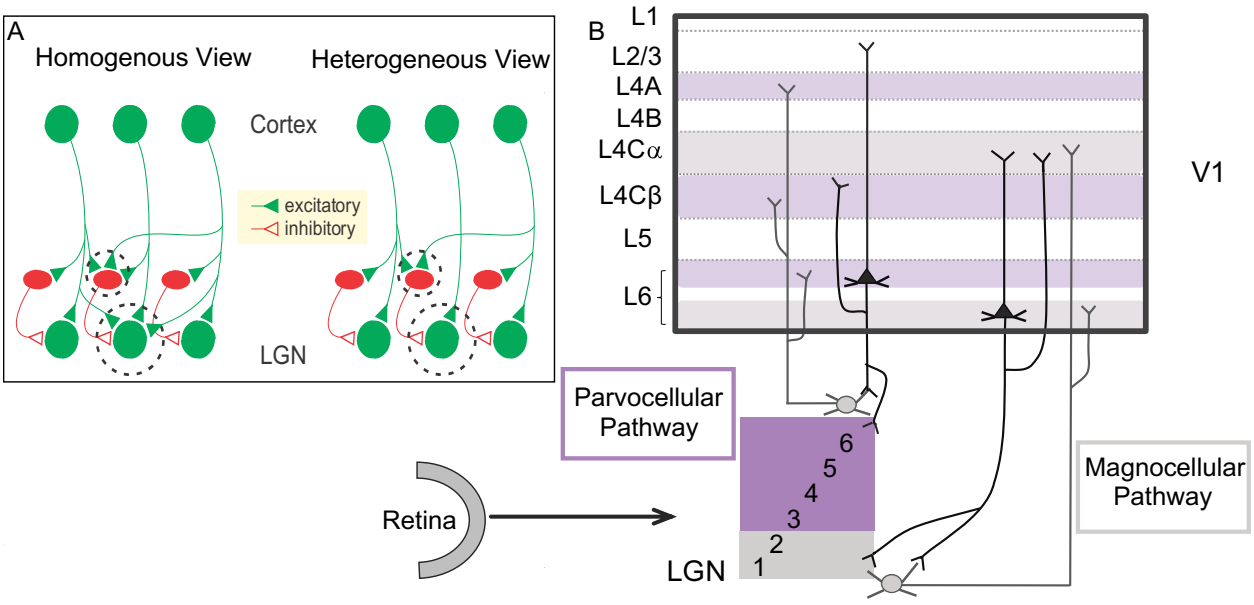

Figure 1. Overview of the Feedback Pathway. A. Two opposing views of how corticogeniculate feedback could function. The traditional view is that feedback's inputs homogeneously excite geniculate cells via monosynaptic excitation (green triangles) or inhibit geniculate cells via disynaptic inhibition (red triangles). An opposing view to a homogenous effect of feedback, feedback cells could have a heterogeneous effect on geniculate relay cells, such as excitatory effects (green triangles) from inputs that have retinogeniculate alignment and inhibitory effects (red triangles) from inputs that have retinogeniculate displacement. B. Overview of the anatomy of the retinogeniculocortical visual pathway. This demonstrates the parallel feedforward pathway of the parvocellular pathway (purple) and the magnocellular pathway (gray) to primary visual cortex (V1). These pathways synapse to unique target layers in V1 and, in addition, receive unique feedback projections form layer 6 feedback cells.

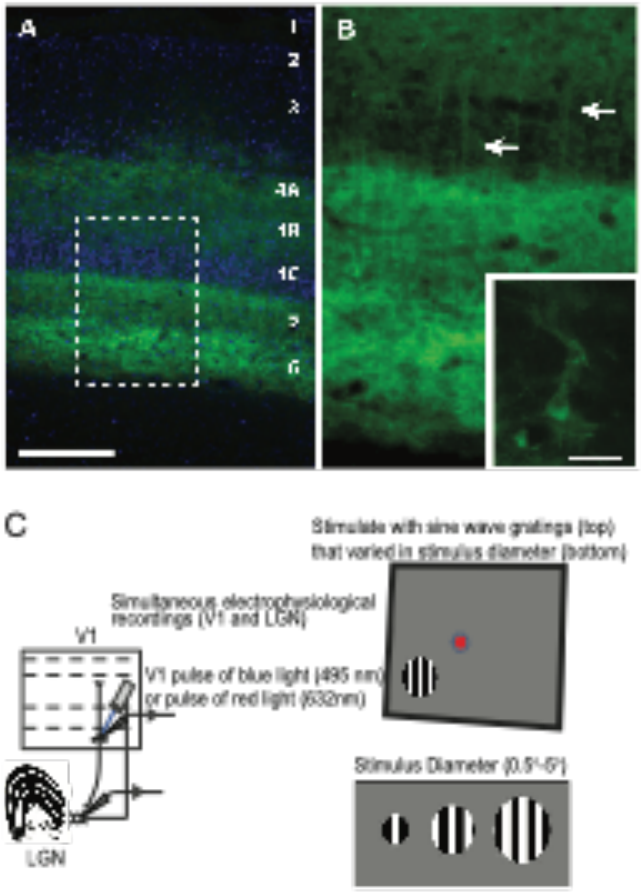

Figure 2. Methods Overview. A. Example optogenetic expression of the optogenetics Jaws (AAV5-hSyn-Jaws-KGC-GFP-ER2-Jaws) in primary visual cortex (V1) against a DAPI counterstain (labelled cells in green, DAPI cells in blue). V1 layers are labelled, Jaws transfection selectively transfected ventral layers of V1. Scale of 500 microns. B. This is an enlarged image of the dotted box from A. Arrows identify example collateral axonal branches from layer 6 cells that are projecting to layer 4 of V1. A labelled cell body is enlarged further, scale of 100 microns C. Overview of awake-behaving recordings. Paired extracellular single-cell recordings were made in the LGN and V1. During optogenetic trials, a pulse of either blue light (495 nm) for mDLX or red light (632 nm) for Jaws was temporarily presented in V1. Animals passively-fixated at a red dot on

a mean luminance gray screen with a set fixation window. Sine-wave gratings that were either stationary or drifting (4 or 5Hz) that was centered over the LGN receptive field. Stimulus diameters ranged from 0.5°(center) to 5°(surround).

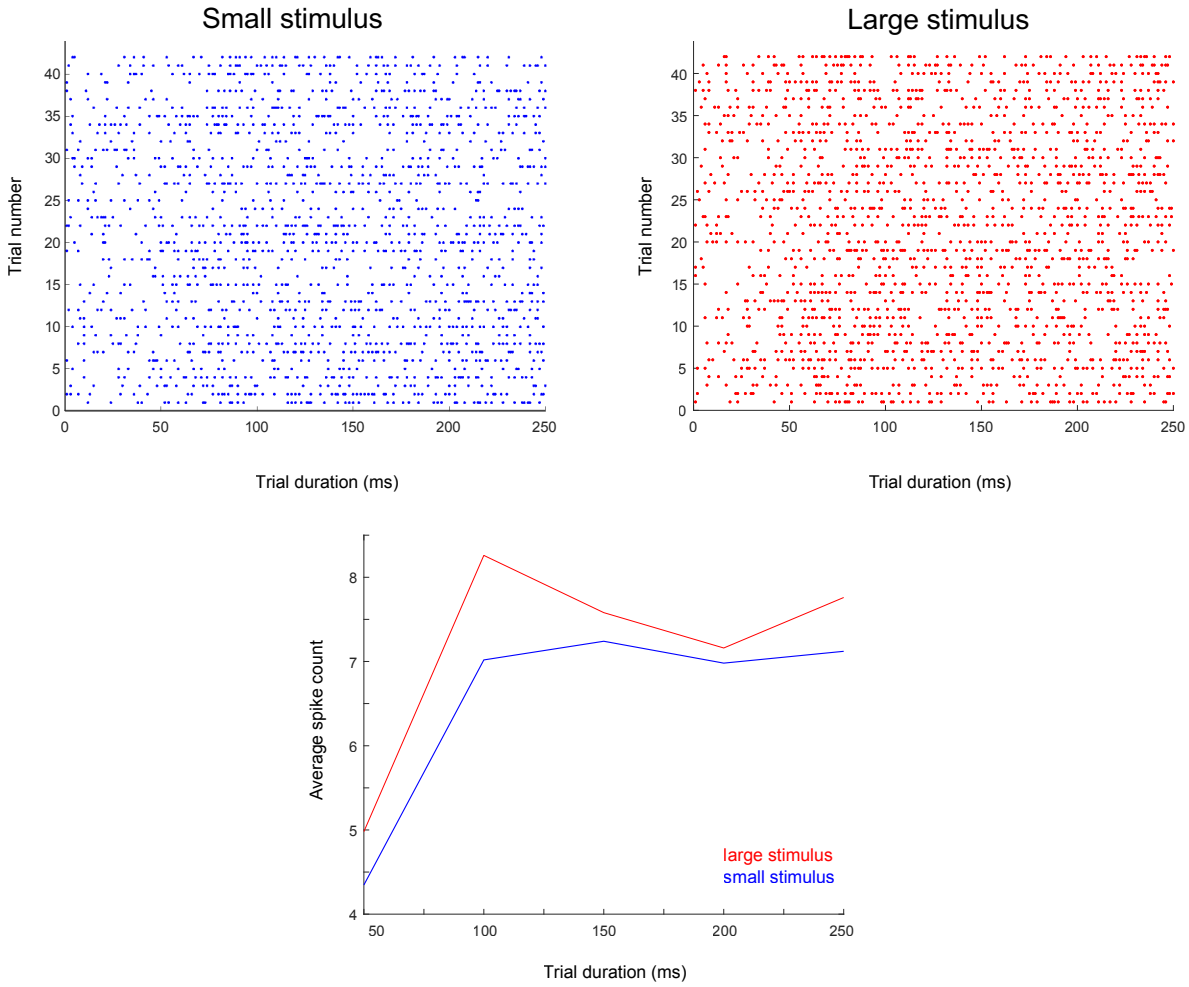

Figure 3. Example geniculate cell area tuning. Two rasters for an example geniculate cell, one for small stimuli (small) and one for large stimuli (red). A total of 42 trials were included in these rasters, each trial lasted 250 ms. An average PSTH response was calculated for large and small stimuli. The average spike count was plotted over the trial duration over 25 ms bins.

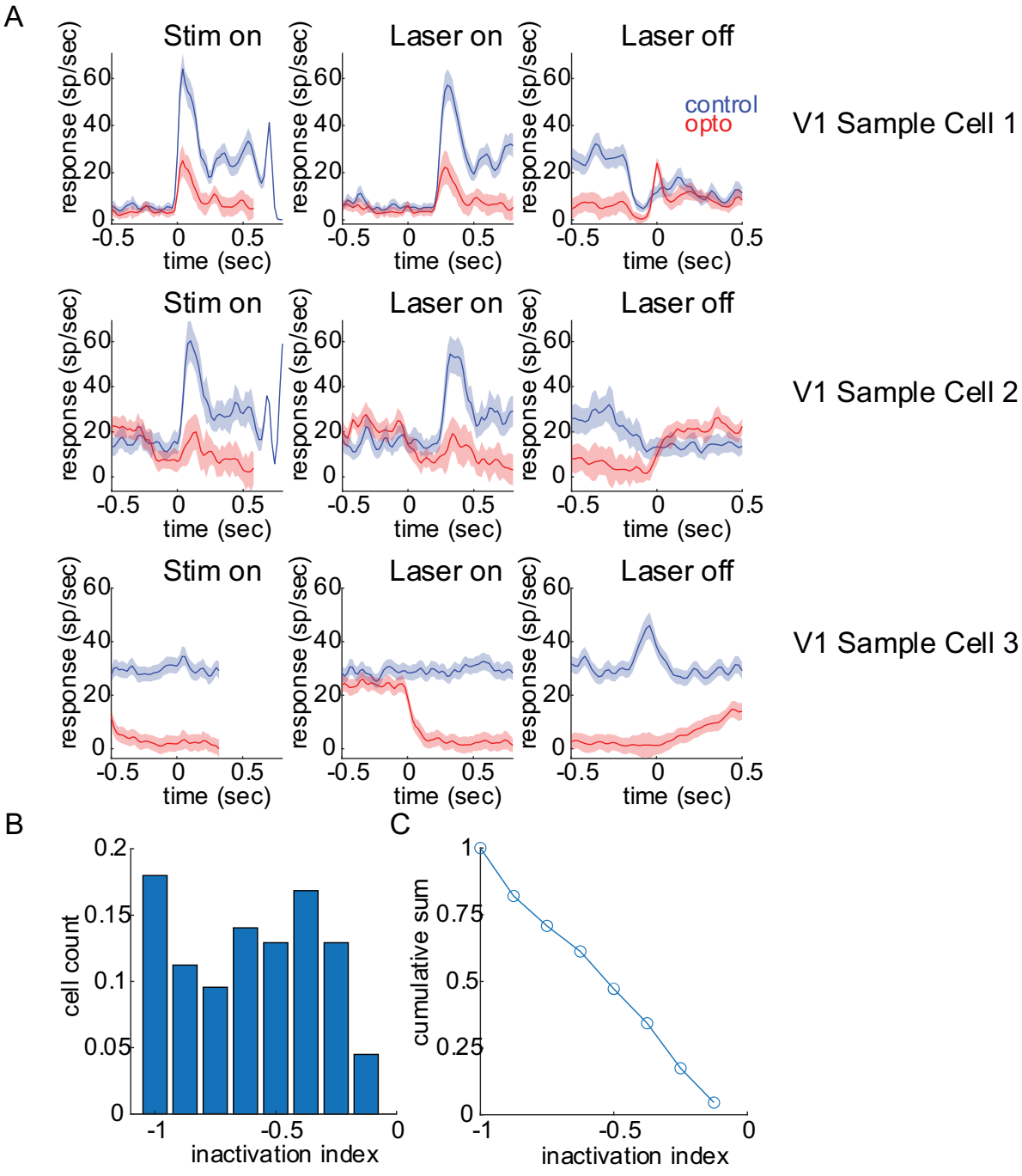

Figure 4. Examples of V1 corticogeniculate feedback cell inactivation. A. Three examples of optogenetic inactivation of feedback cells. Each cell's responses over time under control conditions (blue) was compared to laser inactivation (red). Each example V1 feedback response was analyzed under timeframes during the trial, stimulus onset

(left), laser onset (middle), and laser offset (right). Under all conditions, each V1 feedback cell experienced less activity under optogenetic conditions compared to control conditions. B. Each V1 feedback cell had an inactivation index, and plotted on a histogram of cell count. C. A cumulative sum of the inactivation index was plotted as a function of inactivation index.

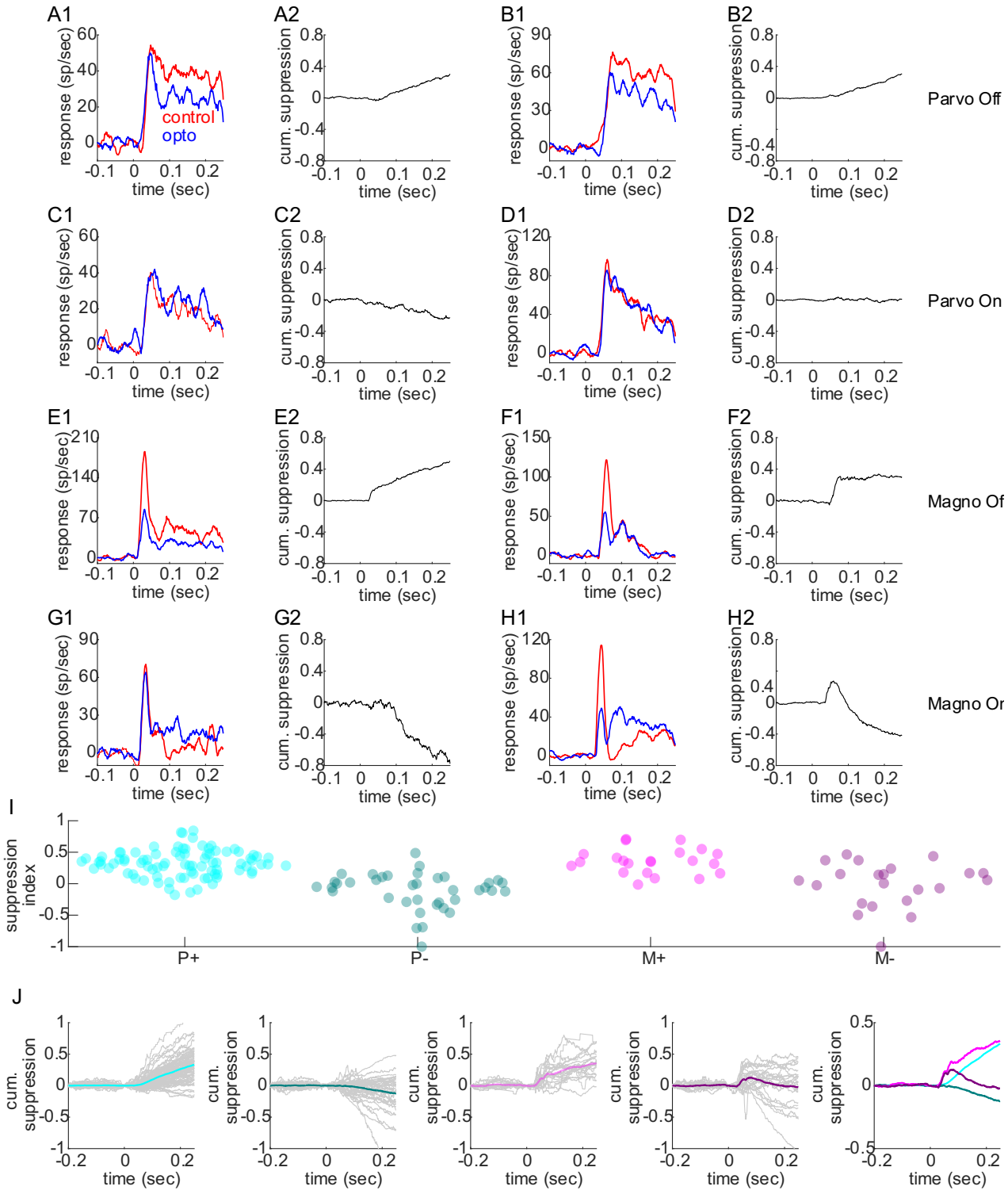

Figure 5. Example cell types with and without feedback. A1-B1. Average spike responses for two example Parvo Off cells under control (red) and feedback inactivation

(blue). C1-D1. Average spike responses for two example Parvo On cells under control (red) and feedback inactivation (blue). E1-F1. Average spike responses for two example Magno Off cells under control (red) and feedback inactivation (blue). G1-H1. Average spike responses for two example Magno On cells under control (red) and feedback inactivation (blue). A2-H2. A cumulative suppression over time (sec) was calculated under control conditions for each example cell. I. A suppression Index was calculated for each cell collected, and plotted according to cell type [P+: Parvo On (n = 45, light blue), P-: Parvo Off (n = 59, green), M+: Magno On (n = 16, pink), M-: Magno Off (n = 22, purple)]. A value of 1 indicates a high suppression index, and -1 indicates a high facilitation index. J. Each cell had cumulative suppression plot and plots were grouped by cell class type. For each cell class type, a population average cumulative suppression plot was calculated. The last plot has each average cell type cumulative suppression plot plotted.

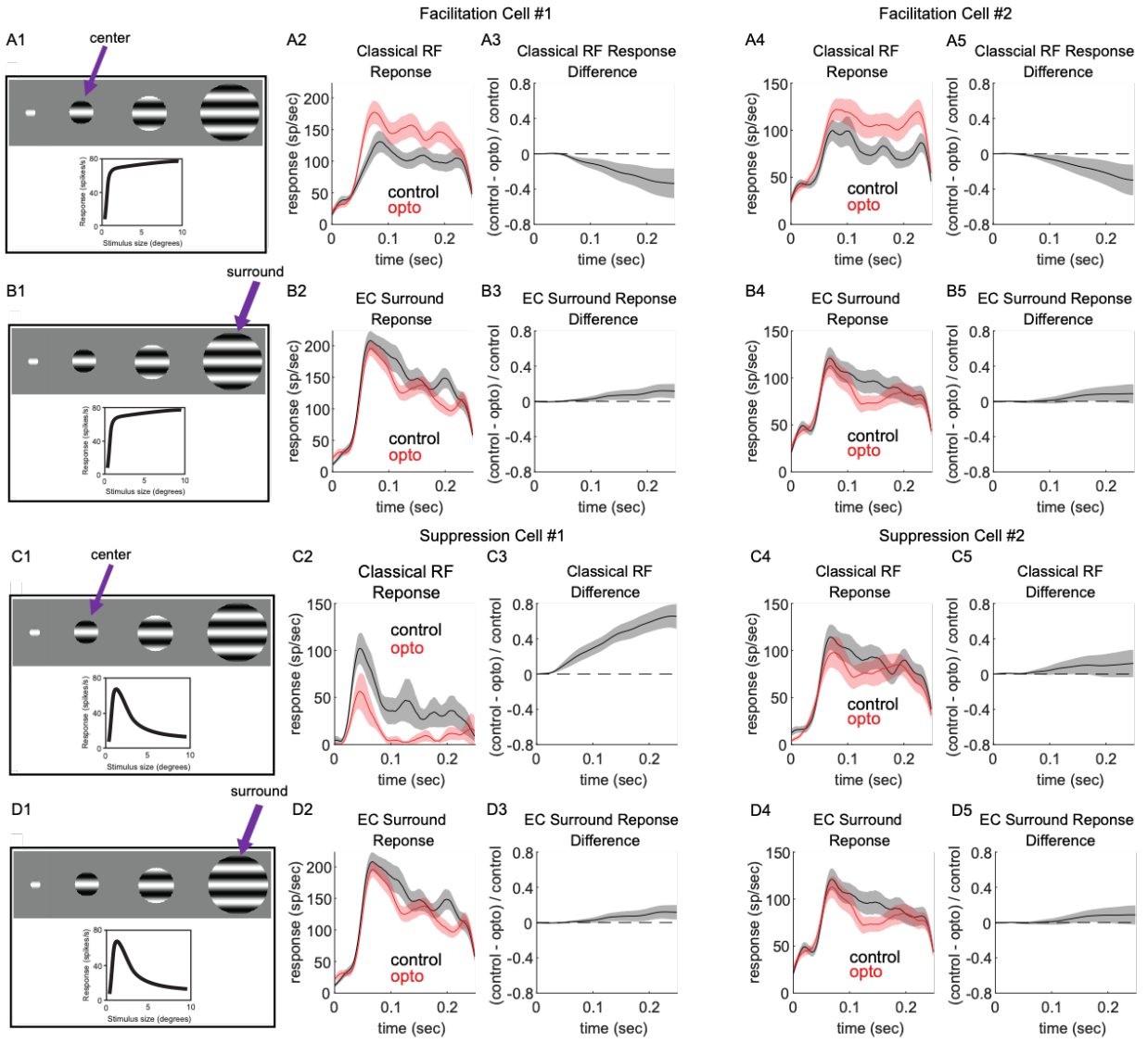

Figure 6. Examples of facilitation and suppression cells with and without feedback. A1-A5. Two examples of facilitation cells and their responses to center stimuli. Their classical receptive field responses were calculated over time (sec) under control (black) and optogenetic (red). An average classical receptive field cumulative difference comparing control to optogenetic trials for center stimuli was calculated and plotted for each example cell. B1-B5. The same examples of facilitation cells and their responses to surround stimuli. Their extraclassical receptive field responses were calculated over

time (sec) under control (black) and optogenetic (red). An average extraclassical surround cumulative difference was calculated comparing control to optogenetic trials for surround stimuli and plotted for each example facilitation cell. C1-C5. Two examples of suppression cells and their responses to center stimuli. Their classical receptive field responses were calculated over time (sec) under control (black) and optogenetic (red). An average classical receptive field cumulative difference comparing control to optogenetic trials for center stimuli was calculated and plotted for each example cell. D1-D5. The same examples of suppression cells and their responses to surround stimuli. Their extraclassical receptive field responses were calculated over time (sec) under control (black) and optogenetic (red). An average extraclassical surround cumulative difference was calculated comparing control to optogenetic trials for surround stimuli and plotted for each example suppression cell.

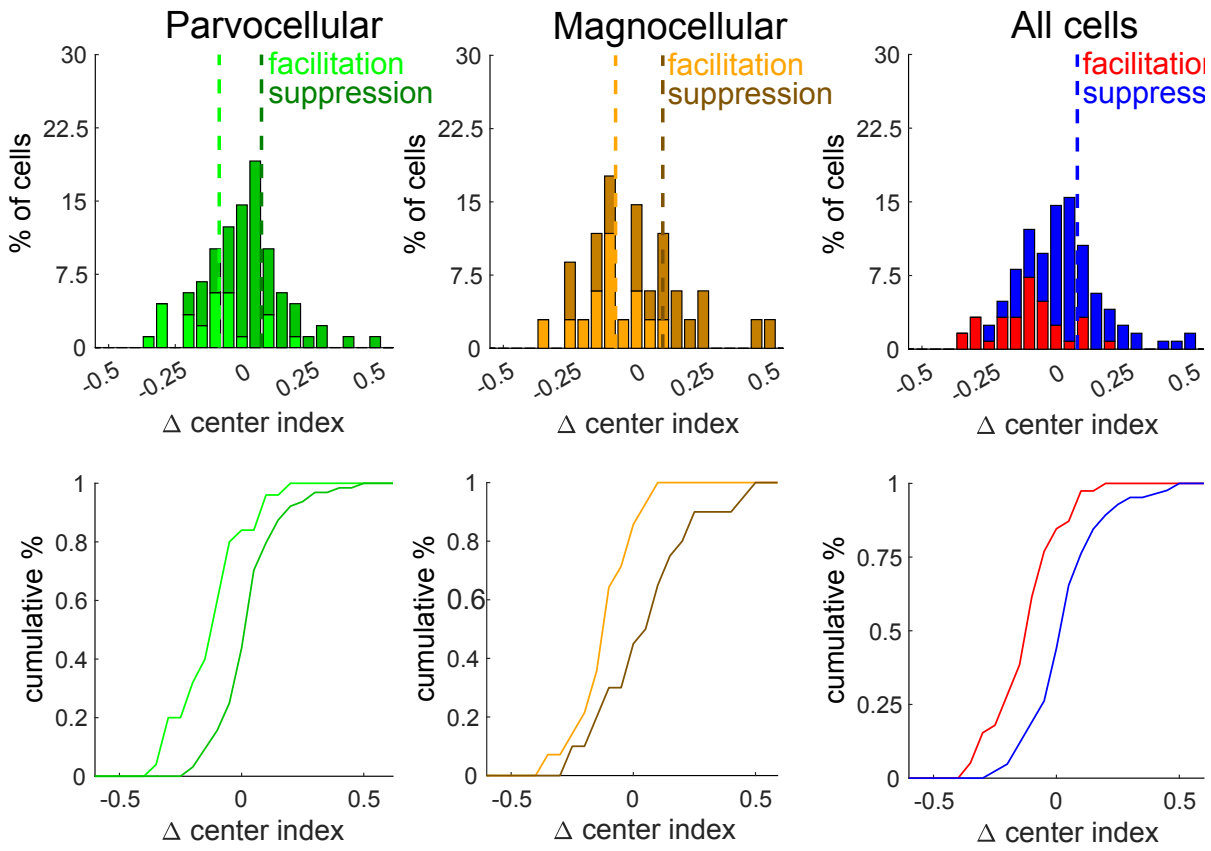

Figure 7. Center Modulation Index by cell type. A center modulation index was calculated for each cell type. Cells were divided into facilitation cells or suppression cells, and plotted under parvocellular geniculate cells (light green/dark green) (facilitation parvocellular cells mean = mean = -0.09 +/- 0.03 SE, p = 0.006, *t-test*; suppression parvocellular cells mean = 0.07 +/- 0.02 SE, *p = 6.03e-05, t-test*) [parvocellular cells mean = 0.03 +/- 0.01 SE, p = 0.0650, *t-test*], magnocellular cells (yellow/brown) (facilitation magnocellular mean = -0.08 +/- 0.03 SE, *p = 0.03, t-test,* suppression magnocellular mean = 0.10 +/- 0.05 SE, p = 0.0593, *t-test*) [magnocellular cells mean = 0.03 +/- 0.03 SE, p = 0.38], and all cells (red/blue) [all cells mean = 0.03 +/- 0.01 SE, *p = 0.0446, t-test*]. Center modulation index was significant for facilitation

(mean = -0.08 +/- 0.02 SE, $p = 3.68e\text{-}04$) and suppression cells (mean = 0.08 +/- 0.02 SE, $p = 1.64e\text{-}05$). Full stats found in Table 2 and Table 3. A percentage of cells for each cell type was plotted based on center modulation index (Δ center index). A cumulative percentage for either facilitation or suppression cells was plotted as a function of Δ center index.

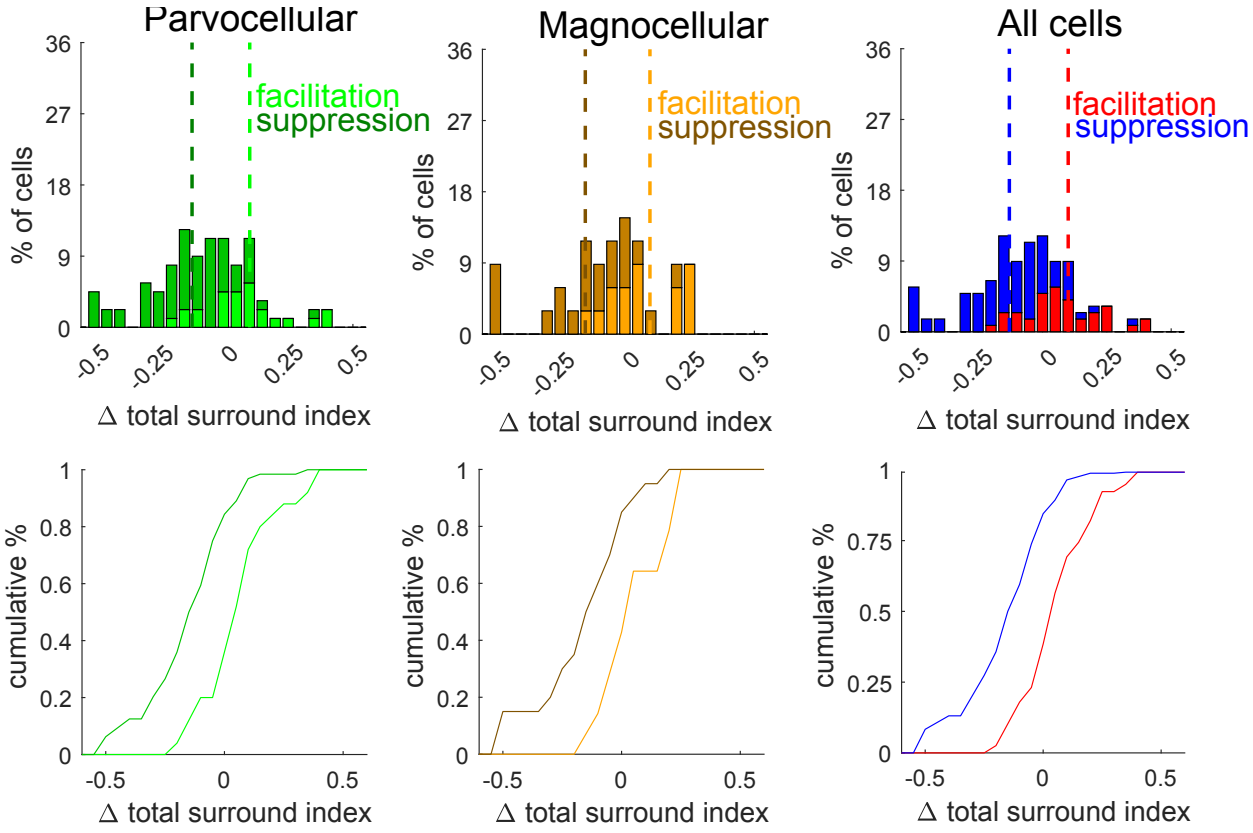

Figure 8. Total Surround Index by cell type. A total surround index was calculated for each cell type. Cells were divided into facilitation cells or suppression cells, and plotted under parvocellular geniculate cells (light green/dark green), magnocellular cells (yellow/brown), and all cells (red/blue). A percentage of cells for each cell type was plotted based on surround modulation index (Δ surround index). A cumulative percentage for either facilitation or suppression cells was plotted as a function of Δ surround index (facilitation total surround index mean = 0.02 +/- 0.02 SE, *p = 3.20e-04, t-test*; suppression total surround index mean = -0.05 +/- 0.02 SE, *p = 1.44e-06, t-test*; facilitation vs. suppression total surround index mean = -0.03 +/- 0.01 SE, *p = 0.01*, *t-test*).

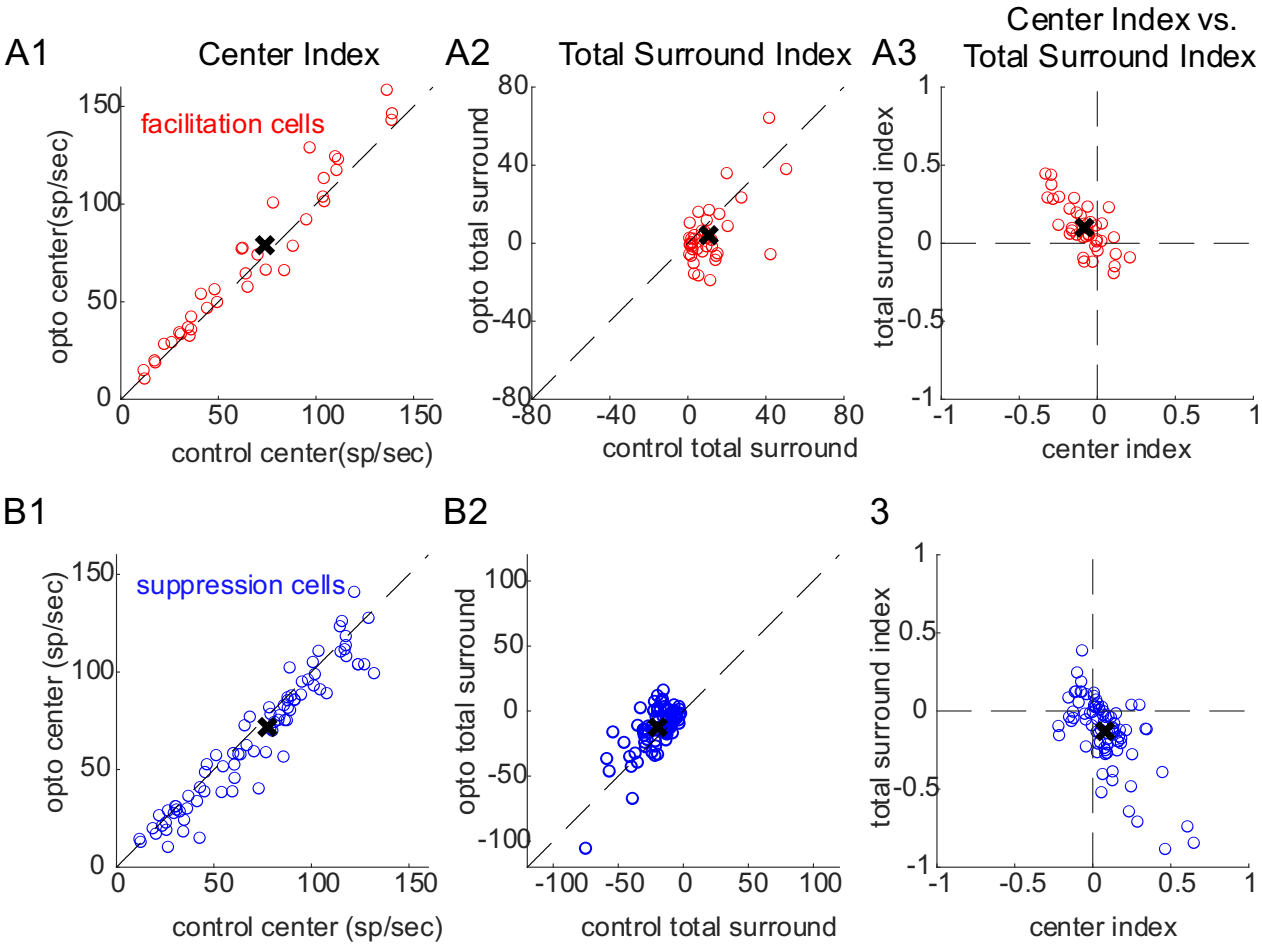

Figure 9. Suppression vs. Facilitation cells. A1. Center Index for each facilitation cell was compared and plotted against one another under control and optogenetic conditions. Slightly increased responses under optogenetic conditions. A2. Total Surround Index for each facilitation cell was compared and plotted against one another under control and optogenetic conditions, with a higher total surround index under control conditions. A3. Each facilitation cell's center index value was plotted against its respective total surround index. B1. Same as A1, but for suppression cells. Slightly higher center index under control conditions. B2. Same as A2, but for suppression cells. Higher total surround index under optogenetic conditions. B3. Same as A3, but for suppression cells.

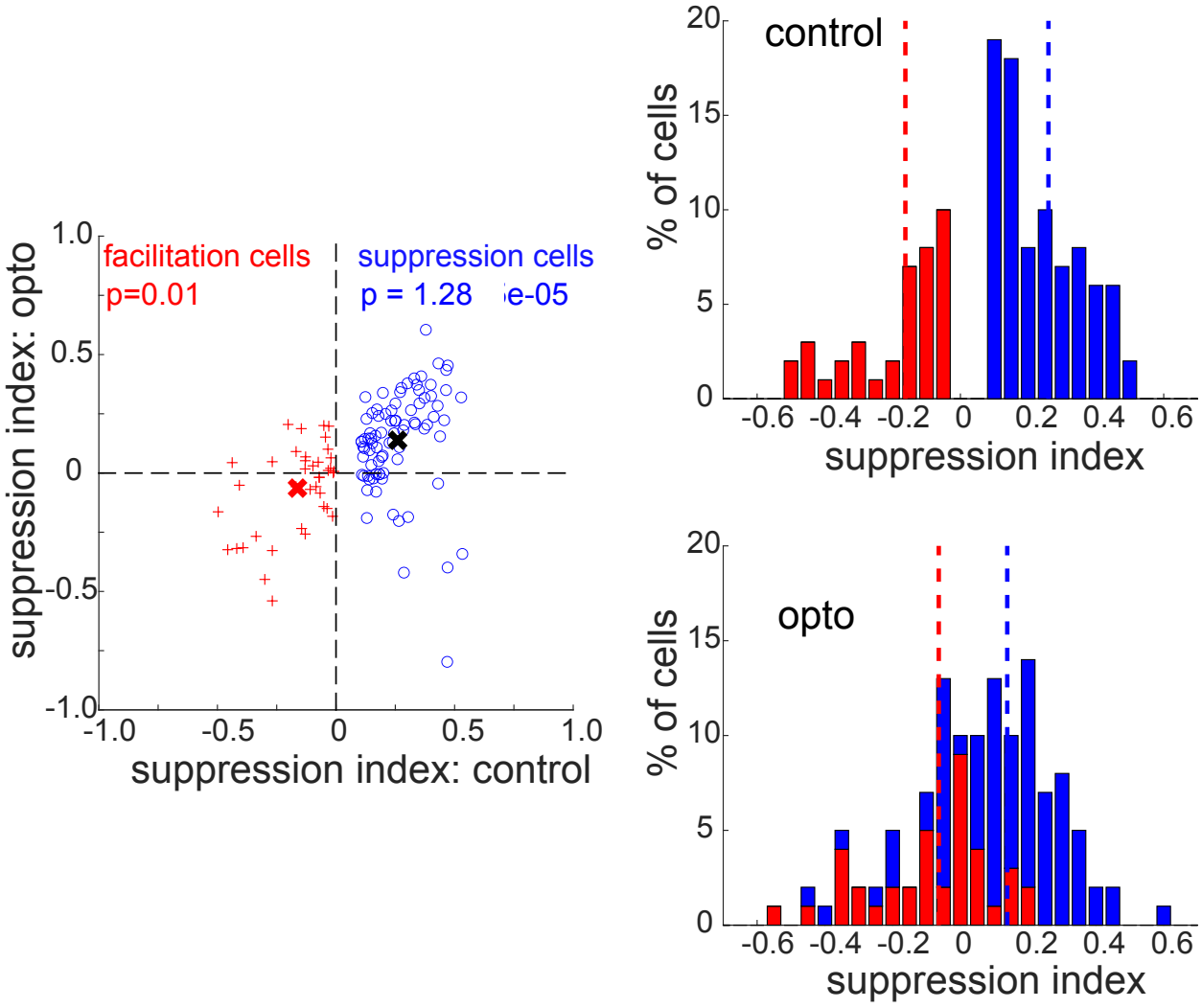

Figure 10. Suppression Index comparisons: facilitation vs. suppression cells. A suppression index was calculated for each individual cell under control and optogenetic trials, these values were compared and plotted against one another, with facilitation cells labelled in red (plus signs) and suppression cells labelled in blue (open circles). The average of each cell type is labelled as with an 'X' (facilitation cells in red and suppression cells in black for visibility). The suppression index for both control and

optogenetic trials was calculated for each individual cell (facilitation control mean = -0.16 +/- 0.02 SE, facilitation optogenetic mean = -0.06 +/- 0.03 SE, *p = 0.01, t-test*; suppression control mean = 0.26 +/- 0.01 SE, suppression optogenetic mean = 0.14 +/- 0.02 SE, *p = 1.28e-05, t-test*). The percentage of cells that fell under a suppression index value were plotted on a histogram for both control and optogenetic conditions (facilitation cells in red and suppression cells in blue). Dotted lines reflect means of each data type under each condition.

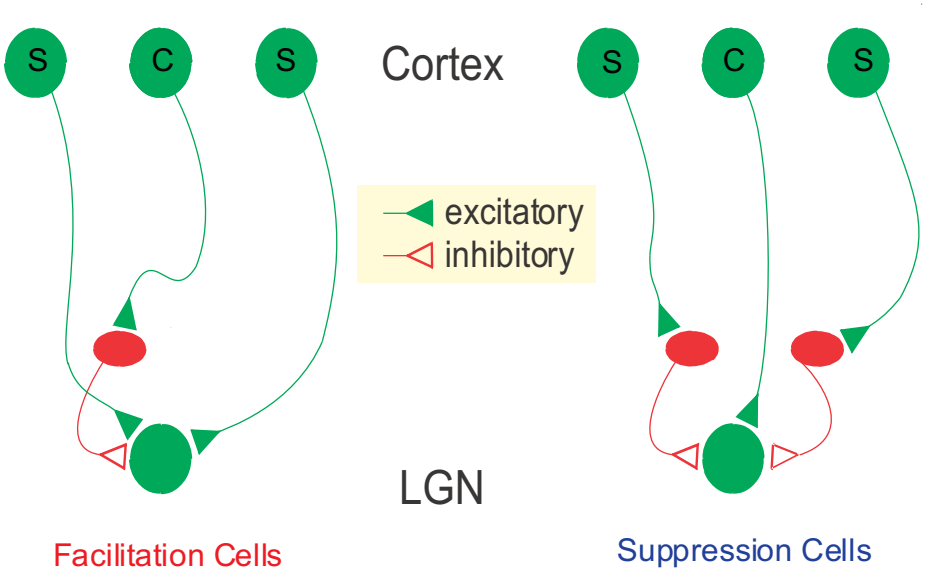

Figure 11. Revised feedback model: facilitation vs. suppression cells. A comparison model of corticogeniculate feedback, in which feedback has opposing effects on facilitation and suppression cells, depending on whether stimuli cover the center, classical receptive field, or extends into the surrounding, extraclassical receptive field. For facilitation cells, feedback provides inhibitory signals to center stimuli and excitatory signals to surround stimuli. In contrast, for suppression cells feedback provides excitatory signals to center stimuli and inhibitory signals to surround stimuli.

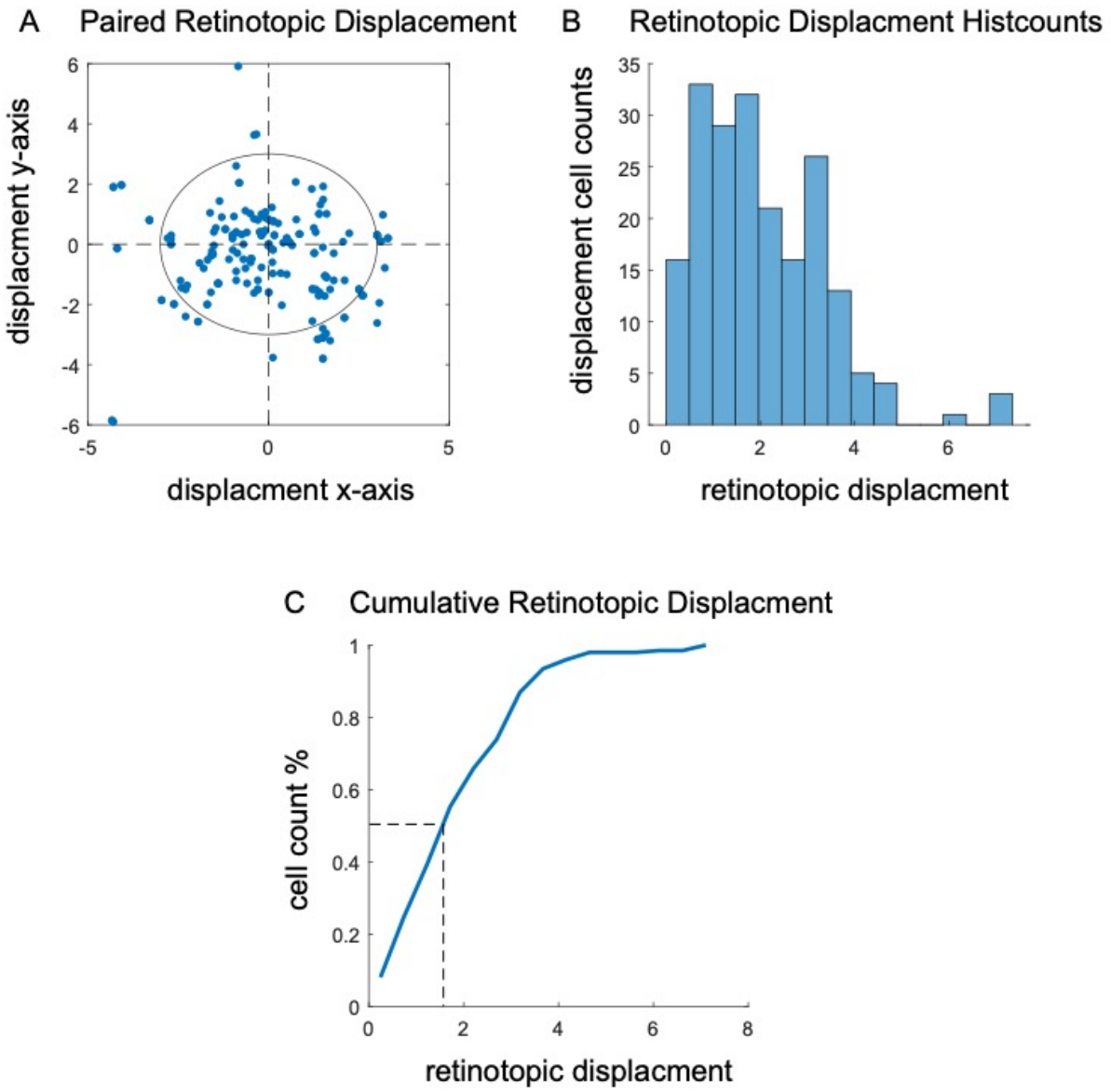

Supplemental Figure 1. Retinal Displacement. A. Paired retinotopic displacement between simultaneously recorded from LGN relay cells and V1 feedback cells. Displacement x-axis was calculated as the difference of x-axis coordinates of the V1 feedback cell receptive field from the x-axis coordinates of the LGN receptive field. Displacement y-axis was calculated as the difference of y-axis coordinates of the V1 feedback cell receptive field from the y-axis coordinates of the LGN receptive field. A circle was placed around 3° displacement. B. Retinotopic displacement histcounts for

retinotopic displacement values. C. A cumulative retinotopic displacement percentage of the histcounts, approximately 50% of cells fell under 2° retinotopic overlap, indicated by the dashed line.

Tables

Table 1
Cell Counts*

Cell Type	Parvo Cells (104)	Magno Cells (38)	Total (142)
ON Cells	45	16	61
OFF Cells	59	22	81
Facilitation Cells (82.05% On cells)	27 (20 ON; 7 OFF)	17 (12 ON; 5 OFF)	44 (32 ON; 12 OFF)
Suppression Cells (82.14% Off cells)	64 (12 ON; 52 OFF)	20 (3 ON; 17 OFF)	84 (15 ON; 69 OFF)
chi-square	**p = 1.19e-07** odd ratio = 17.3333 **Suppression in Off > Suppression in On**	**p = 6.57e-05** odd ratio = 34 **Suppression in Off > Suppression in On**	**p = 9.58e-12** odd ratio = 21.0084 **Suppression in Off > Suppression in On**

****Note: total counts do not always match because cells that had 0 modulation would not fall under either facilitation or suppression.***

Table 2
Center Modulation Index: Center Stimulus Response All Cells

Δ Center Index $= \frac{(control\ center\ response - opto\ center\ response)}{control\ center\ response}$

All Cells	Facilitation	Suppression	All
ON	**mean = -0.080 +/- 0.025 SE** **p = 0.003**	mean = 0.030 +/- 0.026 SE p = 0.27	mean = -0.032 +/- 0.016 SE p = 0.055
OFF	**mean = -0.097 +/- 0.037 SE** **p = 0.038**	**mean = 0.090 +/- 0.020 SE** **p = 3.08e-05**	**mean = 0.071 +/- 0.018 SE** **p = 2.21e-04**
All	**mean = -0.083 +/- 0.021 SE** **p = 3.68e-04**	**mean = 0.079 +/- 0.017 SE** **p = 1.64e-05**	**mean = 0.027 +/- 0.013 SE** **p = 0.0446**

significance indicated by bold

Table 3
Center Modulation Index: Center Stimulus Response by Cell Type

Δ Center Index $= \frac{(control\ center\ response - opto\ center\ response)}{control\ center\ response}$

Cell Type	Parvo Cells	Magno Cells
ON Cells	mean = -0.022 +/- 0.019 SE p = 0.2327	mean = -0.059 +/- 0.034 SE p = 0.1075
OFF Cells	**mean =0.064 +/- 0.020 SE** **p = 0.002**	**mean = 0.091 +/- 0.044 SE** **p = 0.0494**
Facilitation Cells	mean = -0.085 +/- 0.028 SE p = 0.006	**mean = -0.079 +/- 0.032 SE** **p = 0.03**
Suppression Cells	mean = 0.074 +/- 0.017 SE p = 6.03e-05	mean = 0.098 +/- 0.049 SE p = 0.0593
ON Facilitation Cells	**mean = -0.075 +/- 0.034 SE** **p = 0.04**	**mean = -0.088 +/- 0.036 SE** **p = 0.03**
ON Suppression Cells	mean = 0.038 +/- 0.025 SE p = 0.16	mean = -0.004 +/- 0.092 SE p = 0.9699
OFF Facilitation Cells	**mean = -0.127 +/- 0.043 SE** **p = 0.04**	mean = -0.024 +/- 0.050 SE p =0.71
OFF Suppression Cells	**mean = 0.082 +/- 0.020 SE** **p = 1.71e-04**	**mean = 0.116 +/- 0.055 SE** **p = 0.05**
All Cells	mean = 0.027 +/- 0.014 SE p = 0.065	mean = 0.028 +/- 0.031 SE p = 0.38

significance indicated by bold

Table 4
Surround Modulation Index: Surround Stimuli Response All Cells
Δ Surround Index = $\frac{(control\ surround\ response - opto\ surround\ response)}{control\ surround\ response}$**)**

All Cells	Facilitation	Suppression	All
ON	**-**	-	mean = -0.006 +/- 0.015 SE p = 0.68
OFF	-	**-**	**mean = -0.039 +/- 0.018 SE** **p = 0.04**
All	mean = 0.017 +/- 0.017 SE p = 0.32	**mean = -0.049 +/- 0.018 SE** **p = 0.008**	**mean = -0.025 +/- 0.012 SE** **p = 0.0473**

significance indicated by bold

Table 5
Total Surround Index: Total Surround Difference All Cells

Δ total surround index = Δ surround index - Δ center index

All Cells	Facilitation	Suppression	All
ON	-	-	mean = -0.006 +/- 0.015 SE p = 0.27
OFF	-	-	**mean =-0.039 +/- 0.018 SE** **p = 8.19e-05**
All	**mean = 0.017 +/- 0.017 SE** **p = 3.20e-04**	**mean = -0.049 +/- 0.018 SE** **p = 1.44e-06**	**mean = -0.025 +/- 0.012 SE** **p = 0.007**

***significance indicated by bold**

Table 6
Suppression Index by Cell Types for On/Off and Facilitation/Suppression

$$Suppression\ Index = \frac{Response\ to\ surround\ grating}{Response\ to\ center\ grating}$$

Cell Types	Control	Optogenetic	Statistics
On Cells	-0.038 +/- 0.025 SE	-0.011 +/- 0.024 SE	p = 0.4455
Off Cells	**0.231 +/- 0.018 SE**	**0.124 +/- 0.025 SE**	**p = 7.18e-04**
Facilitation Cells	**-0.162 +/- 0.023 SE**	**-0.064 +/- 0.029 SE**	**p = 0.01**
Suppression Cells	**0.260 +/- 0.013 SE**	**0.138 +/- 0.024 SE**	**p = 1.29e-05**
All Cells	**mean = 0.115 +/- 0.018 SE**	**mean = 0.066 +/- 0.019 SE**	**p = 0.0601 (ranksum p = 0.0531)**

significance indicated by bold

Table 7
Suppression Index by Cell Types Magno/Parvo, On/Off, Facilitation/Suppression

$$Suppression\ Index = \frac{Response\ to\ surround\ grating}{Response\ to\ center\ grating}$$

Cell Type	Control	Optogenetic	Statistics
Parvo	0.138 +/- 0.020 SE	0.092 +/- 0.020 SE	p = 0.11
Parvo ON	-0.004 +/- 0.026 SE	0.003 +/- 0.026 SE	p = 0.85
Parvo OFF	**0.245 +/- 0.021 SE**	**0.159 +/- 0.027 SE**	**p = 0.01**
Parvo Suppression	-	-	**p = 2.33e-04**
Parvo Facilitation	-	-	**p = 0.0449**
Magno	0.055 +/- 0.039 SE	-0.004 +/- 0.039 SE	p = 0.29
Magno ON	-0.134 +/- 0.057 SE	-0.052 +/- 0.051 SE	p = 0.30
Magno OFF	**0.192 +/- 0.030 SE**	**0.032 +/- 0.056 SE**	**p = 0.02**
Magno Suppression	-	-	**p = 0.02**
Magno Facilitation	-	-	p = 0.12

significance indicated by bold

Chapter 4: General Discussion

Within the retino-geniculo-cortical visual pathway, the LGN is traditionally viewed as simply a “relay center” of visual information leaving the eye to be sent to cortex. This is in large part due to the driving inputs of retinal ganglion cells that largely determine the visual properties of their LGN relay cell targets. However, as mentioned in Chapter 1, the majority of synapses in the LGN do not come from retinal ganglion cells, but instead come from other extraretinal inputs. Additionally, there are several aspects of LGN visual processing that are important for modifying incoming retinal signals. Of such, visual processing in the LGN includes active encoding of the spatial and temporal influences of response gain of visual signals (i.e., contrast gain control), transforming the temporal structure of its retinal inputs, and preserving retinal inputs while simultaneously increasing the signal-to-noise of its retinal signals. Consequently, LGN encoding is extremely important for appropriate visual processing.

In this dissertation, two unique aspects to LGN relay cells are discussed. First, the membrane of geniculate relay cells has specialized T-type Ca^{2+} channels that allow for a rapid influx of calcium to flow into the cell, triggering a rapid succession of Na+-based action potentials, referred to as “bursts.” This mode of firing is thought to preferentially drives cortical cells in the primary visual cortex due to both temporal summation and a release from synaptic depression. Importantly, after a burst event, LGN relay cells return to tonic firing and a sufficient amount of time is needed before a burst event can occur again. Thus, spikes sent to cortex from the LGN after and between bursts are thought to convey fine details in the visual stimulus whereas bursts may serve as a “wake-up” call to cortex while also conveying course details in the visual stimulus. Uniquely, bursting requires first a de-inactivation of the inactivation gate in T-

type Ca^{2+} channels followed by the opening of the activation gate in T-type Ca^{2+} channels. This results in a rapid influx of Ca^{2+} producing a Ca^{2+} potential that triggers the opening of voltage-gated Na^{+} channels that lead to a rapid train of spikes, a burst. With the time-voltage requirement of an inactivation gate, followed by an activation gate, the phenomena of bursting occurs more readily under low arousal states or following periods of anti-preferred visual stimulation that can hyperpolarize cells. Either way, bursting almost always occurs in response to the initial presentation of a stimulus within the geniculate relay cell's receptive field. Previous literature has proposed this phenomenon of bursting under low arousal states to function as a "wake-up" call to cortex. Within this dissertation, we investigated how bursting changed as a function of the contrast of visual inputs on individual relay cells. We found that burst rate, individual geniculate relay cell reliability, and geniculate relay cell timing precision are all significantly greater with higher contrast stimuli compared to lower contrast stimuli. Additional analysis from simultaneous recordings of synaptically connected retinal ganglion cells and LGN neurons further revealed the time/voltage dynamics underlying burst activity. Together, results presented in Chapter 2 support the hypothesis that stimulus contrast along with the biophysical properties underlying the state of T-type Ca^{2+} channels interact to influence burst activity, presumably to facilitate thalamocortical communication and stimulus detection.

Outside of the biophysical properties of geniculate relay cells, the majority of the inputs coming to the LGN are nonretinal, with most coming from corticogeniculate feedback cells located in layer 6 of V1. Anatomically, corticogeniculate feedback projections onto the LGN have larger terminal fields than those from the retina; they are

also larger than the terminal fields of individual LGN neurons in cortex, approximately 2–3 times larger (Murphy & Sillito 1996). As a result, individual corticogeniculate feedback cells could influence activity across a larger pool of LGN cells compared to individual retinal ganglion cells. Additionally, corticogeniculate feedback cells synapse more distally on axons of the geniculate cells compared to proximal synapses seen from their retinal inputs, but instead synapse distally on the dendrites of geniculate cells. Although corticogeniculate inputs largely outnumber retinogeniculate synapses, individual inputs from corticogeniculate feedback cells have significantly smaller EPSP amplitudes than their retinal ganglion cell counterparts (reviewed in Sherman & Guillery 2009). Consequently, while feedback is the largest proportion of input to individual geniculate relay cells, these feedback synapses are modulatory in nature. In this dissertation, we explored how corticogeniculate feedback modulates individual geniculate relay cells as a function of cell type and the physical size of the visual stimulus. For geniculate cells that experience extraclassical surround facilitation, corticogeniculate feedback provides center suppression and extraclassical surround excitation. Equally, for geniculate relay cells that experience extraclassical surround suppression, corticogeniculate feedback provides center excitation and extraclassical surround suppression. Thus, our data supports the idea that for LGN cells with surround facilitation, corticogeniculate feedback functions to extend receptive field boundaries, improving the system's ability to detect a stimulus. In contrast, for LGN cells with surround suppression, corticogeniculate feedback functions to sharpen receptive field boundaries and improve the system's ability for stimulus discrimination. Importantly, as discussed in Chapter 3, for corticogeniculate feedback activity to effectively modulate

geniculate cells, the animal needs to be awake. Under general anesthesia, corticogeniculate feedback activity is largely silent. Additionally, without a task demand from higher cortical areas, corticogeniculate feedback may not have much of an influence on visual processing. Lastly, it is possible that corticogeniculate feedback is turned off when an animal is unconscious, as the corticothalamic pathway may be involved in a completely different process to uncouple the thalamus from the cortex.

Previous literature has demonstrated that under anesthesia, feedback neurons are largely inactive and geniculate cell activity is low. With this in mind, geniculate bursting and corticogeniculate feedback could interact with one another to allow for normal geniculate relay cell visual processing as the system shifts from a general low arousal state to targeted encoding and processing. As geniculate cell bursting may function as a “wake-up” call to cortex under low arousal states, where bursting functions to signal to cortex that visual stimuli have entered the geniculate cell’s receptive field. When a burst event occurs, it propagates down the geniculate cell’s axon to its synaptic targets. Not only do these axons project to the layer 4C (4Cα for magnocellular axons and 4Cβ for parvocellular axons) of V1, they also project to their respective tiers of layer 6 (parvocellular axons to the upper tier of layer 6 and magnocellular axons to lower tier of layer 6), where corticogeniculate feedback cells reside. Thus, it is possible that bursting functions to not only prime the primary visual cortex to the incoming LGN relay cell signal, but also to activate corticogeniculate feedback cells to modulate and attenuate LGN relay cell activity. Importantly, after a burst event, the geniculate relay shifts back to tonic firing responses to incoming visual signals. This could be a natural product of the inherent timing of the T-type Ca^{2+} channels activity, or the shift into tonic

mode could be facilitated by divergent corticogeniculate feedback projections back onto the LGN. If bursting assists in activating corticogeniculate feedback cell activity and feedback is contributes to size tuning in the LGN, then bursting could be important for both corticogeniculate feedback activity and for the maintenance of receptive field properties in the LGN under low arousal states.

It is also possible that corticogeniculate feedback assists in facilitating burst events in the LGN. Feedback's modulation of classical and extraclassical receptive field responses could promote the ability of geniculate relay cells to produce bursts. Importantly, bursting first requires the de-inactivation T-type Ca^{2+} channels and then the opening of the activation gate in T-type Ca^{2+} channels. With this in mind, the general relationship between a visual stimulus and the receptive field over time is important for geniculate cell activity. If a visual stimulus first occurs in the extraclassical surround of a geniculate cell, corticogeniculate feedback could modulate the membrane potential of the cell, depending on whether the geniculate cell experiences extraclassical surround facilitation or suppression. For geniculate cells that experience extraclassical surround suppression, visual stimuli that exist only in the extraclassical receptive field could modulate the geniculate relay cell into more of a suppressed state, which would allow for the inactivation gate of T-type Ca^{2+} channels to be de-inactivated/primed. Once the visual stimulus enters the classical receptive field of the geniculate cell, the geniculate relay cell would become excited, triggering the opening of the of T-type Ca^{2+} channels activation gate, a rapid influx of Ca^{2+}, and a burst. Simultaneously, corticogeniculate feedback effects from stimuli restricted to the classical receptive for these geniculate cell types is excitatory, further promoting both bursting and subsequent tonic activity. This

could preferentially drive cortex to communicate that a visual stimulus was entering the geniculate cell's receptive field. Conversely, if the geniculate cell was a facilitation cell, visual stimuli over the classical receptive field would receive an inhibitory signal from feedback, assisting in priming the cell's T-type Ca^{2+} channels, and the cell would be able to burst once the visual stimulus entered its extraclassical receptive field, where feedback modulates the geniculate relay cell signal and its facilitation to surround stimuli. This could preferentially drive cortex to communicate that a visual stimulus was leaving the geniculate relay cell's receptive field. Thus, for LGN cells with surround facilitation, corticogeniculate feedback (and bursting) may function together to extend receptive field boundaries, improving the system's ability to detect a stimulus. For LGN cells with surround suppression LGN, feedback (and bursting) may function together to sharpen receptive field boundaries to improve the system's ability for stimulus discrimination.

Lastly, if corticogeniculate feedback is itself modulated by geniculate bursting, feedback's projections to the LGN after bursting could be either excitatory or inhibitory to individual LGN cells as feedback projections provide monosynaptic excitation and/or disynaptic inhibition through either the TRN or local inhibitory neurons. As individual corticogeniculate feedback cell projections have a footprint across multiple LGN cells, feedback cells could modulate individual geniculate cell activity differently depending on retinotopic overlap, such as providing necessary modulatory input onto geniculate cells with receptive field located on the edges of the feedback cell's receptive field. If bursting contributed to feedback projections becoming excitatory, feedback would allow LGN

cells to continue to fire in tonic mode and if the signal from feedback became inhibitory, it would further the ability for geniculate cells to be primed to burst.

As things such as arousal state and task demand are known to change the overall activity in both LGN cells and corticogeniculate feedback cells, it is important to understand the unique feedforward thalamocortical and feedback corticothalamic interactions simultaneously during visual processing. Within this discussion, the relationship of bursting and corticogeniculate feedback is explored in an effort to understand how these two early brain regions function during visual processing. This dissertation highlights unique aspects to geniculate relay cell visual processing that is important and necessary for a functional visual system.

The LGN is a ubiquitous and evolutionarily conserved region of the thalamus important for the visual system. Its relationship with V1can be viewed as a model for other thalamocortical interactions in other sensory systems. In order for neuroscience to achieve an all-encompassing understanding of the importance of the LGN during visual processing, we must first reframe the traditional view of the LGN as a simple relay center to cortex. This dissertation serves as an example of how the LGN is much more than just than a simple relay.

Appendix: Eye to Brain: Parallel Visual Pathways

For citation of this appendix chapter, please use its publication citation: Sanchez, A.N., Alitto, H.J., Usrey, W.M. (2020). Eye to Brain: Parallel Visual Pathways In P. Martin (Eds.), The Senses: A Comprehensive Reference, 2nd Edition. Elsevier. 10.1016/B978-0-12-809324-5.24157-6.

Abstract

Visual processing begins in the eye where neural circuits establish the response properties of multiple classes of retinal ganglion cells (RGCs). Each of these RGC classes has a distinct pattern of projection to targets in the brain, and each serves as a unique filter for different features in the visual scene. Several of these RGC classes innervate relay cells in the lateral geniculate nucleus (LGN) of the dorsal thalamus where their input remains segregated onto different classes of LGN neurons which, in turn, innervate distinct cortical circuits within primary visual cortex (V1). In this way, visual information flows from retina through the thalamus to cortex via multiple, parallel pathways allowing different features of the visual scene to be processed separately and independently from each other. Here, we examine the anatomical and physiological organization of the parallel retino-geniculo-cortical pathways and consider their relationship to the parallel feedback pathways which complete a reciprocal loop of information exchange between thalamus and cortex. Although parallel retino-geniculo-cortical pathways are present in all mammals, we focus on the feline, primate, and rodent, where most research has been done and we have the greatest knowledge.

Synopsis

Multiple streams of retino-geniculo-cortical projections, or parallel pathways, link the retina with the primary visual cortex. Each of these streams provides the cortex with unique information about the visual scene, thus providing flexibility in how the cortex combines and segregates incoming signals for further processing. This review examines the strengths and constraints of parallel processing by comparing and contrasting the functional organization of the retino-geniculo-cortical pathway in felines, primates, and rodents.

Introduction

For all sensory systems, neurons near the periphery serve as filters to capture specific attributes of the sensory world. For the visual system, massive amounts of information are extracted and parceled into parallel pathways beginning in the eye. These parallel pathways are first established in the retina and are transmitted to the brain via the axons of multiple classes of retinal ganglion cells (RGCs), the output cells of the retina, that vary in their responses to stimulus features such as luminance contrast, color, spatial frequency, and temporal frequency. While there are many benefits to parallel processing, including a greater repertoire of signals that can be used for specialized functions in downstream neurons, the number of parallel processing streams leaving the eye has limits, including restrictions imposed by the size of the optic nerve, which contains approximately 1.2 million axons in the macaque monkey (Sanchez, Dunkelberger and Quigley, 1986).

Visual information from the retina is transmitted to visual cortex (V1) via distinct classes of neurons in the lateral geniculate nucleus (LGN) of the dorsal thalamus that individually receive stream-specific input from the different classes of RGCs. The LGN is therefore considered the gateway for visual signals supplied to cortex, and its shape and size reflects the parallel pathways it accommodates (Figure 1). Within V1, a complex architecture of diverse cortical circuits serves to maintain stream specificity as well as combine information traveling in the parallel pathways to generate a broader array of receptive fields and neuronal responses than is present in the inputs to the cortex. In this manner, parallel visual pathways from the eye to brain form the foundation for visual perception and many forms of visually guided behavior.

A brief history of parallel pathways

The concept of parallel pathways can be traced back to the nascent days of brain research and is rooted in descriptions of what we now call “labeled lines”. In the early 19th century, Charles Bell and Francois Magendie independently argued for what Johannes Müller later termed the “specific energy of nerves”, in which the nature of sensory perception is determined by the pathway being activated. In 1860, Helmholtz expanded on this idea in the “Handbook of Physiological Optics” (2000) where he described Thomas Young’s theory of color vision (1807) in the following manner: “The eye is provided with three distinct sets of nervous fibers. Stimulation of the first excites the sensation of red, stimulation of the second the sensation of green, and stimulation of the third the sensation of violet.” Given the technical limitations and knowledge available at the time, these ideas were remarkably insightful and, importantly, established a framework for approaching and investigating parallel pathways.

Parallel pathways begin in the eye

The majority of RGCs have a center-surround organization. In the 1950s, Stephen Kuffler reported that on-center/off-surround and off-center/on-surround cells were found at every location across the entire retina (Kuffler, 1952, 1953). A major implication from this finding is that there are at least two complete and complementary representations of the visual world that travel together, i.e. ‘parallel’, in optic nerve axons. Estimates on the number of complete representations present in the optic nerve has grown rapidly, as we now know that there are at least 19 distinct types of RGCs that tile the eye and provide the brain with visual information (reviewed in Crook, Packer, Troy, and Dacey, 2014). While the details of many of these cell classes remain elusive, we now know a

great deal about the major retinogeniculate pathways in the feline and primate, and information is accumulating for the rodent visual system at an unprecedented rate.

Felines

After the discovery of on- and off-center RGCs, evidence for parallel pathways grew rapidly, as several additional functional classes of RGCs were identified in the cat. In a groundbreaking study, Enroth-Cugell and Robson (1966) distinguished two response classes within the on and off pathways, which they termed X and Y. The visual responses of X cells can be accounted for by simple summation of their excitatory and suppressive inputs (linear summation), whereas the responses of Y cells indicate more complex interactions between inputs (nonlinear summation) as exemplified with a 'null test'. In contrast to X-cells, which have a phase-dependent null point in their responses to counterphasing sinusoidal stimuli (consistent with linear summation of inputs), the responses of Y cells show a phase-dependent frequency doubling. This response property is believed to result from nonlinear subunits (Hochstein and Shapley, 1976; Derrington, Lennie, and Wright, 1979) involving rectifying amacrine cells and bipolar cells (Stafford and Dacey 1997, Demb, Zaghloul, Haarsma and Sterling, 2001).

Although the distinction of X and Y cells on the basis of linear summation may seem rather abstract, X and Y cells also differ from each other in several additional and important ways. The X cells (independently identified and termed beta cells by anatomists) have smaller dendritic fields, smaller receptive fields, slower axonal conduction velocities, longer visual response latencies, respond in a sustained fashion to stationary stimuli, and prefer stimuli with lower temporal frequencies. By contrast, Y cells (independently identified and termed alpha cells by anatomists) have larger

dendritic fields, larger receptive fields, faster axonal conduction velocities, shorter response latencies, respond transiently to stationary stimuli, and follow stimuli at higher temporal frequencies (reviewed in Lennie, 1980; Sherman and Guillery, 2009; Usrey and Alitto, 2015). Unlike their target cells in the cortex, both of these cell types are largely nonselective for stimulus orientation or direction of motion.

Separate from the X and Y cells, a third group of cells, W cells, broadly include all of the cell types that do not fit neatly within the X and Y cell categories. The W cells comprise several unique cell classes that we know relatively little about, except that each is thought to tile the retina. Some of the response properties documented for these cell types include on/off responses and direction selectivity, responses not evident in X and Y cells. Projections from these cell types differ as well. The W cells that innervate the LGN target relay cells that project to the superficial layers of cortex, whereas X and Y RGCs target relay cells that innervate layer 4 (Figure 2; LeVay and Gilbert, 1976; Humphrey, Sur, Uhlrich and Sherman, 1985; see also Carey, Fitzpatrick and Diamond, 1979).

In common with the retina, the cat LGN also contains X cells, Y cells, and W cells (Figure 3). To a first approximation these cell types largely reflect those of their retinal inputs, and the main characteristics of retinal X and Y cells are maintained in the LGN. For example, similar to the RGCs that provide their input, Y-cells in the LGN have larger dendritic fields, larger receptive fields, faster conducting axons, shorter visual response latencies, respond more transiently to visual stimuli, and follow stimuli at higher temporal frequencies in comparison with X-cells (Figure 3; Cleland, Dubin and Levick, 1971a,b; Fukada, 1971; Ikeda and Wright, 1972; Usrey, Reppas and Reid, 1999).

However, there are several nonlinear receptive field properties that are augmented in the LGN by nonretinal processes in both X and Y cells (Jones, Andolina, Oakely, Murphy and Sillito, 2000; see also Alitto and Usrey, 2004). In particular, contrast gain control, contrast-dependent response phase, and extraclassical suppression are more robust in the LGN than in the retina (Fisher, Alitto and Usrey, 2017; Alitto, Rathbun, Fisher, Alexander and Usrey, 2019). While these nonlinear response properties are present in both X and Y cells, they are typically more pronounced in Y cells.

The projections of X, Y, and W cells to the cortex indicates that there is both stream mixing and stream segregation in the geniculocortical pathway. As mentioned above, LGN W cells project to the superficial layers of V1, whereas LGN X and Y cells project to layer 4. Within layer 4, the axons of X and Y cells are partially overlapping. This suggests a substrate for stream mixing, a suggestion supported with studies examining the inputs to individual layer 4 cells (Alonso, Usrey and Reid, 196, 2001), as well as for stream segregation.

Primates

Similar to the cat, the primate retina contains a diversity of cell types that provide the substrate for multiple parallel pathways of information flow to the brain (reviewed in Thoreson and Dacey, 2019; Grünert and Martin, 2020). Many of these cell types project to the LGN which contains three types of layers—the magnocellular, parvocellular, and koniocellular layers. Within each of these categories, there are separate classes of relay cells that convey on and off information. Importantly, cells within the magnocellular, parvocellular, and koniocellular layers differ from each other substantially in their cellular morphology, visual physiology, sources of retinal input, and projections to visual cortex

(Schiller and Logothetis, 1990; Merigan and Maunsell, 1993; Casagrande, 1994; Casagrande and Kaas, 1994; Lee, 1996; Hendry and Reid, 2000; Nassi and Callaway, 2009; Usrey and Alitto, 2015).

Compared to parvocellular LGN neurons, magnocellular neurons have larger cell bodies, larger receptive fields, faster conducting axons, shorter visual response latencies, more transient responses to visual stimuli, and greater response gain than do parvocellular neurons. Magnocellular neurons also have achromatic receptive fields, whereas parvocellular neurons, at least in Old World monkeys and some New World monkeys, have receptive fields that are chromatically selective. Specifically, parvocellular receptive fields are red/green color opponent, where inputs from the long (L) and medium (M) wavelength cones are antagonistically arranged to form the center-surround receptive field (Reid and Shapley, 1992, Reid and Shapley, 2002) More so than in the cat, the axonal projections of magnocellular and parvocellular neurons to primary visual cortex are strictly segregated (Figure 3).

Magnocellular and parvocellular LGN neurons also differ in their projections to primary visual cortex. Magnocellular axons terminate in cortical layer 4Cα and parvocellular axons terminate in layer 4Cβ. Consequently, layer 4C stellate cells with dendrites restricted to either layer 4Cα or 4Cβ receive stream-specific input from the LGN. However, cells in layers 5 and 6 with apical dendrites that pass through layers 4Cα and 4Cβ have the opportunity to sample from both the magnocellular and parvocellular streams.

Similar to W cells in the cat, we know relatively less about neurons in the koniocellular layers than we do for neurons in the magnocellular and parvocellular

layers. The koniocellular layers are located beneath and between each of the magnocellular and parvocellular layers. Neuronal density in the koniocellular layers is lower than that in the magnocellular and parvocellular layers, which explains, in part, why we have more limited information about these cell types. Also similar to W cells, a distinguishing feature of koniocellular neurons is that their axons bypass cortical layer 4 and terminate, instead, in the cytochrome-oxidase rich 'blobs' in the superficial layers of primary visual cortex (Fitzpatrick, Itoh and Diamond, 1983; Casagrande, Yazar, Jones and Ding, 2007). Furthermore, neurons in the koniocellular layers are a diverse group containing multiple subclasses of cells that receive input from distinct classes of RGCs, including the small and large bistratified cells, the recursive monostratified and bistratified cells, the smooth and sparse inner cells, and the narrow and broad thorny cells (Dacey and Packer, 2003; Wässle, 2004; Masland, 2011, 2012; Crook, Packer, Troy and Dacey, 2014; Masri, Percival, Koizumi, Martin and Grünert, 2019). Unlike magnocellular and parvocellular LGN neurons, which have monocular responses, some koniocellular neurons have binocular responses (Zeater, Cheong, Solomon, Dreher and Martin, 2015), suggesting that individual koniocellular neurons combine retinal inputs either directly or through polysynaptic circuits. Like parvocellular neurons, a subset of koniocellular neurons have chromatically selective receptive fields, with input from the short (S) cones being antagonistic to mixed input from the medium (M) and long (L) wave length cones (Dacey and Lee, 1994; Hendry and Reid, 2000). Finally, as further evidence of the diversity of circuits that establish responses in the koniocellular layers, we now have a fairly complete understanding of the circuitry that underlies the orientation and directional tuning of a subset of koniocellular neurons (Cheong, Tailby,

Solomon and Martin, 2013; Percival, Koizumi, Masri, et al., 2014), selectivity that is absent in the parvocellular and magnocellular layers.

Taken together, many of the features that distinguish the magnocellular, parvocellular, and koniocellular streams in the primate are similar to those that distinguish the Y cell, X cell, and W cell streams in the feline.

RODENTS

Research on the mouse visual system has increased rapidly in recent years, due in large part to the wealth of molecular tools for identifying cell types, dissecting neural circuits, and manipulating neuronal activity. Thus, while mice do not rely as heavily on their visual system as do felines and primates, mice offer insight into visual processing that is currently difficult, if not impossible, to study in other species and mice have become a valuable model system for vision science.

Experiments have identified and characterized a greater diversity cell types and response properties in the mouse LGN than has been reported for either cats or primates. Among this diversity are a greater proportion of cells with response properties generally considered more typical of cortical neurons, such as orientation selectivity and direction selectivity, as well as cells with response properties not reported for cats and monkeys, such as selectivity for the axis of motion or the absence of contrast (Huberman, Wei, Elstrott et al., 2009; Marshel, Kaye Nauhaus and Callaway, 2012; Piscopo, El-Danaf, Huberman and Niell, 2013; Scholl, Tan, Corey and Priebe, 2013; Cruz-Martín, El-Danaf and Osakada, et al., 2014; Tang, Ardila Jimenez, Chakraborty and Schultz, 2016; see also Barlow, Hill and Levick, 1964). These cell types are primarily located in the dorsal “shell” region of the LGN (Figure 3). Given our limited

knowledge on the diversity of cell types in the cat W pathway and the primate koniocellular pathway, one might expect the novel cell types identified in the mouse LGN to have counterparts in the W cell and koniocellular pathways. In support of this possibility, anatomical and physiological studies demonstrate a much greater diversity of retinal ganglion cells in the primates with projections to koniocellular layers compared to those with projections to the magnocellular and parvocellular layers (Dacey and Packer, 2003; Wässle, 2004; Masland 2011, 2012; Crook, Packer, Troy and Dacey, 2014; Masri, Percival, Koizumi, Martin and Grünert, 2019; Grünert and Martin, 2020). Thus, results from the mouse may provide important insight into the range of processing strategies utilized across mammals for parallel processing of visual signals from eye to brain.

Parallel pathways from LGN to cortex are matched with parallel feedback pathways

Communication between the LGN and V1 is not uni-directional. Rather, feedback projections from V1 to the LGN complete a reciprocal exchange of information between the two structures. The majority of layer 6 neurons in V1 with axons that leave the cortex project to the LGN (note: these neurons are distinct from those that project to the claustrum (see Katz, 1987)). In addition to their extrinsic projections, layer 6 corticogeniculate neurons also send local axon collaterals to the overlying layers of cortex that receive thalamic input (Brigg, Kiley, Callaway and Usrey, 2016; Gilbert and Wiesel, 1979; Lund and Boothe, 1975; Usrey and Fitzpatrick, 1996). As a consequence of these projections, layer 6 neurons are in a strategic position to influence feedforward communication between the LGN and V1.

In common with the feedforward projection from the retina through the LGN to V1, the corticogeniculate feedback pathway also contains stream-specific projections. This specificity has been best demonstrated in the monkey where the corticogeniculate pathway includes separate classes of corticogeniculate neurons with axons selective for the magnocellular, parvocellular, and possibly even the koniocellular layers of the LGN (Fitzpatrick, Usrey, Schofield and Einstein, 1994; Ichida and Casagrande, 2002; Ichida, Mavity-Hudson and Casagrande, 2014). Thus, based on their anatomy, corticogeniculate neurons appear to form distinct groups with projections that align with the parallel retino-geniculo-cortical pathways. However, unlike retinal synapses that provide driving input to LGN neurons, corticogeniculate synapses are modulatory and serve to adjust geniculate responses to retinal input (see Sherman and Guillery, 2009).

The visual responses of corticogeniculate neurons are also consistent with a pathway that contains parallel streams. Specifically, neurons in the lower tier of layer 6 with projections to the magnocellular layers of the LGN have magnocellular-like response properties: they respond well to low-contrast and fast-moving stimuli and have fast-conducting axons. In contrast, neurons in the upper tier of layer 6 with projections to the parvocellular geniculate layers have parvocellular-like response properties: they prefer higher contrast and slower moving stimuli and have slower conducting axons (Fitzpatrick Usrey, Schofield and Einstein, 1994; Briggs and Usrey, 2009). As a result of this organization, visual stimuli well suited for exciting the magnocellular pathway also excite corticogeniculate neurons with axons selective for the magnocellular layers of the LGN, and visual stimuli better suited for exciting the parvocellular pathway also excite corticogeniculate neurons with axons selective for the parvocellular layers. In this way,

the corticogeniculate pathway appears poised to adjust the gain of its own input in a stream-specific fashion. Although less is known about corticogeniculate neurons in other species, evidence from the rat, cat, ferret, and tree shrew is consistent with the view of parallel streams in the corticogeniculate pathway (Bourassa and Deschênes, 1995; Briggs and Usrey, 2005; Tsumoto and Suda, 1980; Usrey and Fitzpatrick, 1996). It therefore seems likely that corticogeniculate neurons generally serve to influence the feedforward delivery of visual signals to cortex in a stream-specific fashion.

Summary and Conclusions

In summary, parallel pathways originating in the retina and continued through the LGN provide the cortex with complementary representations of the visual world. These pathways are rooted in the circuitry of the retina that gives rise to multiple classes of RGCs selective for distinct stimulus features, including luminance, contrast, color, spatial frequency, and temporal frequency. Much of what we know about parallel retino-geniculo-cortical pathways comes from three animal models: felines, monkey, and mice. In felines and monkeys, two prominent pathways, the X/Y and parvocellular/magnocellular pathways, respectively, each contain on-center and off-center cell types. These pathways share many features in common, as well as some distinct differences, reflecting the animals' survival needs and evolutionary histories. The W-cell or koniocellular pathways are a collection of many pathways originating from a broader diversity of RGCs. Mice are increasingly providing new information about these additional cell classes and this knowledge will likely inform future studies in other model systems. Parallel retino-geniculo-cortical pathways play an important role in supplying the cortex with independent channels of information that can be combined in

specific ways by the complexity of cortical circuits to generate a broader repertoire of visual responses that contribute to visual behavior and perception.

Figures

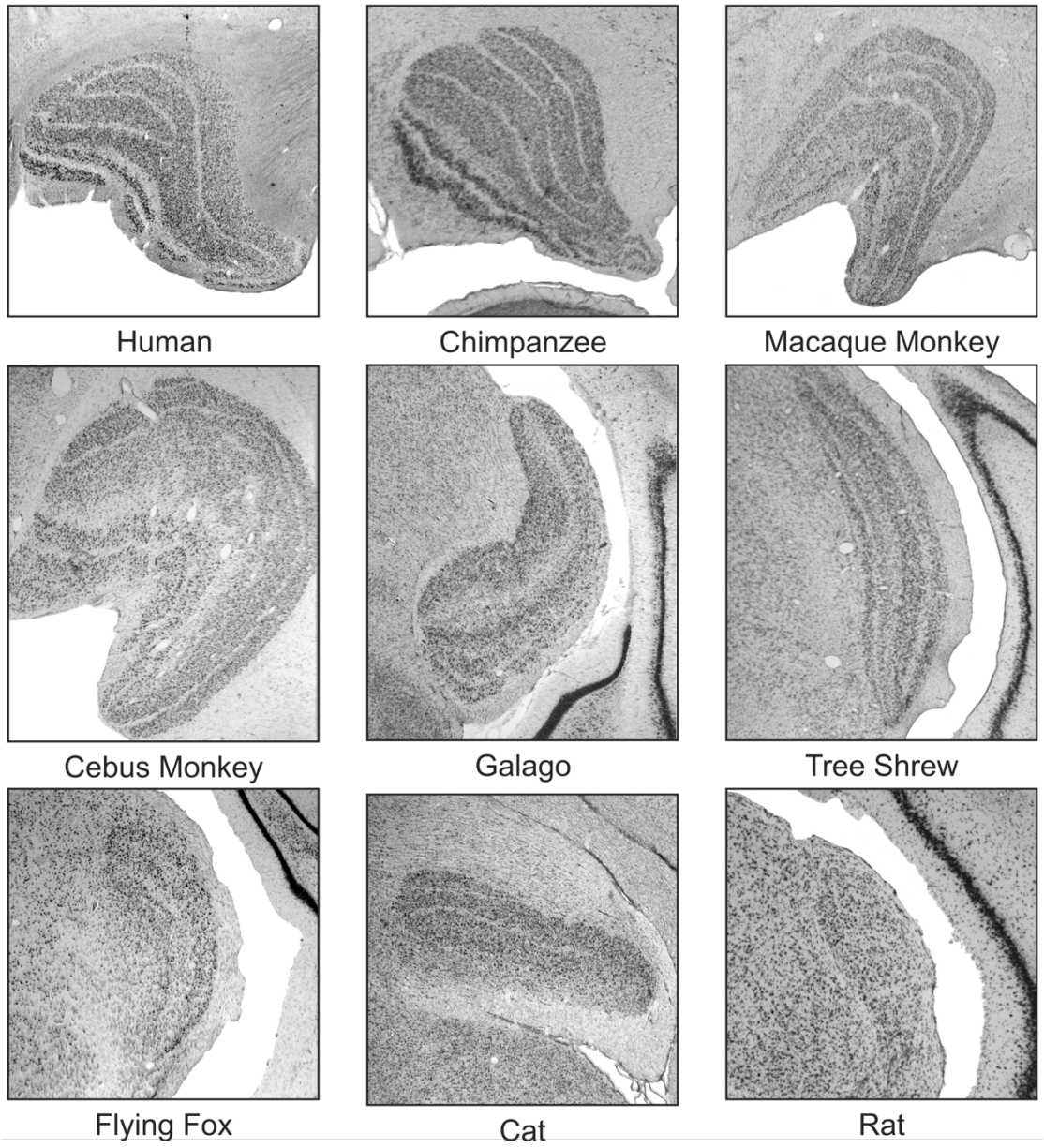

Figure 1. Nissl-stained sections of the lateral geniculate nucleus (LGN) from nine different species illustrating the diversity of shapes, sizes, and lamination patterns that accommodate the parallel retino-geniculo-cortical pathways. Top row: human, chimpanzee, rhesus macaque; middle row: cebus monkey, galago, tree shrew; bottom row: flying fox, domestic cat, rat. Adapted from Usrey and Alitto (2015).

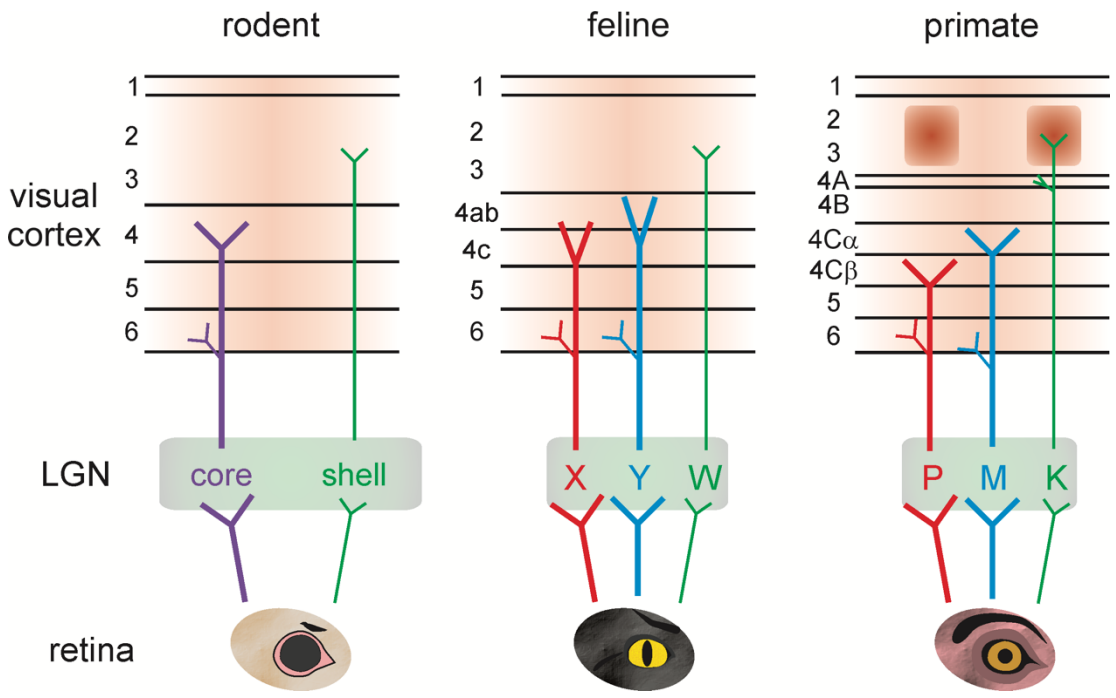

Figure 2. Schematic organization of the retino-geniculo-cortical pathway in the rodent, feline, and primate. In all mammals, including these examples, the geniculo-cortical axons terminate in cortical layer 4, a minority of axons terminate in cortical layers 1-3. In rodents, the LGN can be divided into core and shell regions. Relay cells in the core project primarily to cortical layer 4, whereas relay cells in the shell project primarily to the overlying superficial layers. In the feline, there are three major parallel pathways to cortex—the X-cell pathway terminates primarily in layer 4c, the Y-cell pathway terminates primarily in layer 4ab, and the W-cell pathway terminates in layers 1-3. There are also three parallel pathways in the primate—the parvocellular pathway (P) terminates in layer 4Cα, the magnocellular pathway (M) terminates in layer 4Cβ, and the koniocellular pathway (K) terminates in the layer 1–3 blobs. Adapted from Rathbun and Usrey (2008).

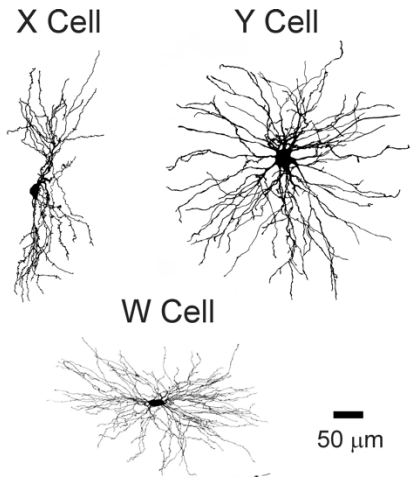

Figure 3. Cell types in the feline LGN. Camera lucida reconstructions of a representative X, Y, and W relay cell labeled with intracellular injection of horseradish peroxidase (HRP). Each cell type receives input from a different class of retinal ganglion cells and give rise to specific projection patterns to primary visual cortex. As is typical for these cell types, the dendritic arbor of the X cell is tufted and is oriented perpendicular to the plane of the layers, the arbor of the Y cell is more spherical, and the W cell arbor is oriented parallel to the layers. *Adapted from Friedlander et al. (1979), Stanford et al. (1981, 1983).*

References

Alitto H.J., Moore B.D. 4th, Rathbun D.L., Usrey W.M. A comparison of visual responses in the lateral geniculate nucleus of alert and anaesthetized macaque monkeys. *J. Physiol.* 2011;589:87–99. [PMC free article] [PubMed] [Google Scholar]

Alitto H.J., Rathbun D.L., Fisher T.G., Alexander P.C., Usrey W.M. Contrast gain control and retinogeniculate communication. *Eur. J. Neurosci.* 2019;49:1061–1068. [PMC free article] [PubMed] [Google Scholar]

Alitto H.J., Rathbun D.L., Vandeleest J.J., Alexander P.C., Usrey W.M. The augmentation of retinogeniculate communication during thalamic burst mode. *J. Neurosci.* 2019;39:5697–5710. [PMC free article] [PubMed] [Google Scholar]

Alitto, H.J. and Usrey, W.M. Influence of contrast on orientation and temporal frequency tuning in ferret primary visual cortex. *J. Neurophys.* 2004;91, 2797–2808.

Alitto H.J., Usrey W.M. Origin and dynamics of extraclassical suppression in the lateral geniculate nucleus of the macaque monkey. *Neuron* 2008;57:135–146, doi:10.1016/j.neuron.2007.11.019, pmid:18184570. [CrossRef] [PubMed] [Google Scholar]

Alitto H.J., Usrey W.M. Surround suppression and temporal processing of visual signals. *J. Neurophysiol.* 2015a;113:2605–2617, doi:10.1152/jn.00480.2014, pmid:25652919. [Abstract/FREE Full Text] [Google Scholar]

Alitto HJ, Usrey WM. Dissecting the dynamics of corticothalamic feedback. *Neuron.* 2015b;86:605–607. doi: 10.1016/j.neuron.2015.04.016. [PubMed] [CrossRef] [Google Scholar]

Alitto H.J., Weyand T.G., Usrey W.M. Distinct properties of stimulus-evoked bursts in the lateral geniculate nucleus. *J. Neurosci.* 2005;25:514–523. [PMC free article] [PubMed] [Google Scholar]

Alonso, J.M., Usrey, W.M. and Reid, R.C. Precisely correlated firing in cells of the lateral geniculate nucleus. *Nature* 1996;383, 815-819.

Alonso J.M., Usrey W.M., Reid R.C. Rules of connection for neurons in the lateral geniculate nucleus and visual cortex. *J Neurosci.* 2001;21:4002–4015. [PMC free article] [PubMed] [Google Scholar]

Angelucci A., Sainsbury K. Contribution of feedforward thalamic afferents and corticogeniculate feedback to the spatial summation area of macaque V1 and LGN. *J. Comp. Neurol.* 2006;498:330–351. [PubMed] [Google Scholar]

Barlow H.B., Fitzhugh R., Kuffler S.W. Resting discharge and dark adaptation in the cat. *J. Physiol.* 1964;125: 28–9P

Bereshpolova Y., Stoelzel C.R., Zhuang J., Amitai Y., Alonso J.M., Swadlow H.A. Getting drowsy? Alert/non-alert transitions and visual thalamocortical network dynamics. *J. Neurosci.* 2011;31:17480–17487. [PMC free article] [PubMed] [Google Scholar]

Bezdudnaya T., Cano M., Bereshpolova Y., Stoelzel C.R., Alonso J.M., Swadlow H.A. Thalamic burst mode and inattention in the awake LGNd. *Neuron.* 2006;49:421–432. [PubMed] [Google Scholar]

Bonin V., Mante V., Carandini M. The suppressive field of neurons in lateral geniculate nucleus. *J. Neurosci.* 2005;25:10844–10856, doi:10.1523/JNEUROSCI.3562-05.2005, pmid:16306397. [Abstract/FREE Full Text] [Google Scholar]

Bondy A.G., Haefner R.M., Cumming B.G. Feedback determines the structure of correlated variability in primary visual cortex. *Nat. Neurosci.* 2018; 21:598–606.

Borden P.Y., Wright N.C., Morrissette A.E., Jaeger D., Haider B., Stanley G.B. Thalamic bursting and the role of timing and synchrony in thalamocortical signaling in the awake mouse. *Neuron.* 2022;110:2836–2853. [PMC free article] [PubMed] [Google Scholar]

Bourassa, J. and Deschênes, M. Corticothalamic projections from the primary visual cortex in rats: A single fiber study using biocytin as an anterograde tracer. *Neuroscience* 1995;66, 253-263.

Briggs, F. and Usrey, W.M. Temporal properties of feedforward and feedback pathways between the thalamus and visual cortex in the ferret. *Thalamus and Related Systems* 2005;3, 133-139.

Briggs F., Usrey W.M. A fast, reciprocal pathway between the lateral geniculate nucleus and visual cortex in the macaque monkey. *J. Neurosci.* 2007;27:5431–36.

Briggs, F. Role of Feedback Connections in Central Visual Processing. *Annual Review of Vision Science*. 2020; https://doi.org/10.1146/annurev-vision-121219-081716.

Briggs F., Usrey W.M. Parallel processing in the corticogeniculate pathway of the macaque monkey. *Neuron.* 2009;62:135–146. doi: 10.1016/j.neuron.2009.02.024. [PMC free article] [PubMed] [CrossRef] [Google Scholar]

Briggs, F. and Usrey, W.M. Corticogeniculate feedback and visual processing in the primate. *The J. of Phys.* 2011; 589: 33 40. https://doi.org/10.1113/jphysiol.2010.193599

Briggs F., Kiley C.W., Callaway E.M., Usrey W.M. Morphological substrates for parallel streams of corticogeniculate feedback originating in both V1 and V2 of the macaque monkey. *Neuron* 2016; 90:388–99.

Brown SP, Masland RH. Spatial scale and cellular substrate of contrast adaptation by retinal ganglion cells. *Nat Neurosci.* 2001 Jan;4(1):44-51. doi: 10.1038/82888. PMID: 11135644.

Buffalo E.A., Fries P., Landman R., Liang H., Desimone R. A backward progression of attentional effects in the ventral stream. *PNAS* 2010;107:361–65.

Butts D.A., Cui Y., Casti A.R.R. Nonlinear computations shaping temporal processing of precortical vision. *J. Neurophysiol.* 2016;116:1344–1357. [PMC free article] [PubMed] [Google Scholar]

Carey S., Diamond R., Woods B. Development of face recognition: A maturational component? *Developmental psychology.* 1980 Jul;16(4):257.

Carey, R.G., Fitzpatrick, D. and Diamond, I.T. Thalamic projections to layer I of striate cortex shown by retrograde transport of horseradish peroxidase. *Science* 1979;203, 556-559.

Casagrande, V.A. A third parallel pathway to primate area V1. *Trends in Neuroscience* 1994;17, 305–310.

Casagrande, V.A. and Kaas, J.H. The afferent, intrinsic, and efferent connections of primary visual cortex in primates. In *Cerebral Cortex. Primary Visual Cortex in Primates*, 1994;Vol. 10, ed. A Peters, KS Rockland, pp. 201–59. New York: Plenum.

Casagrande, V.A., Yazar, F., Jones, K.D. and Ding, Y. The morphology of the koniocellular axon pathway in the macaque monkey. *Cerebral Cortex* 2007;17, 2334-2345.

Cavanaugh J.R., Bair W., Movshon J.A. Nature and interaction of signals from the receptive field center and surround in macaque V1 neurons. *J. Neurophysiol.* 2002a;88:2530–2546. [PubMed] [Google Scholar]

Cheong, S.K., Tailby, C., Solomon, S.G. and Martin, P.R. Cortical-like receptive fields in the lateral geniculate nucleus of marmoset monkeys. *J. Neurosci.* 2013;33, 6864–6876.

Chen Y., Martinez-Conde S., Macknik S.L., Bereshpolova Y., Swadlow H.A., Alonso J.M. Task difficulty modulates the activity of specific neuronal populations in primary visual cortex. *Nat Neurosci.* 2008;11:974–982. doi: 10.1038/nn.2147. [PMC free article] [PubMed] [CrossRef] [Google Scholar]

Chung S., Li X., Nelson S.B. Short-term depression at thalamocortical synapses contributes to rapid adaptation of cortical sensory responses in vivo. *Neuron.* 2002;34:437–446. [PubMed] [Google Scholar]

Cleland BG, Dubin MW, Levick WR. Simultaneous recording of input and output of lateral geniculate neurones. *Nat New Biol.* 1971 Jun 9;231(23):191-2. doi: 10.1038/newbio231191a0. PMID: 4325715.

Cleland BG. The dorsal lateral geniculate nucleus of the cat. In: Pettigrew JD, Sanderson KJ, Levick WR, editors. *Visual Neuroscience.* Cambridge Univ. Press; London: 1986. pp. 111–20. [Google Scholar]

Cleland BG, Harding TH. Response to the velocity of moving visual stimuli of the brisk classes of ganglion cells in the cat retina. J Physiol. 1983 Dec;345:47-63. doi: 10.1113/jphysiol.1983.sp014964. PMID: 6663509; PMCID: PMC1193783.

Cohen HI, Winters RW, Hamasaki DI. Response of X and Y cat retinal ganglion cells to moving stimuli. *Exp Brain Res.* 1980 Feb;38(3):299-303. doi: 10.1007/BF00236649. PMID: 7371732.

Crook, J.D., Packer, O.S., Troy, J.B. and Dacey, D.M. Synaptic mechanisms of color and luminance coding: rediscovering the X-Y dichotomy in primate retinal ganglion cells. *In: The New Visual Neurosciences* (Chalupa LM, Werner JS, eds): MIT press. 2014

Crunelli V., Tóth T.I., Cope D.W., Blethyn K., Hughes S.W. The 'window' T-type calcium current in brain dynamics of different behavioural states. *J. Physiol.* 2005;562:121–129. [PMC free article] [PubMed] [Google Scholar]

Cruz-Martín, A., El-Danaf, R.N., Osakada, F., Sriram, B., Dhande, O.S., et al. A dedicated circuit links direction-selective retinal ganglion cells to the primary visual cortex. *Nature* 2014;507, 358–361

Dan Y., Atick J.J., Reid R.C. Efficient coding of natural scenes in the lateral geniculate nucleus: experimental test of a computational theory. *J. Neurosci.* 1996;16:3351–3362. [PMC free article] [PubMed] [Google Scholar]

Dacey, D.M. and Lee, B.B. The ‘blue-on’ opponent pathway in primate retina originates from a distinct bistratified ganglion cell type. *Nature* 1994;367, 731–735.

Dacey DM. Parallel pathways for spectral coding in primate retina. *Annu Rev Neurosci.* 2000;23:743-75. doi: 10.1146/annurev.neuro.23.1.743. PMID: 10845080.

Dacey, D.M. and Packer, O.S. Colour coding in the primate retina: diverse cell types and cone-specific circuitry. *Current Opinion in Neurobiology* 2003;13, 421–427.

Demb, J.B., Zaghloul, K., Haarsma, L. and Sterling, P. Bipolar cells contribute to nonlinear spatial summation in the brisk-transient (Y) ganglion cell in mammalian retina. *J. Neurosci.* 2001;21, 7447-7454

Denning K.S., Reinagel P. Visual control of burst priming in the anesthetized lateral geniculate nucleus. *J. Neurosci.* 2005;25:3531–3538. [PMC free article] [PubMed] [Google Scholar]

Derrington, A.M., Lennie, P.M. and Wright, J. The mechanism of peripherally evoked responses in retinal ganglion cells. J. Phys. 2009;289, 299-310.

Deschenes M., Paradis M., Roy J.P., Steriade M. Electrophysiology of neurons of lateral thalamic nuclei in cat: resting properties and burst discharges. *J. Neurophysiol.* 1984;51:1196–1219. [PubMed] [Google Scholar]

Destexhe A., Sejnowski T.J. The initiation of bursts in thalamic neurons and the cortical control of thalamic sensitivity. *Philos. Trans. R. Soc. Lond. B Biol. Sci.* 2002;357:1649–1657. [PMC free article] [PubMed] [Google Scholar]

DeYoe E.A., Van Essen D.C. Concurrent processing streams in monkey visual cortex. *Trends Neurosci.* 1988 May;11(5):219-26. doi: 10.1016/0166-2236(88)90130-0. PMID: 2471327.

Dreher B., Fukuda Y. and Rodieck R. Identification, X-like and Y-like properties in the lateral geniculate nucleus of old world primates*. J. Physiol*. 1976;258, 433-452.

Edwards G., Vetter P., McGruer F., Petro L.S., Muckli L. Predictive feedback to V1 dynamically updates with sensory input. *Sci. Rep.* 2017;7:16538.

Enroth-Cugell C, Robson JG. The contrast sensitivity of retinal ganglion cells of the cat. *J Physiol.* 1966 Dec;187(3):517-52. doi: 10.1113/jphysiol.1966.sp008107. PMID: 16783910; PMCID: PMC1395960.

Enroth-Cugell C, Robson JG, Schweitzer-Tong DE, Watson AB. Spatio-temporal interactions in cat retinal ganglion cells showing linear spatial summation. *J Physiol.* 1983 Aug;341:279-307. doi: 10.1113/jphysiol.1983.sp014806. PMID: 6620181; PMCID: PMC1195335.

Erisir A., Van Horn S.C., Bickford M.E., Sherman S.M. Immunocytochemistry and distribution of parabrachial terminals in the lateral geniculate nucleus of the cat: a comparison with corticogeniculate terminals. *J. Comp. Neurol.* 1997a; 377:535–49

Erisir A., Van Horn S.C., Sherman S.M. Relative numbers of cortical and brainstem inputs to the lateral geniculate nucleus. *PNAS* 1997b; 94:1517–20

Fisher T.G., Alitto H.A., Usrey W.M. Retinal and non-retinal contributions to extraclassical surround suppression in the lateral geniculate nucleus. *J. Neurosci.* 2017;37:226–235. [PMC free article] [PubMed] [Google Scholar]

Fitzpatrick, D., Itoh, K. and Diamond, I.T. The laminar organization of the lateral geniculate body and the striate cortex in the squirrel monkey Saimiri sciureus. *J. Neurosci.* 1983;3, 673–702.

Fitzpatrick D., Usrey W.M., Schofield B.R., Einstein G. The sublaminar organization of corticogeniculate neurons in layer 6 of macaque striate cortex. *Vis. Neurosci.* 1994;11:307–15.

Friedlander, M.J., Lin, C.-S. and Sherman, S.M. Structure of physiologically identifed X and Y cells in the cat's lateral geniculate nucleus. *Science* 1979;204, 1114-1117.

Fukada, Y. Receptive field organization of cat optic nerve fibers with special reference to conduction velocity. *Vision Research* 1971;11, 209–226.

Gil Z., Connors B.W., Amitai Y. Efficacy of thalamocortical and intracortical synaptic connections: quanta, innervation, and reliability. *Neuron.* 1999;23:385–397. [PubMed] [Google Scholar]

Gilbert, C.D. and Wiesel T.N. Morphology and intracortical connections of functionally characterized neurones in the cat visual cortex. *Nature* 1979;280, 120-125.

Gregoriou G.G., Gotts S.J., Zhou H., Desimone R. High-frequency, long-range coupling between prefrontal and visual cortex during attention. *Science* 2009;324:1207–10

Guido W., Lu S.M., Vaughan J.W., Godwin D.W., Sherman S.M. Receiver operating characteristic (ROC) analysis of neurons in the cat's lateral geniculate nucleus during tonic and burst response mode. *Vis. Neurosci.* 1995;12:723–741. [PubMed] [Google Scholar]

Grünert, U. and Martin, P.R. Cell types and cell circuits in primate retina. *Progress in Retinal and Eye Research.* 2020;Feb 4:100844. doi: 10.1016/j.preteyeres.2020.100844. [Epub ahead of print].

Guillery R.W. A quantitative study of synaptic interconnections in the dorsal lateral geniculate nucleus of the cat. Z. Zellforsch. Mikrosk. *Anat.*1969;96:39–48

Hasse J.M., Bragg E.M., Murphy A.J., Briggs F. Morphological heterogeneity among corticogeniculate neurons in ferrets: quantification and comparison with a previous report in macaque monkeys. *J. Comp. Neurol.* 2019;527:546–57

Hamasaki, D. I., Cohen, H. I. Differential response of X and Y retinal ganglion cells to moving stimuli results from a difference in the surround mechanism. *Brain Research, 1977;122*(1), 157–161. https://doi.org/10.1016/0006-8993(77)90673-4

Helmholtz, H. “Handbook of Physiological Optics” (J. P. C. Southall, ed.), 2000;Vol. 2, p. 143. Thoemmes Press, Bristol, UK.

Hendry, S.H. and Reid, R.C. The koniocellular pathway in primate vision. *Annual Review of Neuroscience* 2000;23, 127–153.

Hirai D., Nakamura K.C., Shibata Ki, et al. Shaping somatosensory responses in awake rats: cortical modulation of thalamic neurons. *Brain Struct. Funct.* 2018;223:851–872. [PubMed] [Google Scholar]

Hochstein, S. and Shapley, R.M. Linear and nonlinear spatial subunits in Y cat retinal ganglion cells. *J. Phys.* 1976;262, 265-284.

Hong S.Z., Kim H.R., Fiorillo C.D. T-type calcium channels promote predictive homeostasis of input-output relations in thalamocortical neurons of lateral geniculate nucleus. *Front. Comput. Neurosci.* 2014;8:98. [PMC free article] [PubMed] [Google Scholar]

Hubel D.H., Wiesel T.N. Integrative action in the cat's lateral geniculate body. *J. Physiol.* 1961;155:385–398. [PMC free article] [PubMed] [Google Scholar]

Huberman, A.D., Wei, W., Elstrott, J., Stafford, B.K., Feller, M.B. and Barres, B.A. Genetic identification of an On-Off direction-selective retinal ganglion cell subtype reveals a layer-specific subcortical map of posterior motion. *Neuron* 2009;62, 327–334.

Huguenard J.R. Low-threshold calcium currents in central nervous system neurons. *Annu. Rev. Physiol.* 1996;58:329–348. [PubMed] [Google Scholar]

Huguenard J.R., McCormick D.A. Simulation of the currents involved in rhythmic oscillations in thalamic relay neurons. *J. Neurophysiol.* 1992;68:1373–1383. [PubMed] [Google Scholar]

Humphrey, A.L., Sur, M., Uhlrich, D.J. and Sherman, S.M. Projection patterns of individual X- and Y-cell axons from the lateral geniculate nucleus to cortical area 17 in the cat. *J. Comp. Neur.* 1985;233, 159-189

Ichida, J.M. and Casagrande, V.A. Organization of the feedback pathway from striate cortex (V1) to the lateral geniculate nucleus (LGN) in the owl monkey (Aotus trivirgatus). *J. Comp. Neur.* 2002;454, 272-283.

Ichida, J.M., Mavity-Hudson, J.A. and Casagrande, V.A. Distinct patterns of corticogeniculate feedback to different layers of the lateral geniculate nucleus. *Eye Brain 6* (Suppl 1) 2014;57-73.

Ikeda, H. and Wright, M.J. Receptive field organization of ‘sustained’ and ‘transient’ retinal ganglion cells which subserve different function roles. *J. Phys.* 2017;227, 769–800.

Jahnsen H., Llinás R. Electrophysiological properties of Guinea-pig thalamic neurones: an in vitro study. *J. Physiol.* 1984;349:205–226. [PMC free article] [PubMed] [Google Scholar]

Jones H.E., Andolina I.M., Oakely N.M., Murphy P.C., Sillito A.M. Spatial summation in lateral geniculate nucleus and visual cortex. *Exp Brain Res* 2000;135:279–284,

doi:10.1007/s002210000574, pmid:11131514. [CrossRef] [PubMed] [Google Scholar]

Jones H.E., Andolina I.M., Oakely N.M., Murphy P.C., Sillito A.M. Spatial summation in lateral geniculate nucleus and visual cortex. *Exp. Brain Res.* 2000;135:279–284. [PubMed] [Google Scholar]

Kapadia M.K., Westheimer G., Gilbert C.D. Dynamics of spatial summation in primary visual cortex of alert monkeys. *Proc. Natl. Acad. Sci. USA*. 1999;96:12073–12078. [PMC free article] [PubMed] [Google Scholar]

Kaplan E, Shapley R.M. The origin of the S (slow) potential in the mammalian lateral geniculate nucleus. *Exp Brain Res.* 1984;55:111–116. [PubMed] [Google Scholar]

Kaplan E, Shapley R.M. The primate retina contains two types of ganglion cells, with high and low contrast sensitivity. *Proc. Natl. Acad. Sci. USA*. 1986 Apr;83(8):2755-7. doi: 10.1073/pnas.83.8.2755. PMID: 3458235; PMCID: PMC323379.

Katz LC. Local circuitry of identified projection neurons in cat visual cortex brain slices. *J Neurosci.* 1987 Apr;7(4):1223-49. doi: 10.1523/JNEUROSCI.07-04-01223.1987. PMID: 3553446; PMCID: PMC6569009.

Kepecs A., Wang X.-J., Lisman J. Bursting neurons signal input slope. *J. Neurosci.* 2002;22:9053–9062. [PMC free article] [PubMed] [Google Scholar]

Kuffler S.W. Neurons in the retina; organization, inhibition and excitation problems. Cold Spring Harb. *Symp. Quant. Biol.* 1952;17: 281–92

Kuffler S.W. Discharge patterns and functional organization of mammalian retina. *J. Neurophysiol.* 1953;16:37–68. [PubMed] [Google Scholar]

Lee, B.B. Receptive field structure in the primate retina. *J. Comp. Neur.* 1996;36, 631–644.

Lennie, P. Parallel visual pathways: a review. *Vision Research* 1980;20, 561-594.

Lesica N.A., Stanley G.B. Encoding of natural scene movies by tonic and burst spikes in the lateral geniculate nucleus. *J. Neurosci.* 2004;24:10731–10740. [PMC free article] [PubMed] [Google Scholar]

Lesica N.A., Weng C., Jin J., Yeh C.-I., Alonso J.-M., Stanley G.B. Dynamic encoding of natural luminance sequences by LGN bursts. *PLoS Biol.* 2006;4 [PMC free article] [PubMed] [Google Scholar]

LeVay S., Sherk H. The visual claustrum of the cat. I. Structure and connections. *J Neurosci.* 1981 Sep;1(9):956-80. doi: 10.1523/JNEUROSCI.01-09-00956.1981. PMID: 6169810; PMCID: PMC6564105.

Levitt J.B., Lund J.S. The spatial extent over which neurons in macaque striate cortex pool visual signals. *Vis. Neurosci.* 2002;19:439–452. [PubMed] [Google Scholar]

Lin C.S., Kaas J.H. Projections from cortical visual areas 17, 18, and MT onto the dorsal lateral geniculate nucleus in owl monkeys. *J. Comp. Neurol.* 1977;173:457–74

Livingstone MS, Hubel DH. Effects of sleep and arousal on the processing of visual information in the cat. *Nature.* 1981;291:554–561. doi: 10.1038/291554a0. [PubMed] [CrossRef] [Google Scholar]

Livingstone M., Hubel D. Segregation of form, color, movement, and depth: anatomy, physiology, and perception. *Science.* 1988 May 6;240(4853):740-9. doi: 10.1126/science.3283936. PMID: 3283936.

Llinás R., Jahnsen H. Electrophysiology of mammalian thalamic neurones in vitro. *Nature.* 1982;297:406–408. [PubMed] [Google Scholar]

Lu S.M., Guido W., Sherman S.M. Effects of membrane voltage on receptive field properties of lateral geniculate neurons in the cat: contributions of the low-threshold Ca^{2+} conductance. *J. Neurophysiol.* 1992;68:1285–1298. [PubMed] [Google Scholar]

Lund, J.S. and Boothe, R. Interlaminar connections and pyramidal neuron organization in the visual cortex, area 17, of the macaque monkey. *J. Comp. Neur.* 1975;159, 305-334.

Marshel, J.H., Kaye, A.P., Nauhaus, I. and Callaway, E.M. Anterior-posterior direction opponency in the superficial mouse lateral geniculate nucleus. *Neuron* 2012;76, 713–720.

Martinez L.M., Molano-Mazón M., Wang X., Sommer F.T., Hirsch J.A. Statistical wiring of thalamic receptive fields optimizes spatial sampling of the retinal image. *Neuron.* 2014;81:943–956. [PMC free article] [PubMed] [Google Scholar]

Masland, R.H. Cell populations of the retina: the Proctor lecture. *Investigative Ophthalmology & Visual Science* 2011;52:4581–4591.

Masland, R.H. The neuronal organization of the retina. *Neuron* 2012;76, 266–280.

Masri, R.A., Percival, K.A., Koizumi, A., Martin, P.R. and Grünert, U. Survey of retinal ganglion cell morphology in marmoset. *J. Comp. Neurol.* 2019;527, 236-258.

Mastronarde D.N. Two classes of single-input X-cells in cat lateral geniculate nucleus. II. Retinal inputs and the generation of receptive-field properties. *J Neurophysiol.* 1987;57:381–413. [PubMed] [Google Scholar]

McClurkin J.W., Optican L.M., Richmond B.J. (1994). Cortical feedback increases visual information transmitted by monkey parvocellular lateral geniculate nucleus neurons. *Visual Neuroscience*, 11(3), 601–617. [PubMed] [Google Scholar]

McCormick D.A., Huguenard J. A model of the electrophysiological properties of thalamocortical relay neurons. *J. Neurophysiol.* 1992;68:1384–1400. [PubMed] [Google Scholar]

Mease R.A., Krieger P., Groh A. Cortical control of adaptation and sensory relay mode in the thalamus. *Proc. Natl. Acad. Sci. USA.* 2014;111:6798–6803. [PMC free article] [PubMed] [Google Scholar]

Mease R.A., Kuner T., Fairhall A.L., Groh A. Multiplexed spike coding and adaptation in the thalamus. *Cell Rep.* 2017;19:1130–1140. [PMC free article] [PubMed] [Google Scholar]

Merigan WH, Maunsell JH. How parallel are the primate visual pathways? *Annu. Rev. Neurosci.* 1993;16:369-402. doi: 10.1146/annurev.ne.16.030193.002101. PMID: 8460898.

Michalareas G, Vezoli J, van Pelt S, Schoffelen J-M, Kennedy H, Fries P. 2016. Alpha-beta and gamma rhythms subserve feedback and feedforward influences among human visual cortical areas. *Neuron* 89:384–97.

Moore B.D., 4th, Rathbun D.L., Usrey W.M., Freeman R.D.. Spatiotemporal flow of information in the early visual pathway. *Eur J Neurosci.* 2014;39:593–601. doi: 10.1111/ejn.12418. [PMC free article] [PubMed] [CrossRef] [Google Scholar]

Mukherjee, P., Kaplan, E. Dynamics of neurons in the cat lateral geniculate nucleus: in vivo electrophysiology and computational modeling. *J. Neurophysiol.* 1995;74:1222-1243.

Murphy, A.J., Shaw, L., Hasse, J.M., Goris, R.L.T., Briggs, F. Optogenetic activation of corticogeniculate feedback stabilizes response gain and increases information coding in LGN neurons. *J. Comput Neurosci.* 2021 Aug;49(3):259-271. doi: 10.1007/s10827-020-00754-5. Epub 2020 Jul 6. PMID: 32632511; PMCID: PMC7785653.

Nassi, J.J. and Callaway, E.M. Parallel processing strategies of the primate visual system. *Nature Reviews Neuroscience* 2009;10, 360–372.

Noudoost B., Chang M.H., Steinmetz N.A., Moore T. Top-down control of visual attention. *Curr. Opin. Neurobiol.* 2010;20:183–90.

Pennartz C.M.A., Dora S., Muckli L., Lorteije J.A.M. Towards a unified view on pathways and functions of neural recurrent processing. *Trends Neurosci.* 2019;42:589–603

Percival, K.A., Koizumi, A., Masri, R.A., Buzás, P., Martin, P.R. and Grünert U. Identification of a pathway from the retina to koniocellular layer K1 in the lateral geniculate nucleus of marmoset. *J. Neurosci.* 2014;34, 3821–3825.

Perez-Reyes E. Molecular physiology of low-voltage-activated t-type calcium channels. *Physiol. Rev.* 2003;83:117–1161. [PubMed] [Google Scholar]

Piscopo, D.M., El-Danaf, R.N., Huberman, A.D. and Niell, C.M. Diverse visual features encoded in mouse lateral geniculate nucleus. *J. Neurosci.* 2013;33, 4642–4656.

Rao R.P.N., Ballard D.H. Predictive coding in the visual cortex: a functional interpretation of some extra-classical receptive-field effects. *Nat. Neurosci.* 1999;2:79–87.

Rathbun D.L., Alitto H.J., Warland D.K., Usrey W.M. Stimulus contrast and retinogeniculate signal processing. *Front. Neural Circ.* 2016;10:8. [PMC free article] [PubMed] [Google Scholar]

Rathbun D.L., Warland D.K., Usrey W.M. Spike timing and information transmission at retinogeniculate synapses. *J. Neurosci.* 2010;30:13558–13566. [PMC free article] [PubMed] [Google Scholar]

Reid RC, Alonso JM. Specificity of monosynaptic connections from thalamus to visual cortex. *Nature.* 1995;378:281–284. doi: 10.1038/378281a0. [PubMed] [CrossRef] [Google Scholar]

Reid, R.C. and Shapley, R.M. Spatial structure of cone inputs to receptive fields in primate lateral geniculate nucleus. *Nature* 1992;356, 716–718.

Reid, R.C. and Shapley, R.M. Space and time maps of cone photoreceptor signals in macaque lateral geniculate nucleus. *J. Neurosci.* 2002;22, 6158–6175.

Reid R.C., Usrey W.M. Functional connectivity in the pathway from retina to striate cortex. In: Chalupa LM, Werner JS, editors. *The visual neurosciences.* Cambridge, MA: MIT; 2004. pp. 673–679. [Google Scholar]

Reinagel P., Godwin D., Sherman S.M., Koch C. Encoding of visual information by LGN bursts. *J. Neurophysiol.* 1999;81:2558–2569. [PubMed] [Google Scholar]

Rivadulla C., Martinez L., Grieve K.L., Cudeiro J. Receptive field structure of burst and tonic firing in feline lateral geniculate nucleus. *J. Physiol.* 2003;553:601–610. [PMC free article] [PubMed] [Google Scholar]

Sanchez, R.M., Dunkelberger, G.R. and Quigley, H.A. The number and diameter distribution of axons in the monkey optic nerve. *Investigative Ophthalmology and Visual Science* 1986;27, 1342-1350.

Sceniak M.P., Chatterjee S., Callaway E.M. Visual spatial summation in macaque geniculocortical afferents. *J. Neurophysiol.* 2006;96:3474–3484. [PubMed] [Google Scholar]

Sceniak M.P., Hawken M.J., Shapley R. Visual spatial characterization of macaque V1 neurons. *J. Neurophysiol.* 2001;85:1873–1887. [PubMed] [Google Scholar]

Sceniak M.P., Ringach D.L., Hawken M.J., Shapley R. Contrast's effect on spatial summation by macaque V1 neurons. *Nat. Neurosci.* 1999;2:733–739. [PubMed] [Google Scholar]

Schiller P.H., Logothetis N.K., Charles E.R. Functions of the colour-opponent and broad-band channels of the visual system. *Nature*. 1990; Jan 4;343(6253):68-70. doi: 10.1038/343068a0. PMID: 2296292.

Scholl, B., Tan, A.Y.Y., Corey, J. and Priebe, N.J. Emergence of orientation selectivity in the mammalian visual pathway. *J. Neurosci.* 2013;33, 10616–10624.

Shapley, R., Perry, V. H. Cat and monkey retinal ganglion cells and their visual functional roles. *Trends in Neurosciences,* 1986;*9*(5), 229–235. https://doi.org/10.1016/0166-2236(86)90064-0

Shapley R.M., Victor J.D. The effect of contrast on the transfer properties of cat retinal ganglion cells. *J Physiol.* 1978;285:275–298. doi: 10.1113/jphysiol.1978.sp012571. [PMC free article] [PubMed] [CrossRef] [Google Scholar]

Shapley, R. M., & Victor, J. D. How the contrast gain control modifies the frequency responses of cat retinal ganglion cells. *J. Physiol.* 1981; *318*(1), 161-179. https://doi.org/10.1113/jphysiol.1981.sp013856

Sherman S.M. Thalamic relays and cortical functioning. *Prog Brain Res.* 2005;149:107-26. doi: 10.1016/S0079-6123(05)49009-3. PMID: 16226580.

Sherman S.M. Thalamus plays a central role in ongoing cortical functioning. *Nat Neurosci.* 2016; Apr;19(4):533-41. doi: 10.1038/nn.4269. PMID: 27021938.

Sherman S.M. Thalamocortical interactions. *Curr Opin Neurobiol.* 2012;Aug;22(4):575-9. doi: 10.1016/j.conb.2012.03.005. Epub 2012 Apr 11. PMID: 22498715; PMCID: PMC3398163.

Sherman S.M. Functioning of Circuits Connecting Thalamus and Cortex. *Compr Physiol.* 2017;Mar 16;7(2):713-739. doi: 10.1002/cphy.c160032. PMID: 28333385.

Sherman S.M., Guillery R.W. second ed. MIT Press; Cambridge, MA: 2009. Exploring the Thalamus and its Role in Cortical Function. [Google Scholar]

Sherman S.M., Guillery R.W. The role of the thalamus in the flow of information to the cortex. Philos Trans R Soc Lond B *Biol Sci.* 2002;Dec 29;357(1428):1695-708. doi: 10.1098/rstb.2002.1161. PMID: 12626004; PMCID: PMC1693087.

Sherman S.M., Guillery R.W. Distinct functions for direct and transthalamic corticocortical connections. *J. Neurophysiol.* 2011;Sep;106(3):1068-77. doi: 10.1152/jn.00429.2011. Epub 2011 Jun 15. PMID: 21676936.

Sherman, S.M., Wilson, J.R., Kaas, J.H., Webb, S.V. X- and Y-Cells in the Dorsal Lateral Geniculate Nucleus of the Owl Monkey (Aotus trivirgatus). *Science*, 1976;*192*(4238), 475–477. http://www.jstor.org/stable/1741358

Sillito A.M., Jones H.E. Corticothalamic interactions in the transfer of visual information*. Philos Trans R Soc Lond B Biol Sci 2002;* 357*:*1739–1752, doi:10.1098/rstb.2002.1170, pmid:12626008*. [*Abstract/FREE Full Text] [Google Scholar]

Sillito A.M., Jones H.E., Gerstein G.L., West D.C. Feature-linked synchronization of thalamic relay cell firing induced by feedback from the visual cortex. *Nature*, 1994; *369*(6480), 479-482. https://doi.org/10.1038/369479a0

Sincich L.C., Adams D.L., Economides J.R., Horton J.C. Transmission of spike trains at the retinogeniculate synapse. *J. Neurosci.* 2007;27:2683–2692. [PMC free article] [PubMed] [Google Scholar]

Sincich L.C., Horton J.C. The circuitry of V1 and V2: integration of color, form, and motion. *Annu Rev Neurosci.* 2005;28:303-26. doi: 10.1146/annurev.neuro.28.061604.135731. PMID: 16022598.

Smith M.A., Bair W., Movshon J.A. Dynamics of suppression in macaque primary visual cortex. *J. Neurosci.* 2006;26:4826–4834. [PMC free article] [PubMed] [Google Scholar]

Solomon S.G., White A.J., Martin P.R. Extraclassical receptive field properties of parvocellular, magnocellular, and koniocellular cells in the primate lateral geniculate nucleus. *J. Neurosci.* 2002;22:338–349, pmid:11756517. [Abstract/FREE Full Text] [Google Scholar]

Stoelzel C.R., Huff J.M., Bereshpolova Y., Zhuang J., Hei X., Alonso J.M., Swadlow H.A. Hour-long adaptation in the awake early visual system. *J Neurophysiol.* 2015;114:1172–1182. doi: 10.1152/jn.00116.2015. [PMC free article] [PubMed] [CrossRef] [Google Scholar]

Stafford, D.K. and Dacey, D.M. Physiology of the A1 amacrine: a spiking, axon-bearing interneuron of the macaque monkey retina. *Visual Neuroscience* 1997;14, 507–522.

Stanford, L.R., Friedlander, M.J. and Sherman, S.M. Morphology of physiologically identified W-cells in the C laminae of the cat's lateral geniculate nucleus. *J. Neurosci.* 1981;1, 578-584.

Stanford, L.R., Friedlander, M.J. and Sherman, S.M. Morphological and physiological properties of geniculate W-cells of the cat: a comparison with X- and Y-cells. *J. Neurophys.* 1983;50, 582-608.

Stratford K.J., Tarczy-Hornoch K., Martin K.A., Bannister N.J., Jack J.J. Excitatory synaptic inputs to spiny stellate cells in cat visual cortex. *Nature.* 1996;382:258–261. [PubMed] [Google Scholar]

Stoelzel C.R., Bereshpolova Y., Alonso J-M., Swadlow H.A. Axonal conduction delays, brain state, and corticogeniculate communication. *J. Neurosci.* 2017;37:6342–58.

Sutter E.E. *Advanced Methods of Physiological Systems Modeling.* Vol. 1. University of Southern California; Los Angeles: 1987. A practical non-stochastic approach to nonlinear time-domain analysis; pp. 303–315. [Google Scholar]

Suzuki S., Rogawski M.A. T-type calcium channels mediate the transition between tonic and phasic firing in thalamic neurons. *Proc. Natl. Acad. Sci. USA.* 1989;86:7228–7232. [PMC free article] [PubMed] [Google Scholar]

Swadlow H.A., Gusev A.G. The impact of 'bursting' thalamic impulses at a neocortical synapse. *Nat. Neurosci.* 2001;4:402–408. [PubMed] [Google Scholar]

Tang, J., Ardila Jimenez, S.C., Chakraborty, S. and Schultz, S.R. Visual receptive field properties of neurons in the mouse lateral geniculate nucleus. *PLoS One*. 2016;7;11(1):e0146017. doi: 10.1371/journal.pone.0146017. eCollection 2016.

Thoreson, W.B. and Dacey, D.M. Diverse Cell Types, Circuits, and Mechanisms *for Color Vision in the Vertebrate Retina. Physiological Reviews* 2019;99, 1527-1573.

Tsien R.W., Lipscombe D., Madison D.V., Bley K.R., Fox A.P. Multiple types of neuronal calcium channels and their selective modulation. *Trends Neurosci.* 1988;11:431–438. [PubMed] [Google Scholar]

Tsumoto, T. and Suda, K. Three groups of cortico-geniculate neurons and their distribution in binocular and monocular segments of cat striate cortex. *J. Comp. Neur.* 1980;193, 223-236.

Uglesich R., Casti A., Hayot F., Kaplan E. Stimulus size dependence of information transfer from retina to thalamus. *Front Syst Neurosci.* 2009;3:10.

doi: 10.3389/neuro.06.010.2009. [PMC free article] [PubMed] [CrossRef] [Google Scholar]

Usrey, W.M. The organization of layer VI neurosn in tre shrew and macaque monkey striate cortex. Doctoral dissertation, Duke University Medical Center. 1994

Usrey W.M. Spike timing and visual processing in the retinogeniculocortical pathway. *Phil. Trans. Roy. Soc. Lond.: Biol. Sci.* 2002;357:1729–1737. [PMC free article] [PubMed] [Google Scholar]

Usrey W.M., Alitto H.J. Visual functions of the thalamus. *Annu. Rev. Vis. Sci.* 2015;1:351–371. [PMC free article] [PubMed] [Google Scholar]

Usrey W.M., Alonso J.M., Reid R.C. Synaptic interactions between thalamic inputs to simple cells in cat visual cortex. *J. Neurosci.* 2000;20:5461–5467. [PMC free article] [PubMed] [Google Scholar]

Usrey W.M., Sherman S.M. Corticofugal circuits: communication lines from the cortex to the rest of the brain. *J. Comp. Neurol.* 2019;527:640–650. [PMC free article] [PubMed] [Google Scholar]

Usrey W.M., Sherman S.M. Oxford University Press; 2022. Exploring Thalamocortical Interactions: Circuitry for Sensation, Action, and Cognition. [Google Scholar]

Usrey W.M., Reppas J.B., Reid R.C. Paired-spike interactions and synaptic efficacy of retinal inputs to the thalamus. *Nature.* 1998;395:384–387. [PubMed] [Google Scholar]

Usrey W.M., Reppas J.B., Reid R.C. Specificity and strength of retinogeniculate connections. *J. Neurophysiol.* 1999;82:3527–3540. [PubMed] [Google Scholar]

van Kerkoerle T., Self M.W., Dagnino B., Gariel-Mathis M-A., Poort J., et al. Alpha and gamma oscillations characterize feedback and feedforward processing in monkey visual cortex. *PNAS* 2014; 111:14332–41

Vinck M., van Wingerden M., Womelsdorf T., Fries P., Pennartz C.M.A. The pairwise phase consistency: a bias-free measure of rhythmic neuronal synchronization. *Neuroimage.* 2010;51:112–122. [PubMed] [Google Scholar]

Walker G.A., Ohzawa I., Freeman R.D. Suppression outside the classical cortical receptive field. *Vis. Neurosci.* 2000;17:369–379. [PubMed] [Google Scholar]

Wang X.J., Rinzel J., Rogawski M.A. A model of the T-type calcium current and the low-threshold spike in thalamic neurons. *J. Neurophysiol.* 1991;66:839–850. [PubMed] [Google Scholar]

Wang X., Wei Y., Vaingankar V., Wang Q., Koepsell K., Sommer F.T., Hirsch J.A. Feedforward excitation and inhibition evoke dual modes of firing in the cat's visual thalamus during naturalistic viewing. *Neuron.* 2007;55:465–778. [PMC free article] [PubMed] [Google Scholar]

Wässle H, Boycott BB. Functional architecture of the mammalian retina. *Physiol Rev.* 1991 Apr;71(2):447-80. doi: 10.1152/physrev.1991.71.2.447. PMID: 2006220.

Webb B.S., Tinsley C.J., Vincent C.J., Derrington A.M. Spatial distribution of suppressive signals outside the classical receptive field in lateral geniculate nucleus. *J. Neurophysiol.* 2005;94:1789–1797. [PubMed] [Google Scholar]

Weyand T.G. Retinogeniculate transmission in wakefulness. *J. Neurophysiol.* 2007;98:769–785. [PubMed] [Google Scholar]

Weyand T.G., Boudreaux M., Guido W. Burst and tonic response modes in thalamic neurons during sleep and wakefulness. *J. Neurophysiol.* 2001;85:1107–1118. [PubMed] [Google Scholar]

Young, T. Bakerian Lecture: On the Theory of Light and Colours. *Philosophical Transactions of the Royal Society of London* 1802;92, 12-48.

Zeater, N., Cheong, S.K., Solomon, S.G., Dreher, B. and Martin, P.R. Binocular Visual Responses in the Primate Lateral Geniculate Nucleus. *Current Biology* 2015;25, 3190-3195.

Zeldenrust F., Chameau P., Wadman W.J. Spike and burst coding in thalamocortical relay cells. *PLoS Comput. Biol.* 2018;14 [PMC free article] [PubMed] [Google Scholar]